Supporting Information

for

Temperature-Modulated Diastereoselective Transformations of 2-Vinylindoles to Tetrahydrocarbazoles and Tetrahydrocycloheptadiindoles

*Imtiyaz Ahmad Wani, Aditya Bhattacharyya, Masthanvali Sayyad, and Manas K. Ghorai**

Department of Chemistry, Indian Institute of Technology, Kanpur 208016, India

E-mail: mkghorai@iitk.ac.in

Table of Contents

1. X-ray crystallographic studies

The crystals used in the analyses were glued to a glass fiber and mounted on SMART APEX diffractometer. The instrument was equipped with CCD area detector and data were collected using graphite-monochromated Mo Kα radiation (λ = 0.71069 Å) at low temperature (100 K). Cell constants were obtained from the least-squares refinement of three-dimensional centroids through the use of CCD recording of narrow ω rotation frames, completing almost all-reciprocal space in the stated θ range. All data were collected with SMART 5.628 and were integrated with the SAINT[1] program. An empirical absorption correction was applied to collect reflections with SADABS[2] using XPREP.[3] The structure was solved using SIR-97[4] and refined using SHELXL-97.[5] The space group of the compounds was determined based on the lack of systematic absence and intensity statistics. Full matrix least squares / difference Fourier cycles were performed which located the remaining non-hydrogen atoms. All non-hydrogen atoms were refined with anisotropic displacement parameters. All the hydrogen atoms are fixed by using geometrical constrains using idealized geometries and have been defined isotropically.

2. X-ray crystallographic structure of 2c

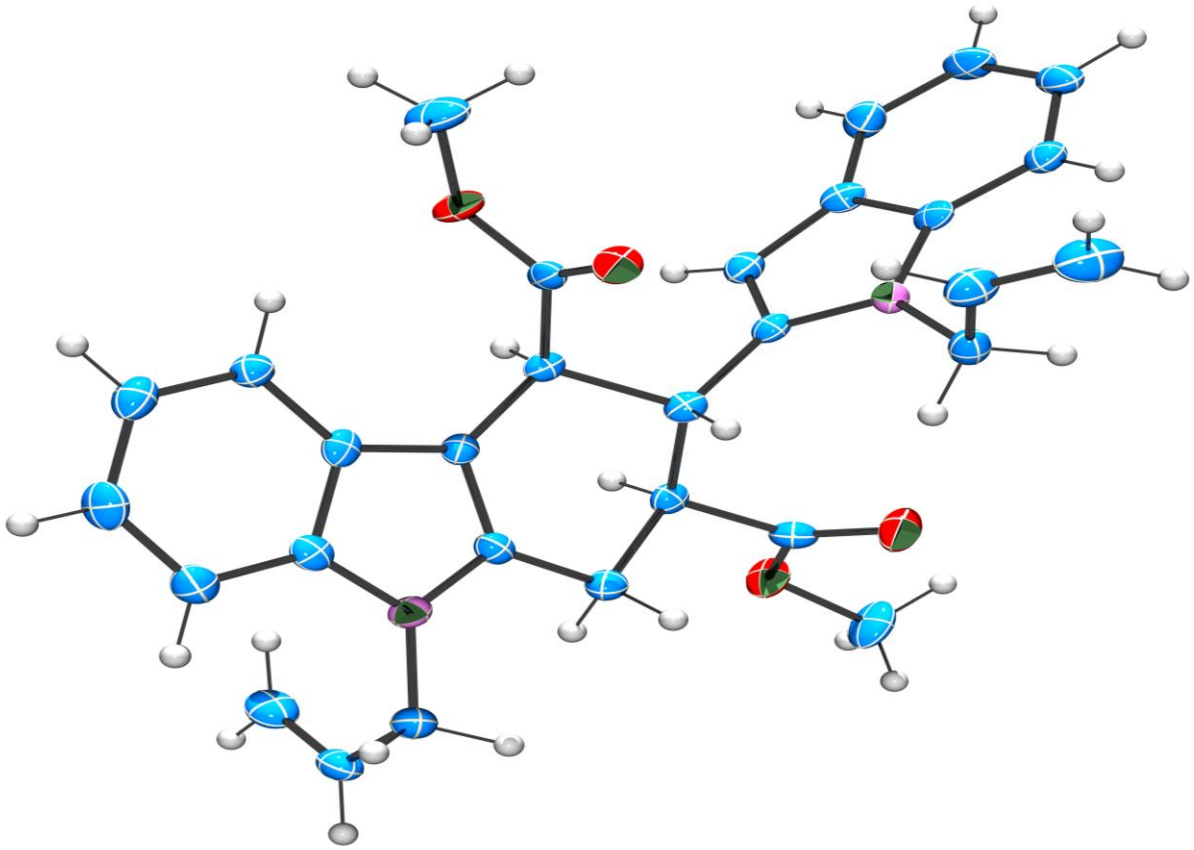

Figure S1. X-ray crystallographic structure of **2c** (ORTEP view with 50% thermal ellipsoid contour probability, CCDC 1562218)

3. X-ray crystallographic structure of 3m

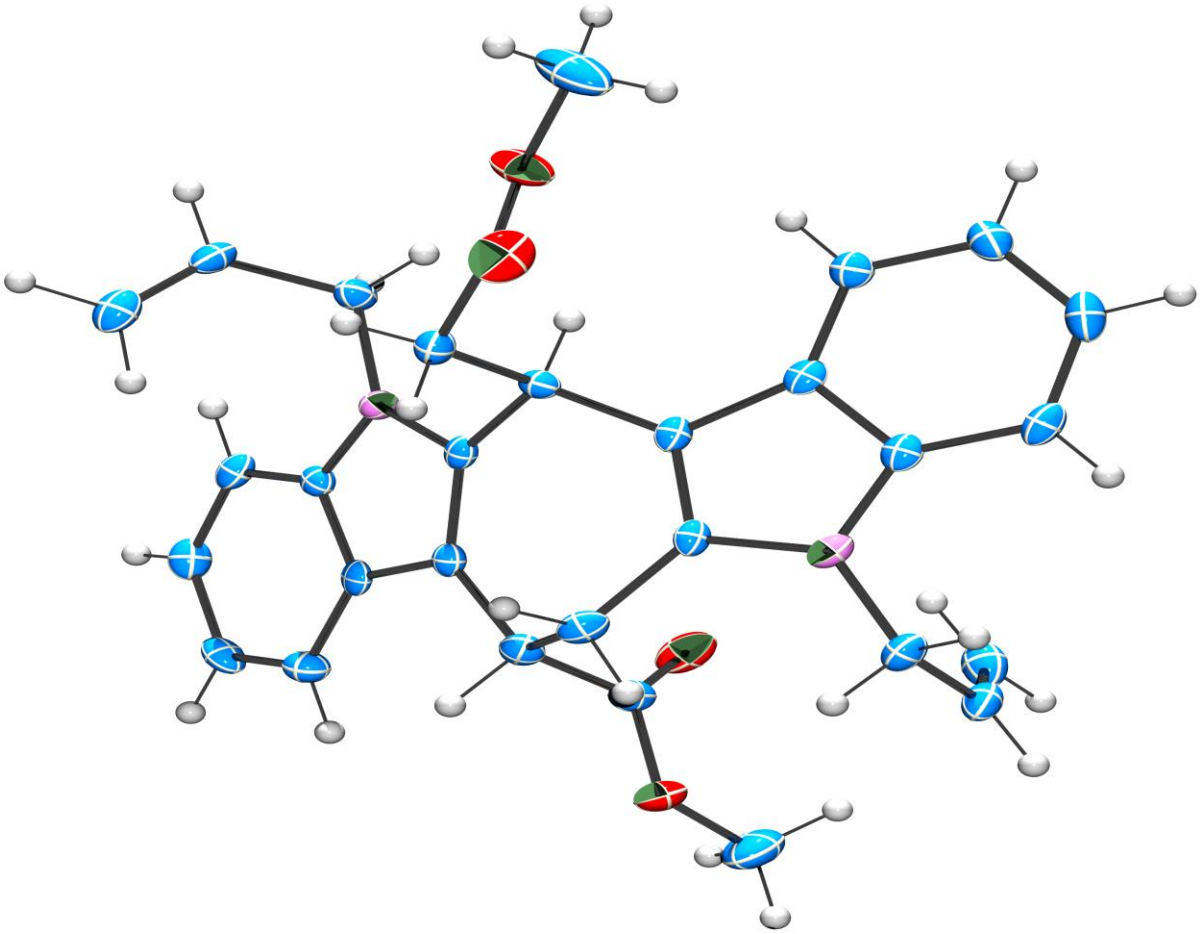

Figure S2. X-ray crystallographic structure of **3m** (ORTEP view with 50% thermal ellipsoid contour probability, CCDC 1562219)

4. X-ray crystallographic structure of 5

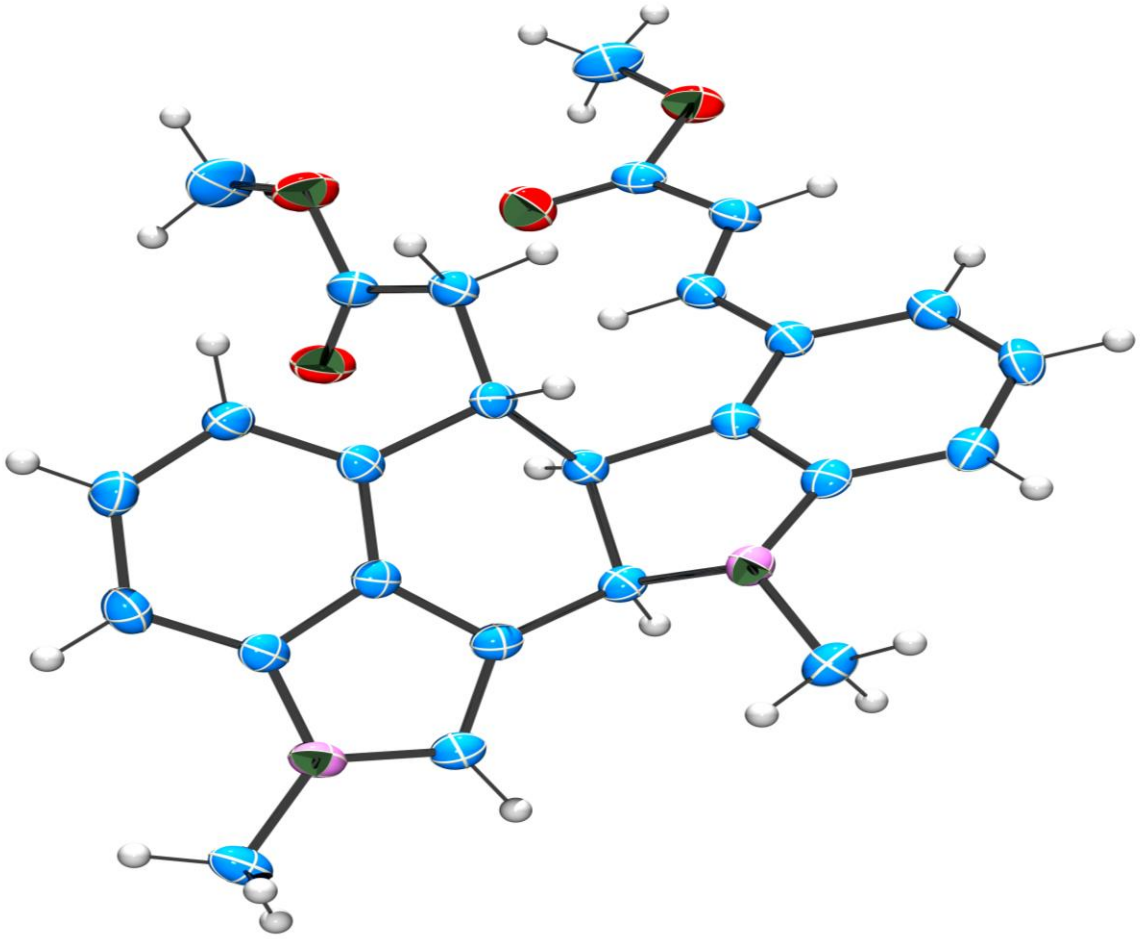

Figure S3. X-ray crystallographic structure of **5** (ORTEP view with 50% thermal ellipsoid contour probability, CCDC 1562220)

5. X-ray crystallographic data and structure refinement

Compound	**2c**	**3m**	**5**
Formula	$C_{30}H_{30}N_2O_4$	$C_{60}H_{60}N_4O_8$	$C_{26}H_{26}N_2O_4$
Formula weight	482.56	965.12	430.49
CCDC No.	1562218	1562219	1562220
Crystal color, habit	white, prism	yellow, prism	yellow, prism
T / K	100(2)	100(2)	100(2)
Crystal system	Triclinic	Triclinic	Triclinic
Space group	P-1 (no. 2)	P-1 (no. 2)	P-1 (no. 2)
a/Å	9.795(5)	13.1542(9)	7.581(5)
b/Å	10.469(5)	13.3153(9)	10.819(5)
c/Å	12.397(5)	15.7230(11)	13.144(5)
α/°	87.898(5)	103.217(2)	89.938(5)
β/°	81.097(5)	113.154(2)	87.155(5)
γ/°	82.861(5)	93.739(2)	82.887(5)
V/Å^3	1246.0(10)	2427.7(3)	1068
Z	2	2	2
D_c/g cm^{-3}	1.286	1.32	1.338
μ/mm^{-1}	0.086	0.088	0.091
Reflections measured	19105	30641	13025
Unique reflections	6199	8984	3789
Reflections used [$I > 2\sigma(I)$]	2583	5196	2964
R_1[a], wR_2[b] [$I > 2\sigma(I)$]	$R_1 = 0.0870$[a] $wR_2 = 0.1476$[b]	$R_1 = 0.064$[a] $wR_2 = 0.134$[b]	$R_1 = 0.0505$[a] $wR_2 = 0.1261$[b]
R_1[a], wR_2[b](all data)	R_1=0.2425[a] wR_2=0.1989[b]	R_1=0.132[a] wR_2=0.164[b]	R_1=0.0678[a] wR_2=0.1352[b]
GOF on F^2	0.985	0.976	1.049

[a] $R_1 = \Sigma||F_o| - |F_c||/\Sigma|F_o|$. [b] $wR_2 = \{\Sigma[w\,(|F_o|^2 - |F_c|^2)^2]/\,\Sigma[w(|F_o|^2)^2]\}^{1/2}$

6. Computational Details[6–8]

All DFT calculations were performed using Gaussian 09 program.[6] Optimizations were carried out with the modeled geometry using B3LYP functional[7] with a 6-311+G(d) basis set.[6] To confirm the nature of the stationary points, frequency calculations were also performed at the same level of theory used for geometry optimization. No imaginary frequency was found for all the optimized structures. Corresponding optimized diagrams were made using Chemcraft[8] visualization program.

7. References

1. SAINT+ 6.02ed.; Bruker AXS, Madison, WI, 1999.

2. Sheldrick, G. M. SADBAS, Empirical Absorption Correction Program, University of Göttingen, Göttingen, Germany, 1997.

3. XPREP, 5.1ed. Siemens Industrial Automation Inc., Madison, WI, 1995.

4. A. Altomare, M. C. Burla, M. Camalli, G. L. Cascarano, C. Giacovazzo, A. Guagliardi, A. G. G. Moliterni, G. Polidori, R. Spagna, *J. Appl. Cryst.* **1999**, *32*, 115.

5. Sheldrick, G. M. SHELXL-97: Program for Crystal Structure Refinement (University of Göttingen, Göttingen, Germany, 1997).

6. (a) I. J. Galpin, A. K. A. Mohammed, A. Patel *Tetrahedron,*1988, **44**, 1783. (b) M. J. Frisch, G. W. Trucks, H. B. Schlegel, G. E. Scuseria, M. A. Robb, J. R. Cheeseman, G. Scalmani, V. Barone Izmaylov, B. Mennucci, G. A. Petersson, H. Nakatsuji, M. Caricato, X. Li, H. P. Hratchian, A. F., J. Bloino, G. Zheng, J. L. Sonnenberg, M. Hada, M. Ehara, K. Toyota, R. Fukuda, J. Hasegawa, M. Ishida, T. Nakajima, Y. Honda, O. Kitao, H. Nakai, T. Vreven, J. A. Montgomery Jr., J. E. Peralta, F. Ogliaro, M. Bearpark, J. J. Heyd, E. Brothers, K. N. Kudin, V. N. Staroverov, R. Kobayashi, J. Normand, K. Raghavachari, A. Rendell, J. C. Burant, S. S. Iyengar, J. Tomasi, M. Cossi, N. Rega, N. J. Millam, M. Klene, J. E. Knox, J. B. Cross, V. Bakken, C. Adamo, J. Jaramillo, R. Gomperts, R. E. Stratmann, O. Yazyev, A. J. Austin, R. Cammi, C. Pomelli, J. W. Ochterski, R. L. Martin, K. Morokuma, V. G. Zakrzewski, G. A. Voth, P. Salvador, J. J. Dannenberg, S. Dapprich, A. D. Daniels, Ö. Farkas, J. B. Foresman, J. V. Ortiz, J. Cioslowski and D. J. Fox, Gaussian 09, revision C.01, Gaussian, Inc., Wallingford, CT, 2010.

7. (a) A. D. Becke, *J. Chem. Phys.*, 1993, **98**, 5648–5652; (b) C. Lee, W. Yang and R. G. Parr, *Phys. Rev. B*, 1988, **37**, 785–789; (*c*) P. J. Stevens, F. J. Devlin, C. F. Chabalowski and M. J. Frisch, *J. Phys. Chem.* 1994, **98**, 11623–11627.

8. http://www.chemcraftprog.com/

8. Computational studies of 2a and 3a

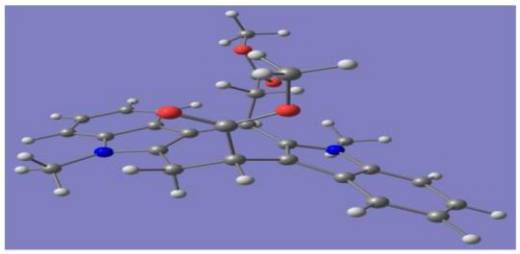

-1417.1946483 a.u.

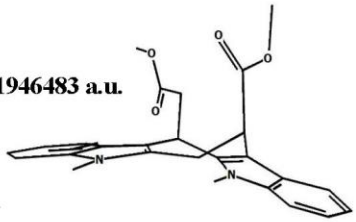

end product

4 +3 thermodynamic product

intermediate

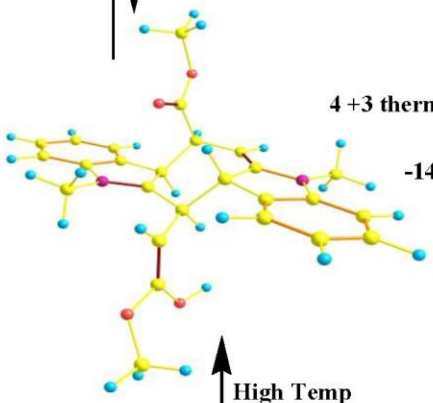

-1417.4993824 a. u.

High Temp

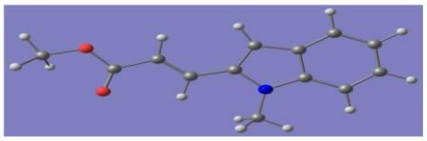

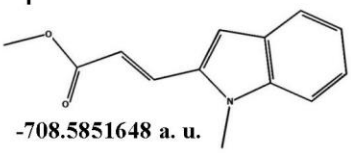

-708.5851648 a. u.

Low Temp

intermediate

4 +2 kinetic product

or

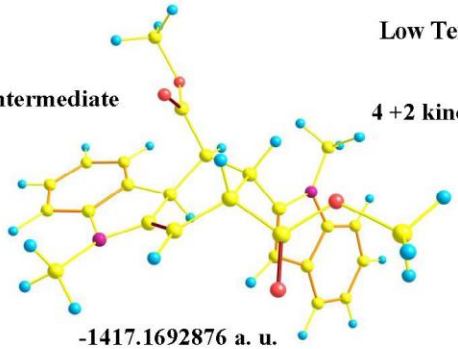

-1417.1692876 a. u.

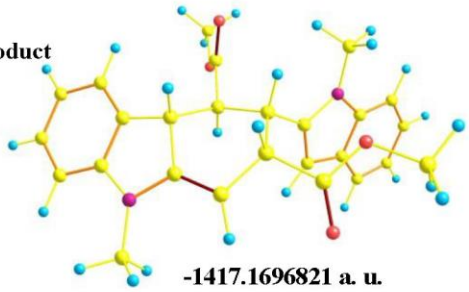

-1417.1696821 a. u.

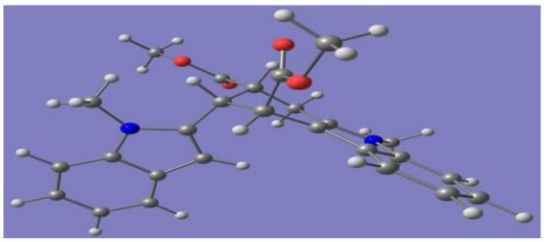

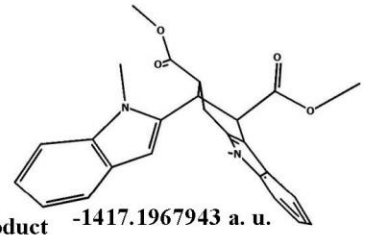

end product -1417.1967943 a. u.

9. Copies of NMR spectra

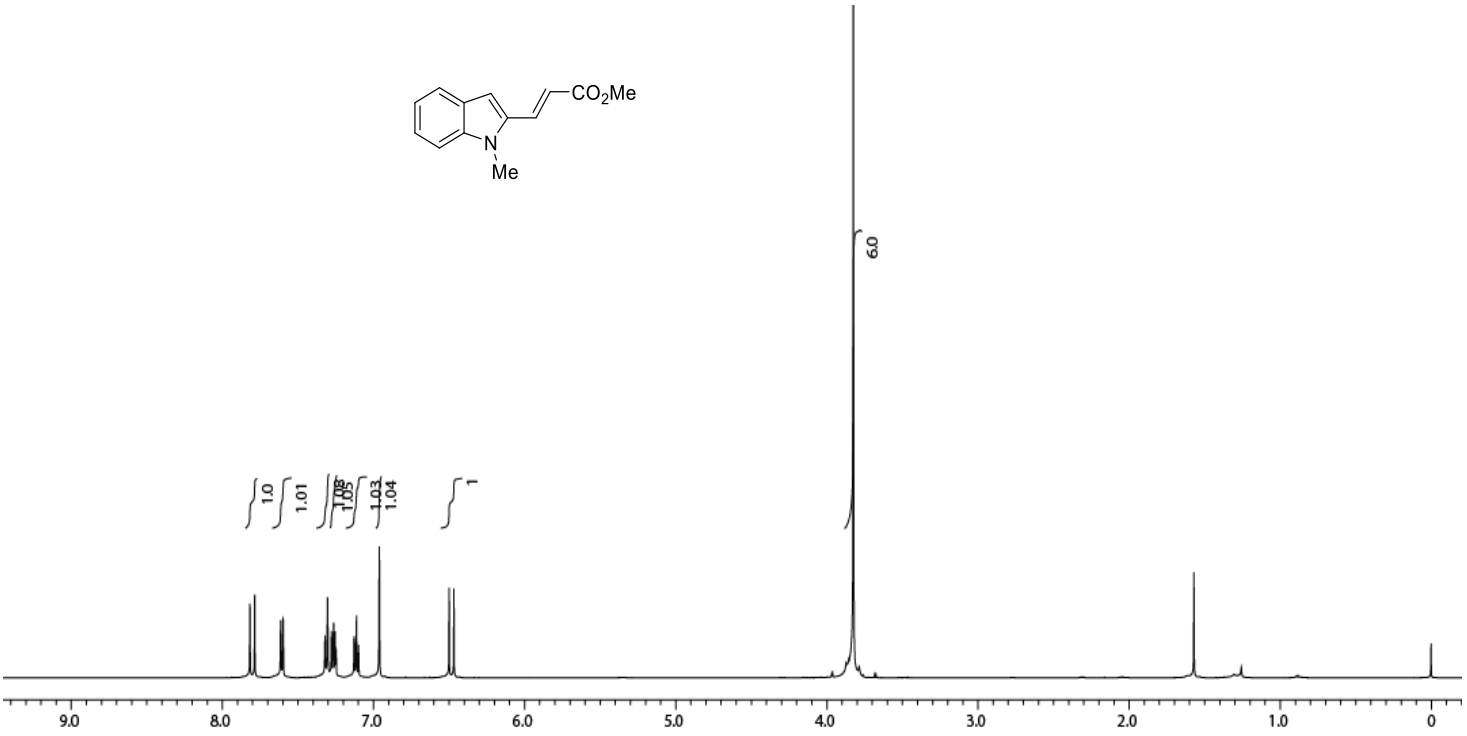

Figure S4. ^{1}H NMR spectrum of **1a** ($CDCl_3$, 500 MHz)

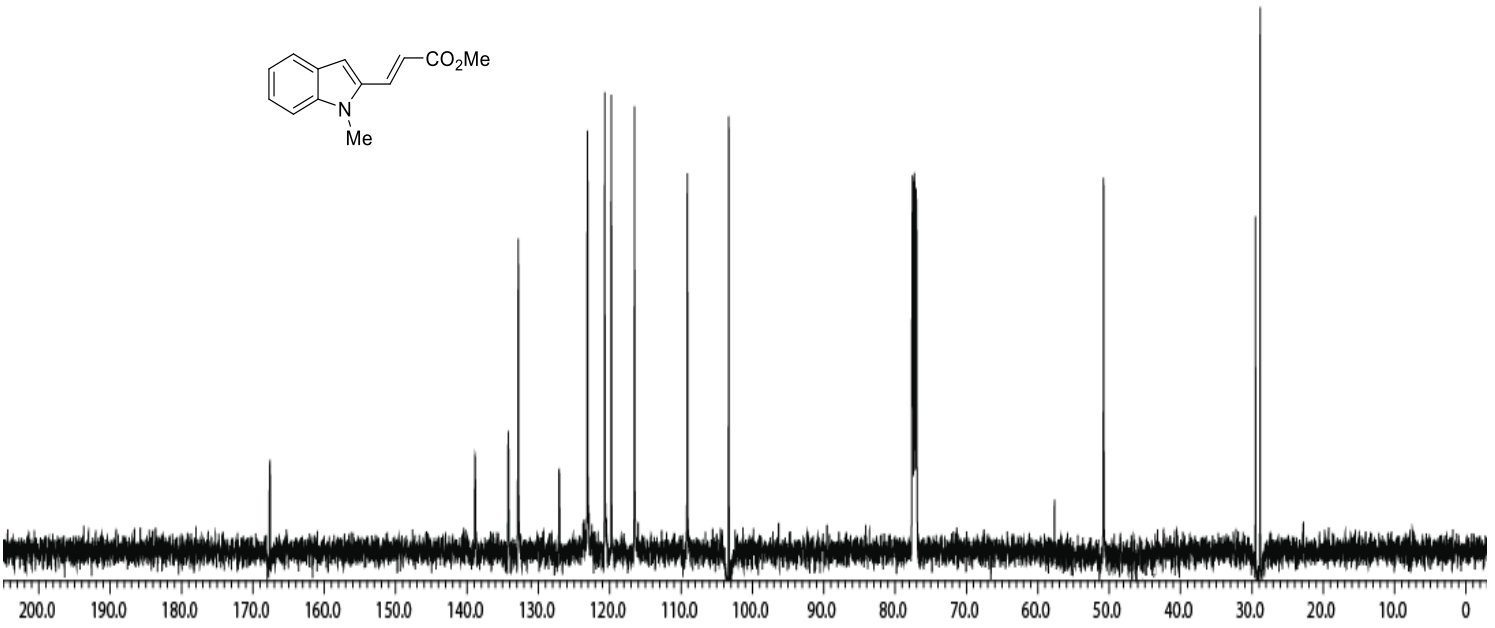

Figure S5. $^{13}C\{^{1}H\}$ NMR spectrum of **1a** ($CDCl_3$, 125 MHz)

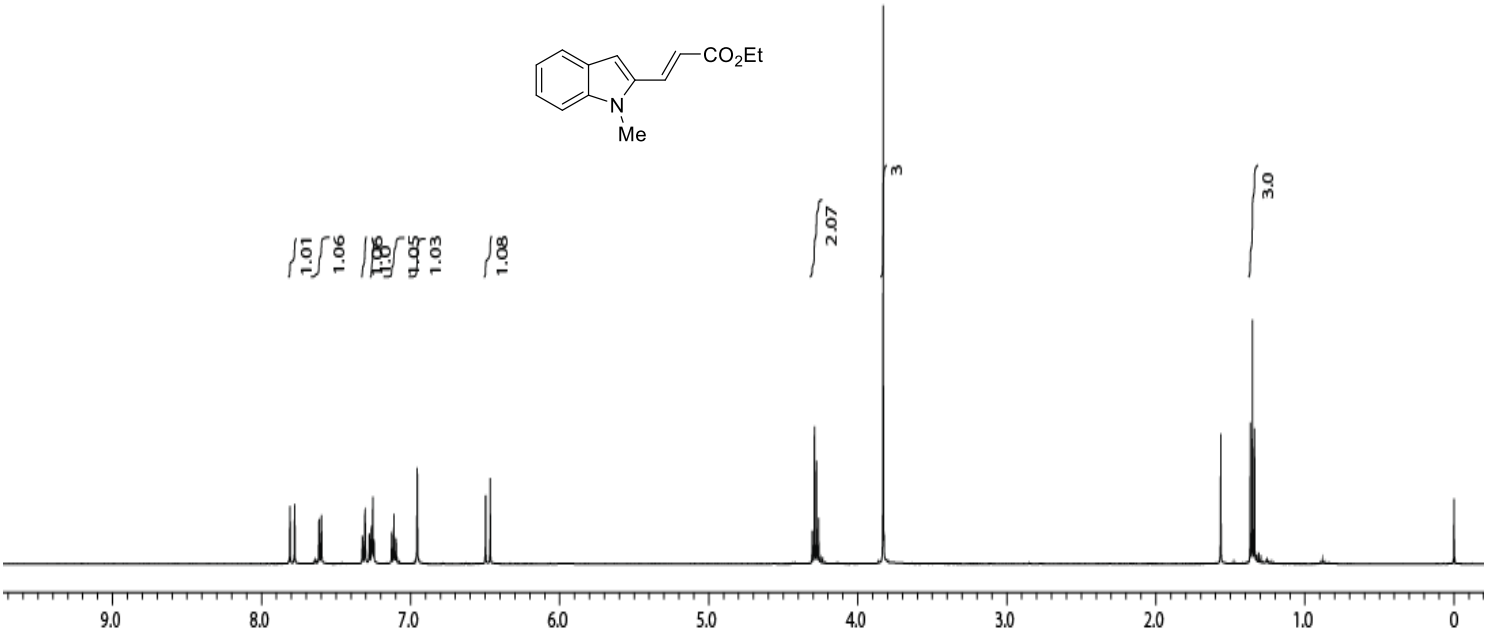

Figure S6. ^{1}H NMR spectrum of **1b** ($CDCl_3$, 500 MHz)

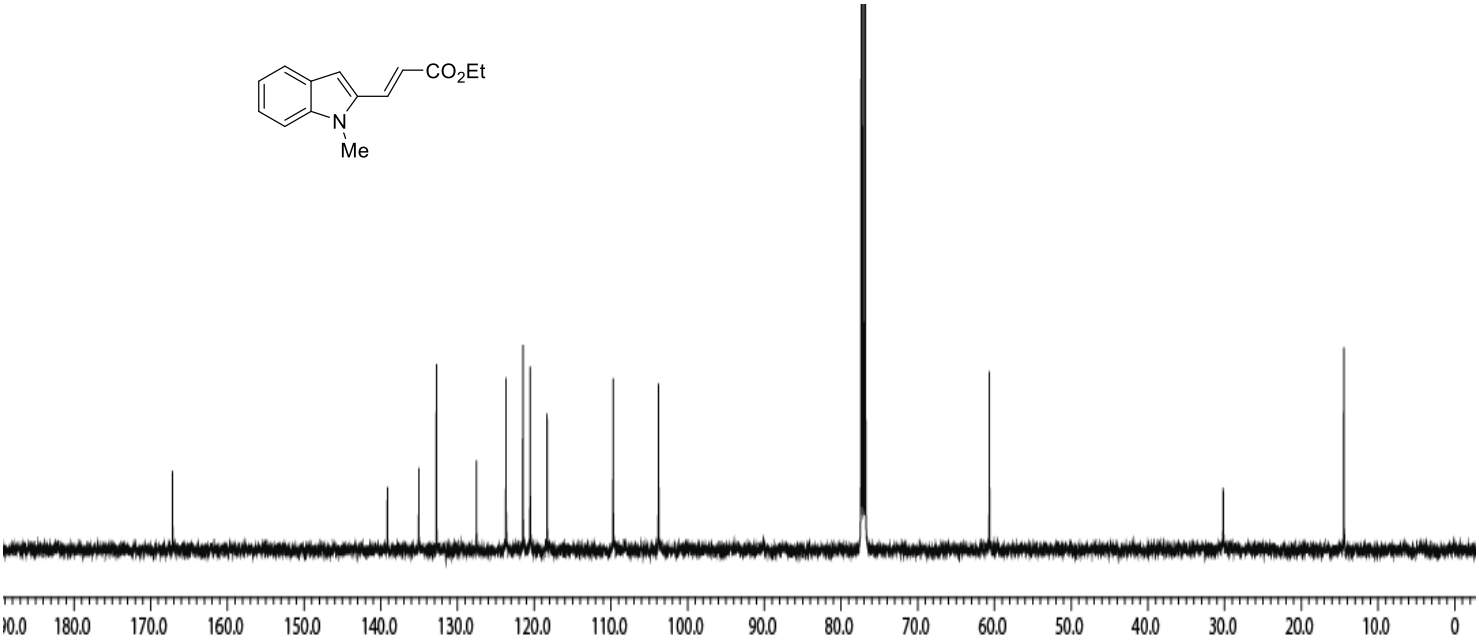

Figure S7. $^{13}C\{^{1}H\}$ NMR spectrum of **1b** ($CDCl_3$, 125 MHz)

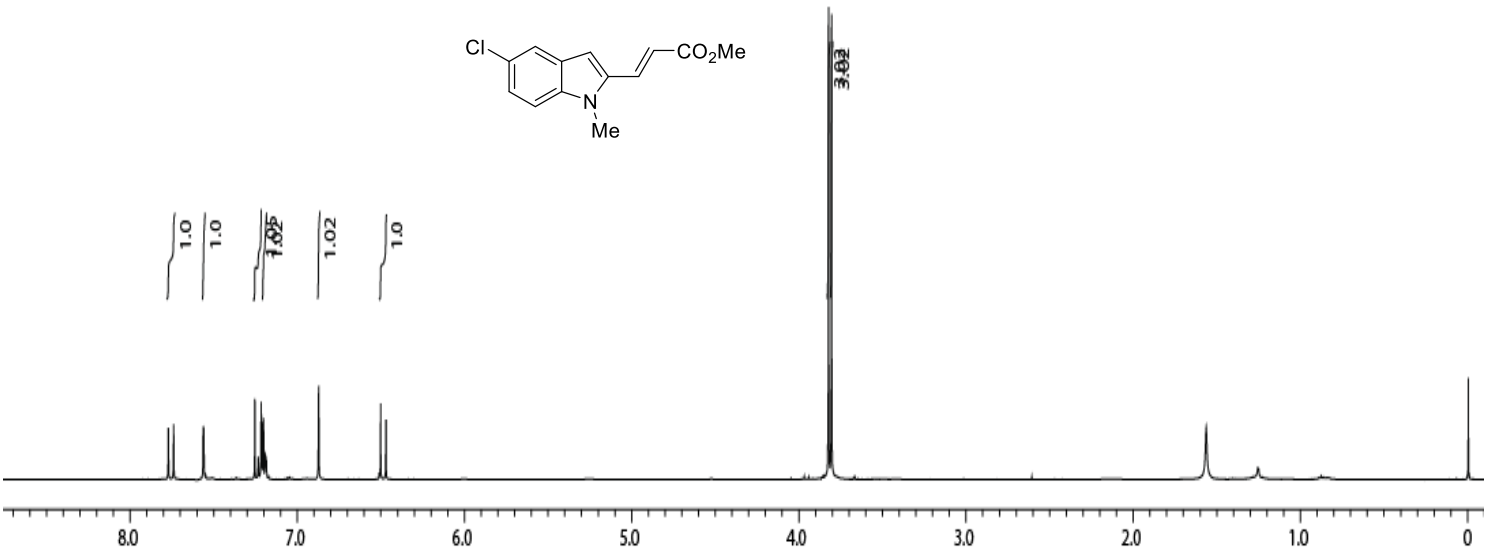

Figure S8. ^{1}H NMR spectrum of **1e** ($CDCl_3$, 500 MHz)

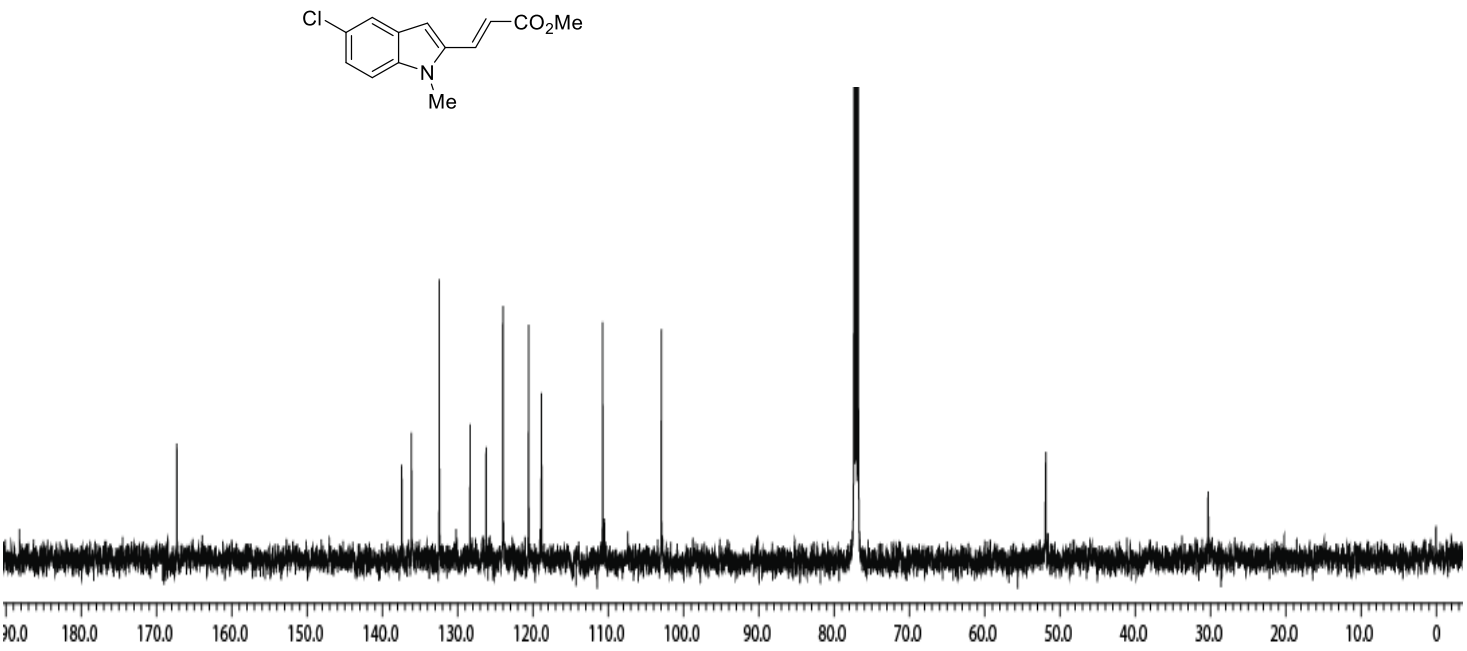

Figure S9. $^{13}C\{^{1}H\}$ NMR spectrum of **1e** ($CDCl_3$, 125 MHz)

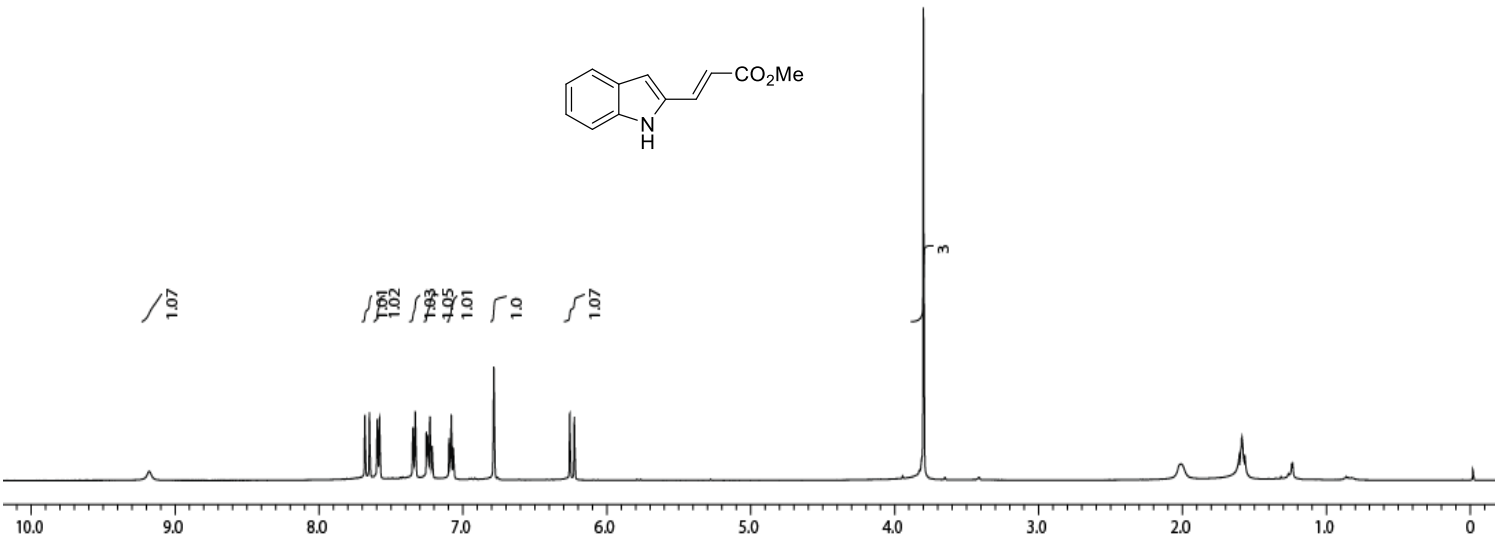

Figure S10. ^{1}H NMR spectrum of **1i** ($CDCl_3$, 500 MHz)

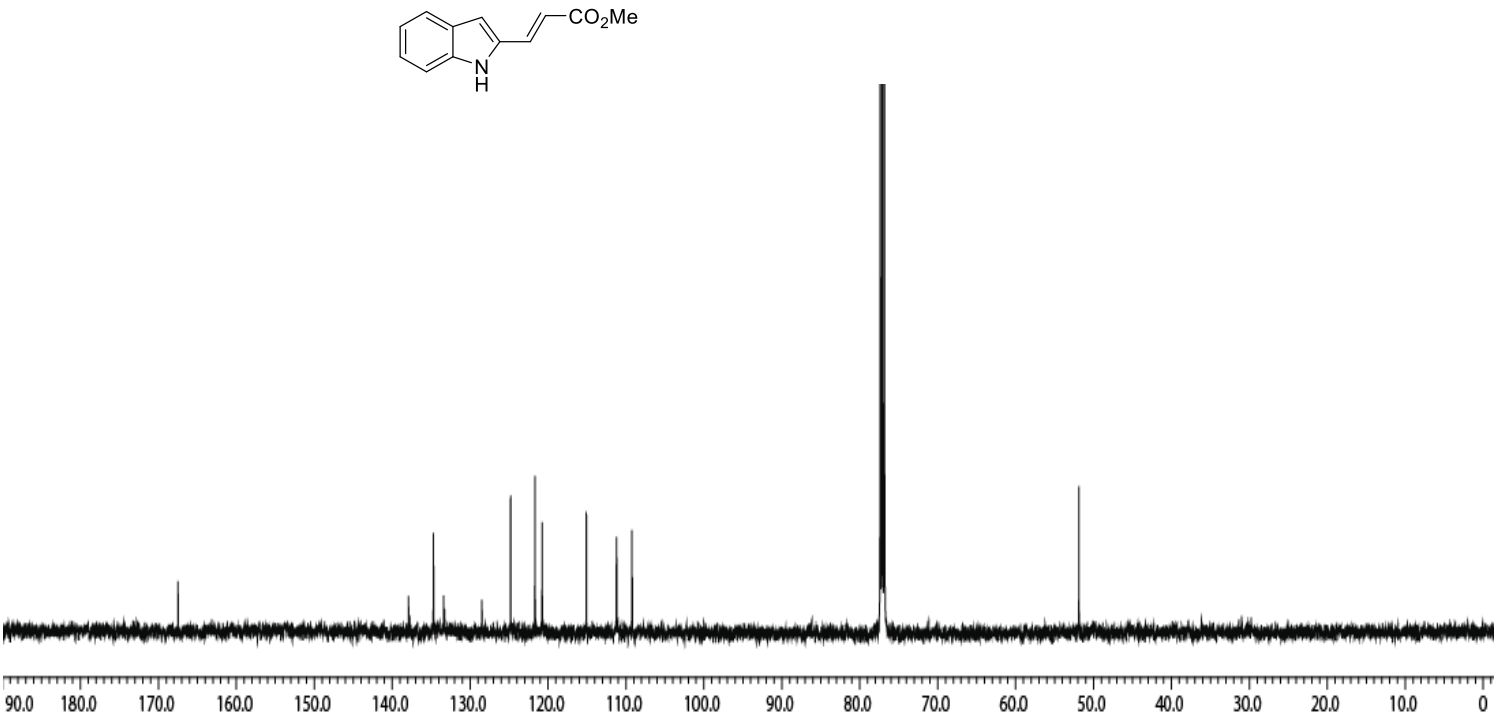

Figure S11. $^{13}C\{^{1}H\}$ NMR spectrum of **1i** ($CDCl_3$, 125 MHz)

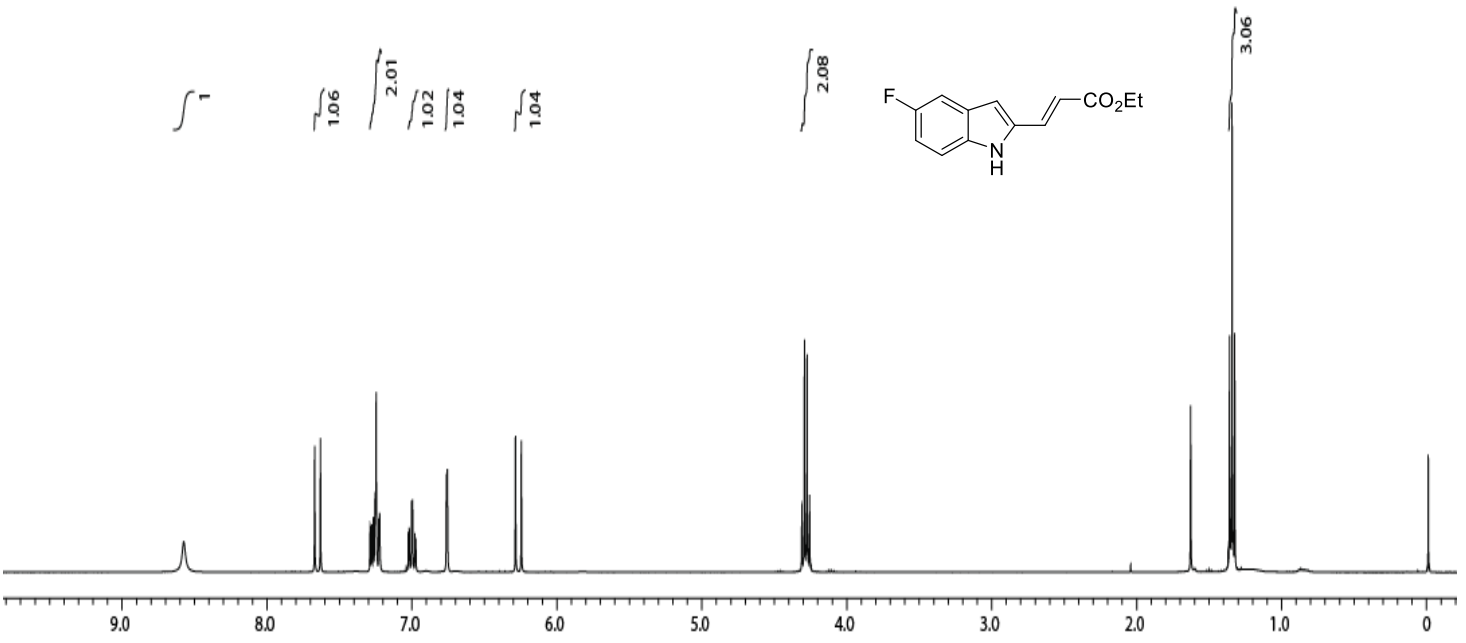

Figure S12. ^{1}H NMR spectrum of **1k** ($CDCl_3$, 500 MHz)

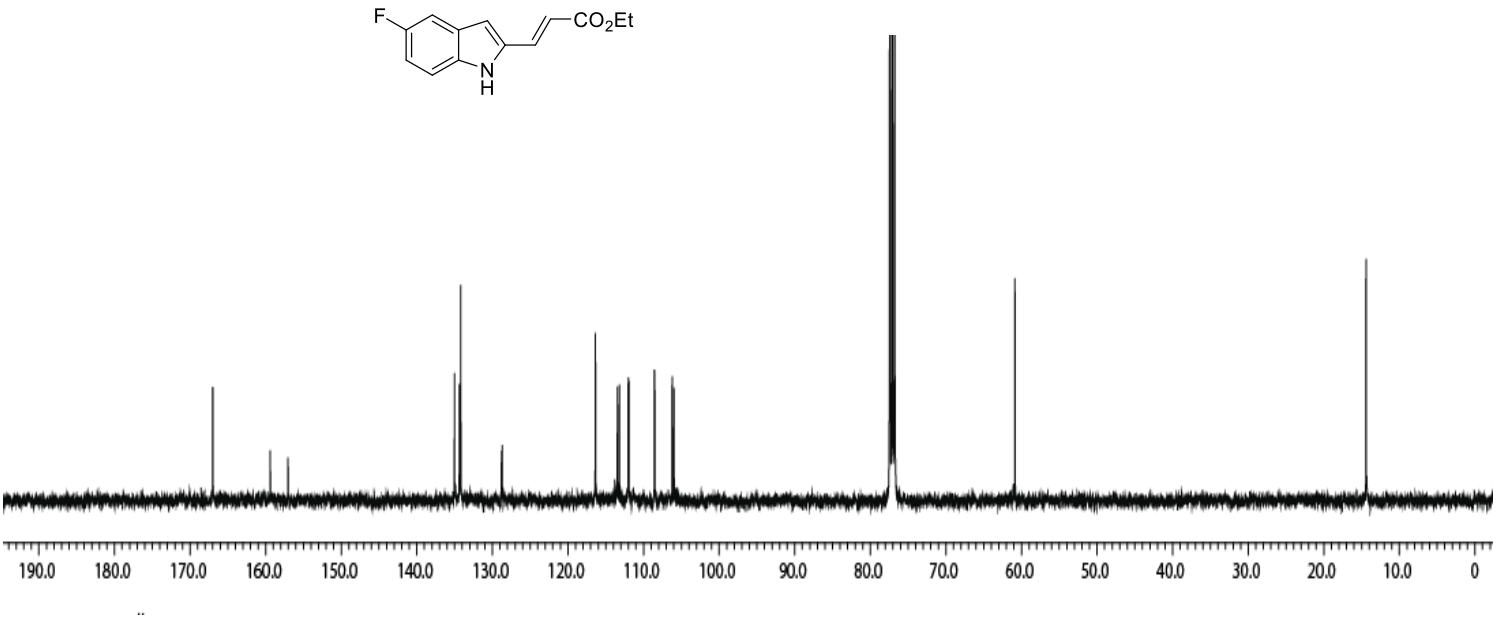

Figure S13. $^{13}C\{^{1}H\}$ NMR spectrum of **1k** ($CDCl_3$, 125 MHz)

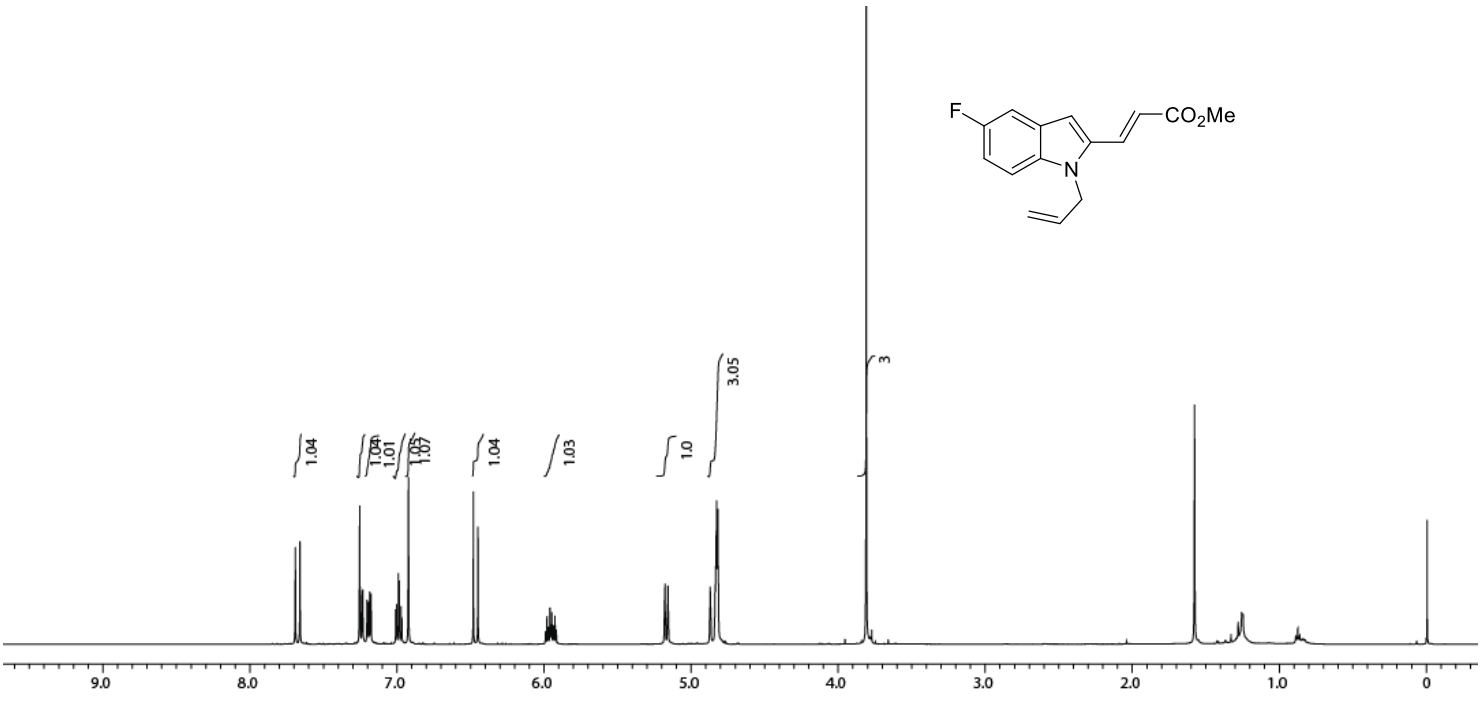

Figure S14. ^{1}H NMR spectrum of **1l** ($CDCl_3$, 500 MHz)

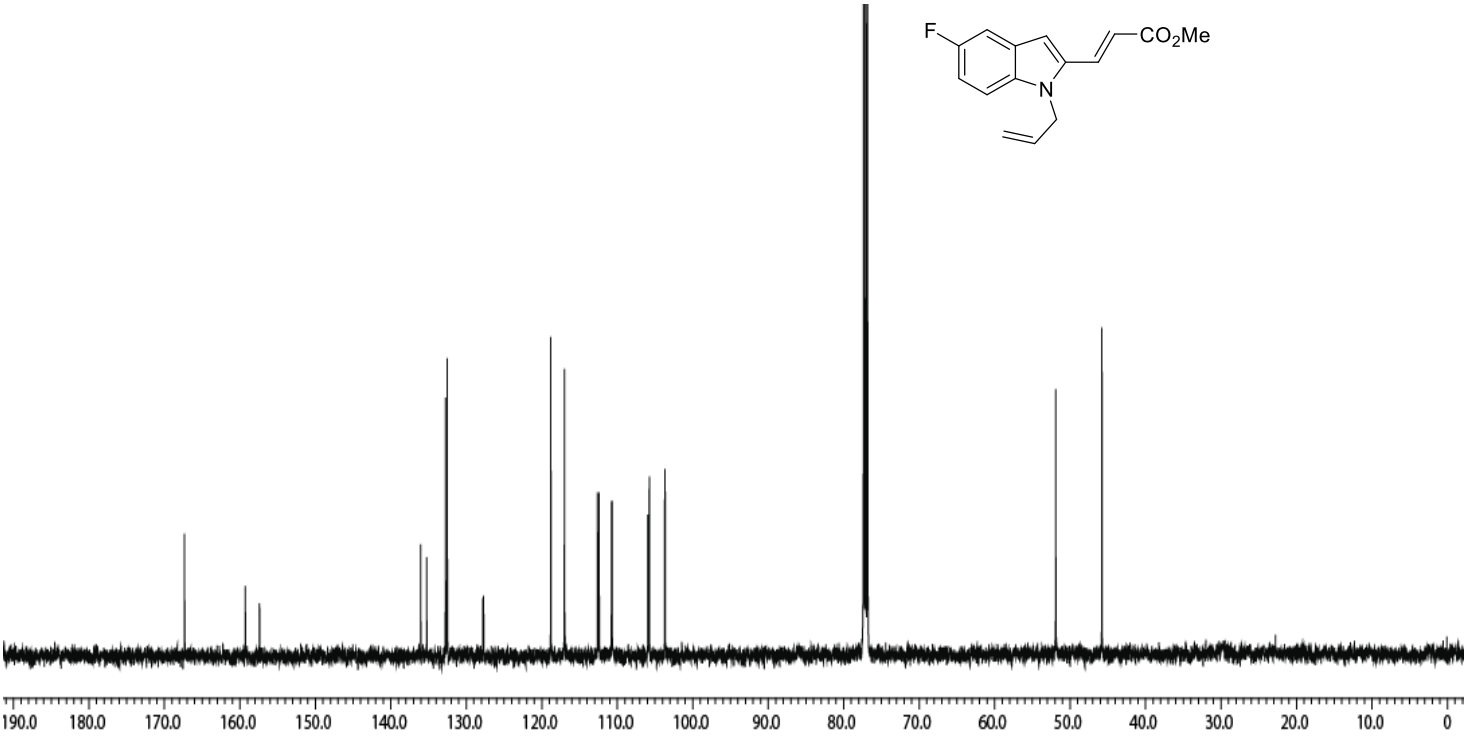

Figure S15. $^{13}C\{^{1}H\}$ NMR spectrum of **1l** ($CDCl_3$, 125 MHz)

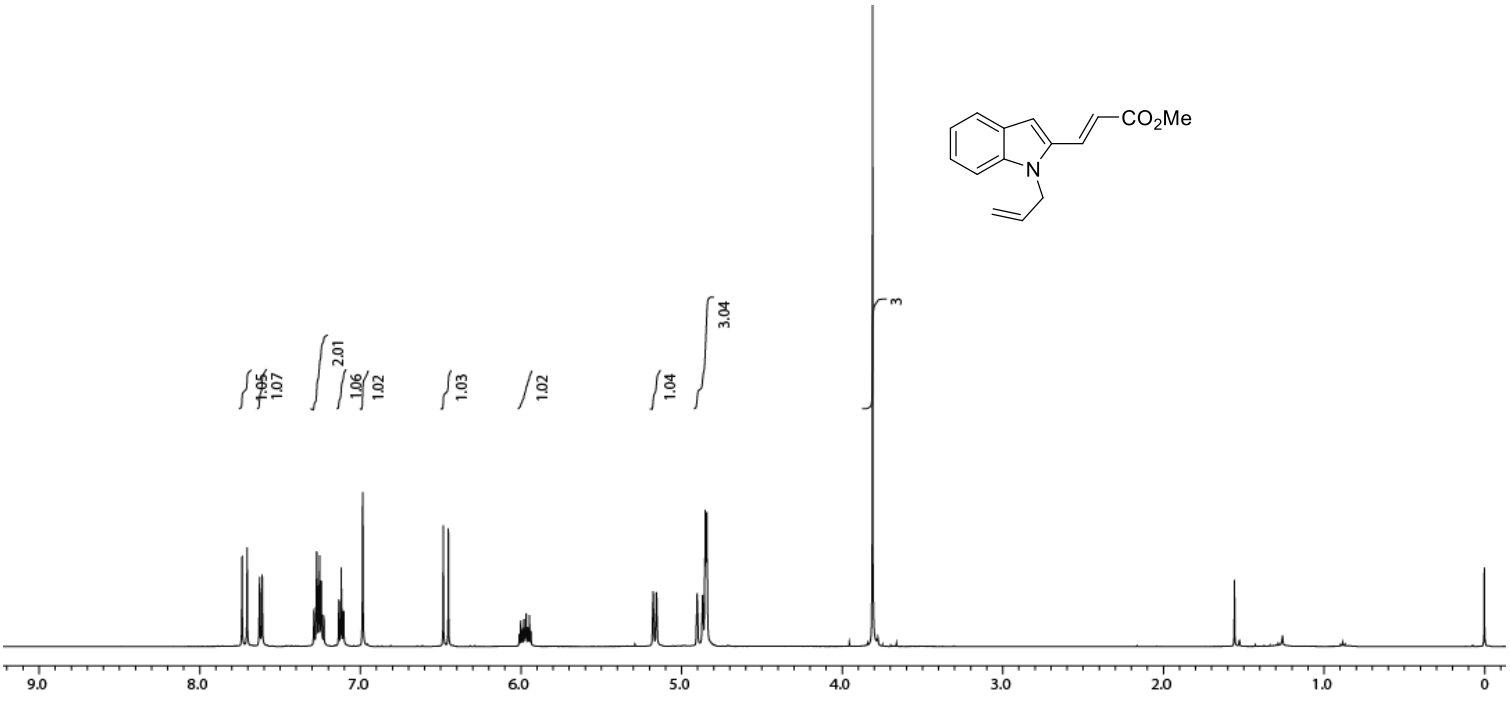

Figure S16. ^{1}H NMR spectrum of **1m** ($CDCl_3$, 500 MHz)

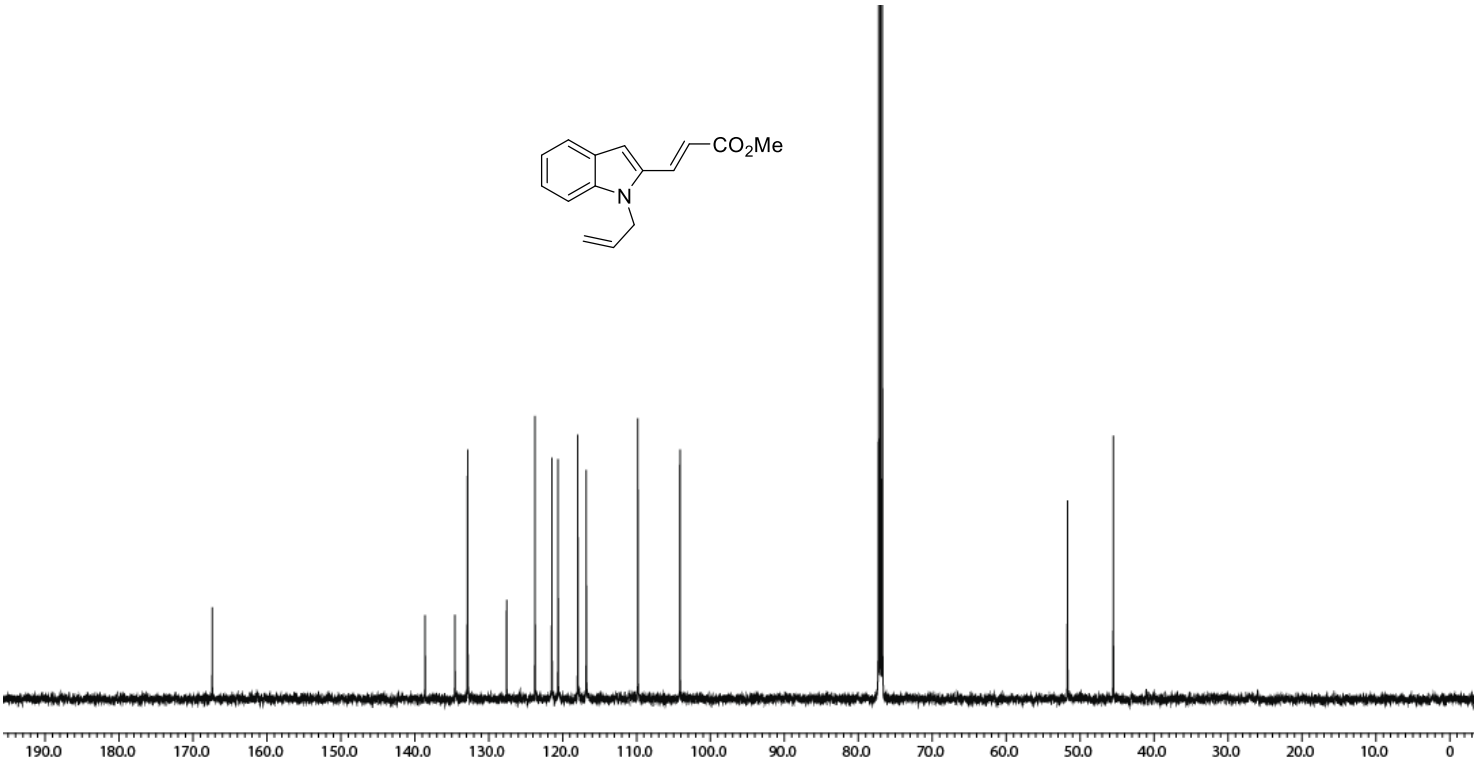

Figure S17. $^{13}C\{^{1}H\}$ NMR spectrum of **1m** ($CDCl_3$, 125 MHz)

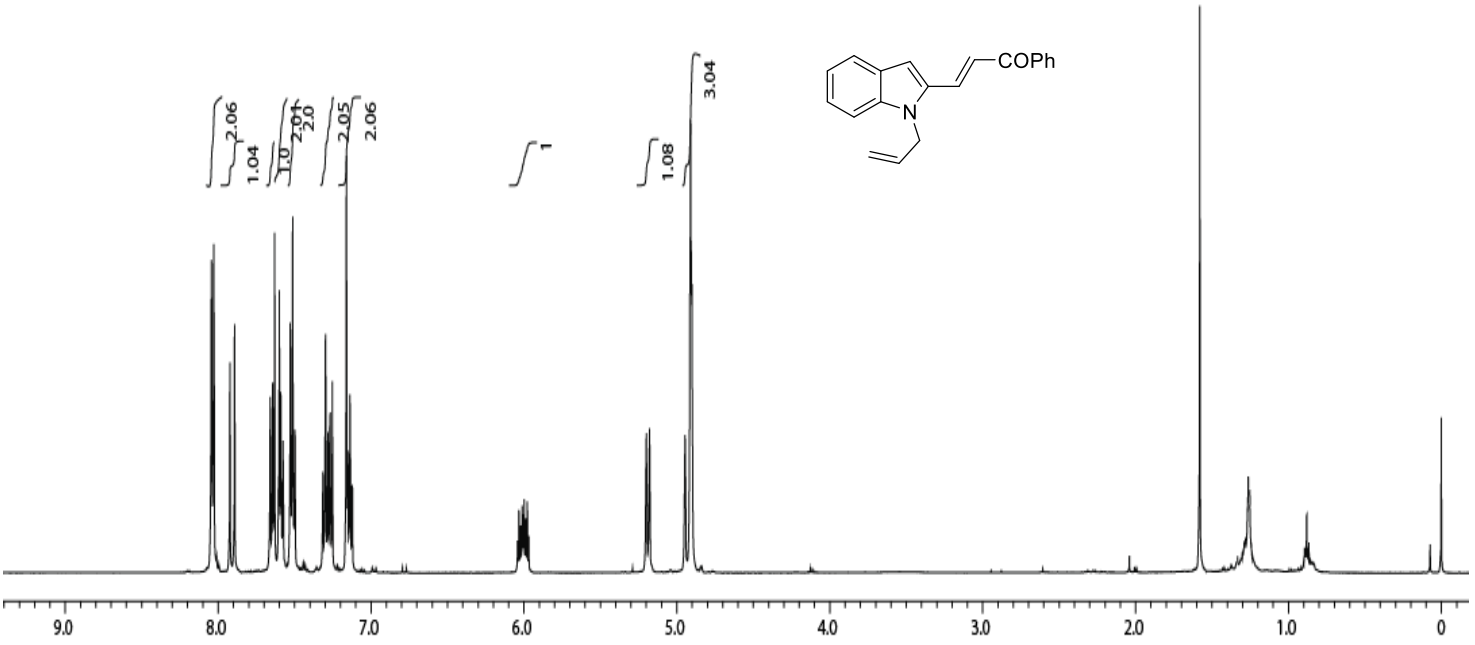

Figure S18. ^{1}H NMR spectrum of **1o** ($CDCl_3$, 500 MHz)

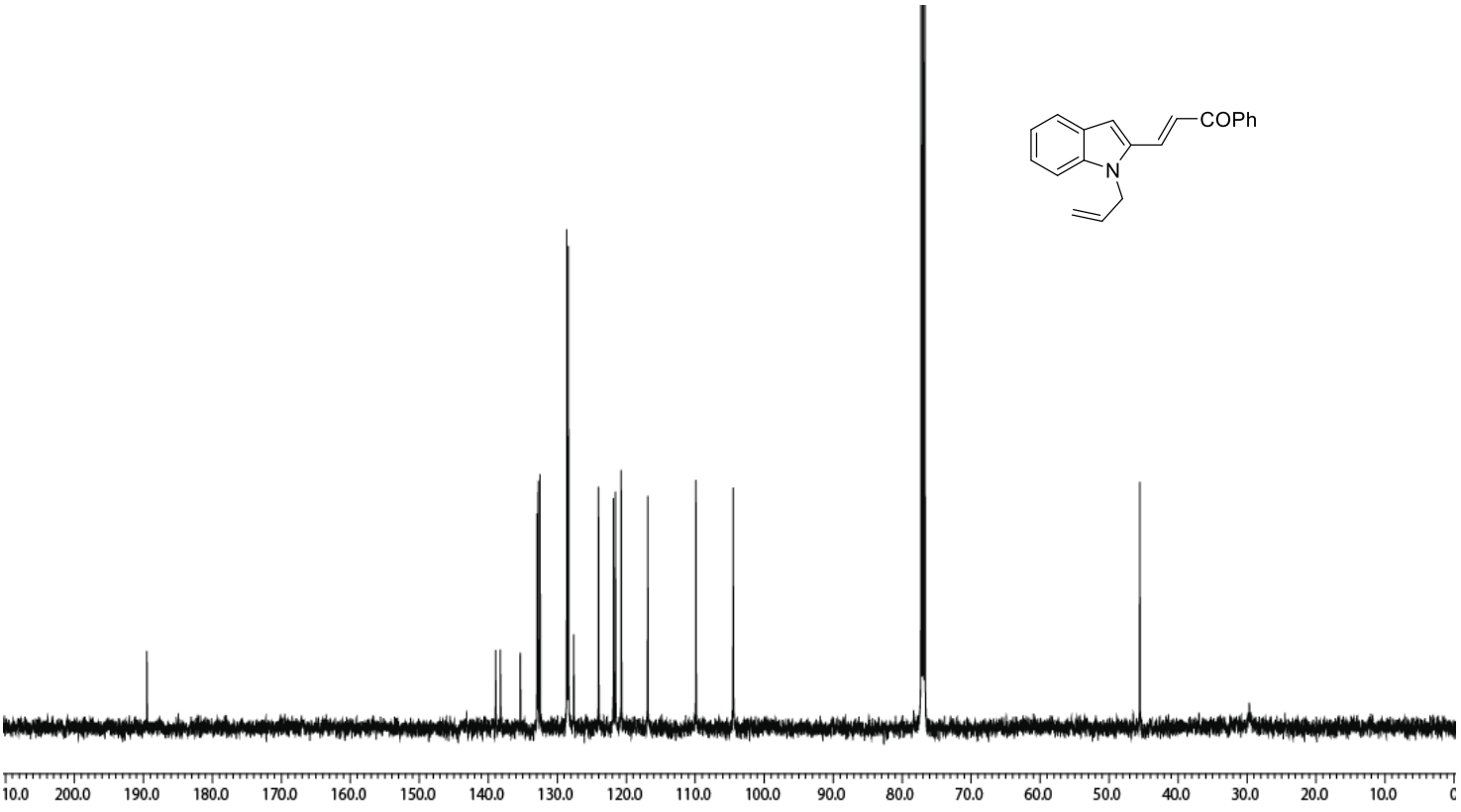

Figure S19. $^{13}C\{^{1}H\}$ NMR spectrum of **1o** ($CDCl_3$, 125 MHz)

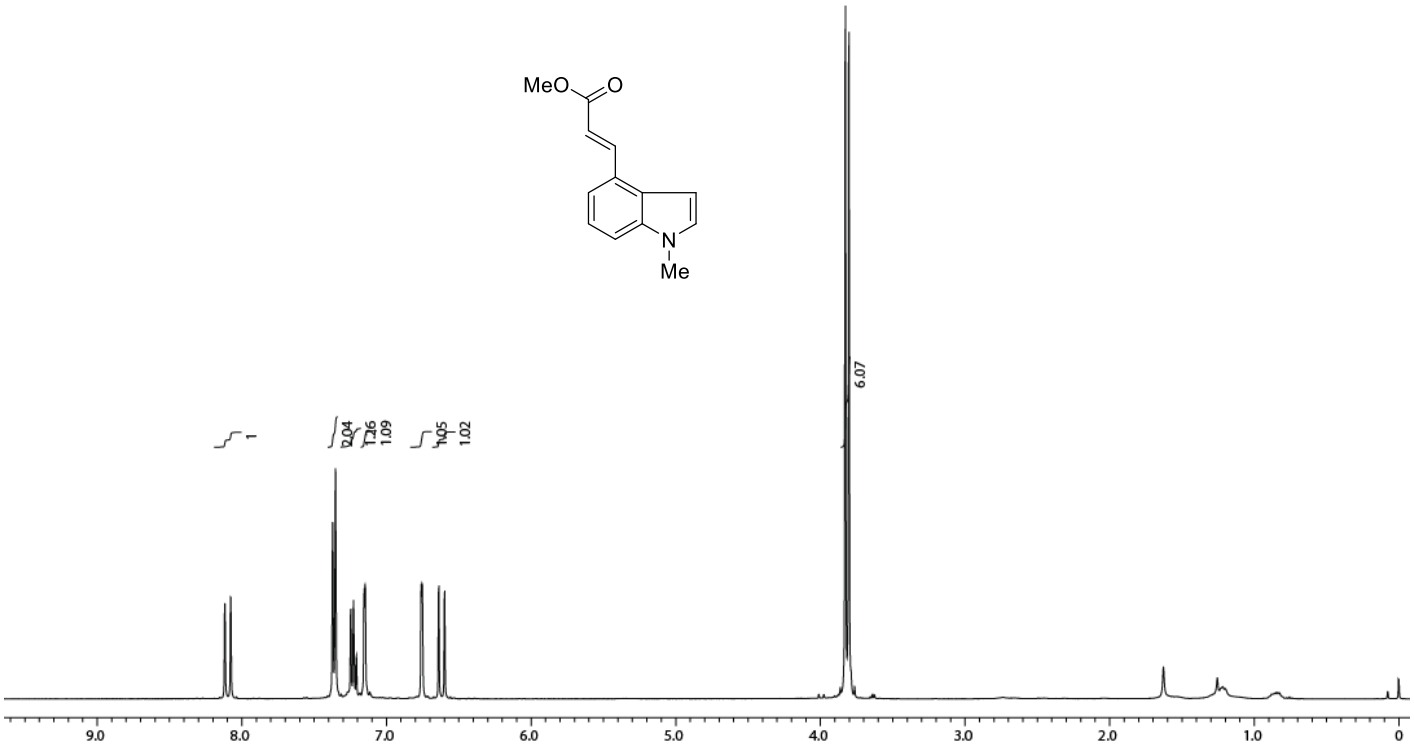

Figure S20. ^{1}H NMR spectrum of **4** ($CDCl_3$, 500 MHz)

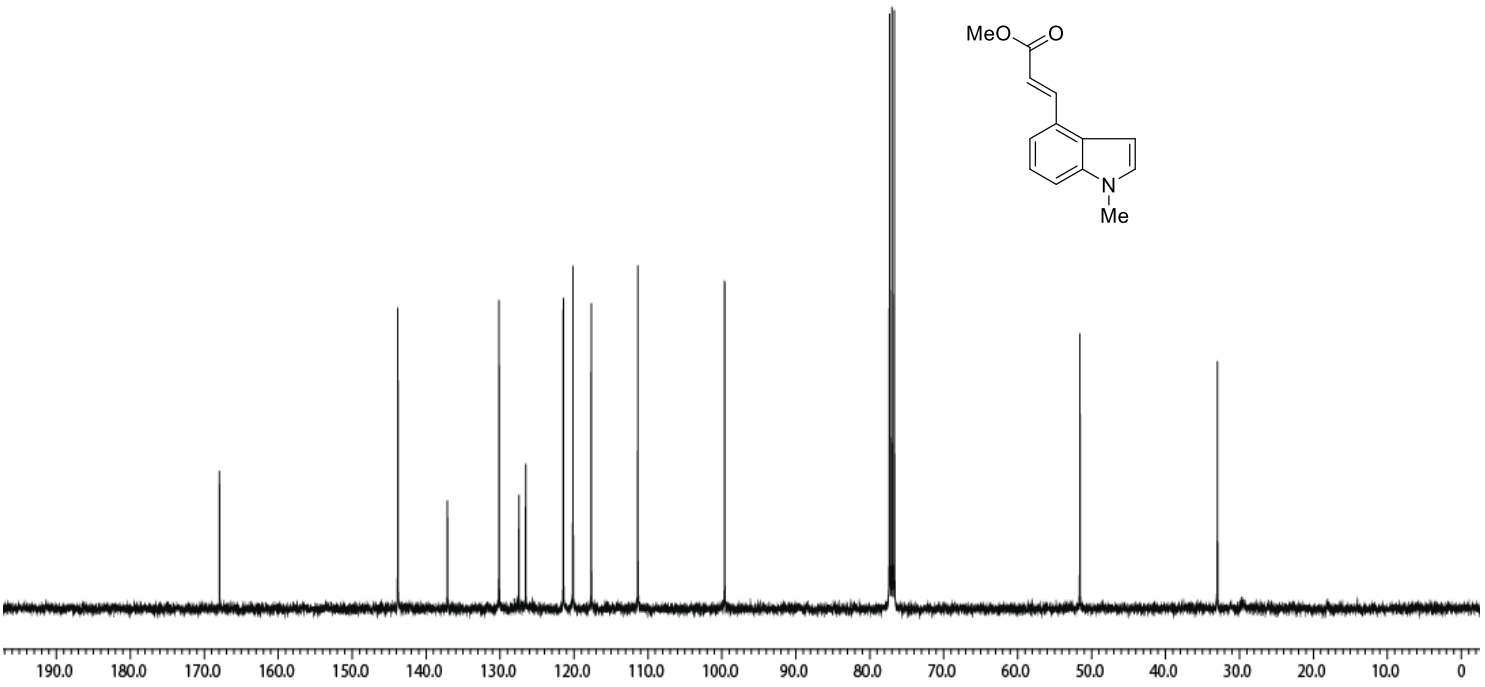

Figure S21. $^{13}C\{^{1}H\}$ NMR spectrum of **4** ($CDCl_3$, 125 MHz)

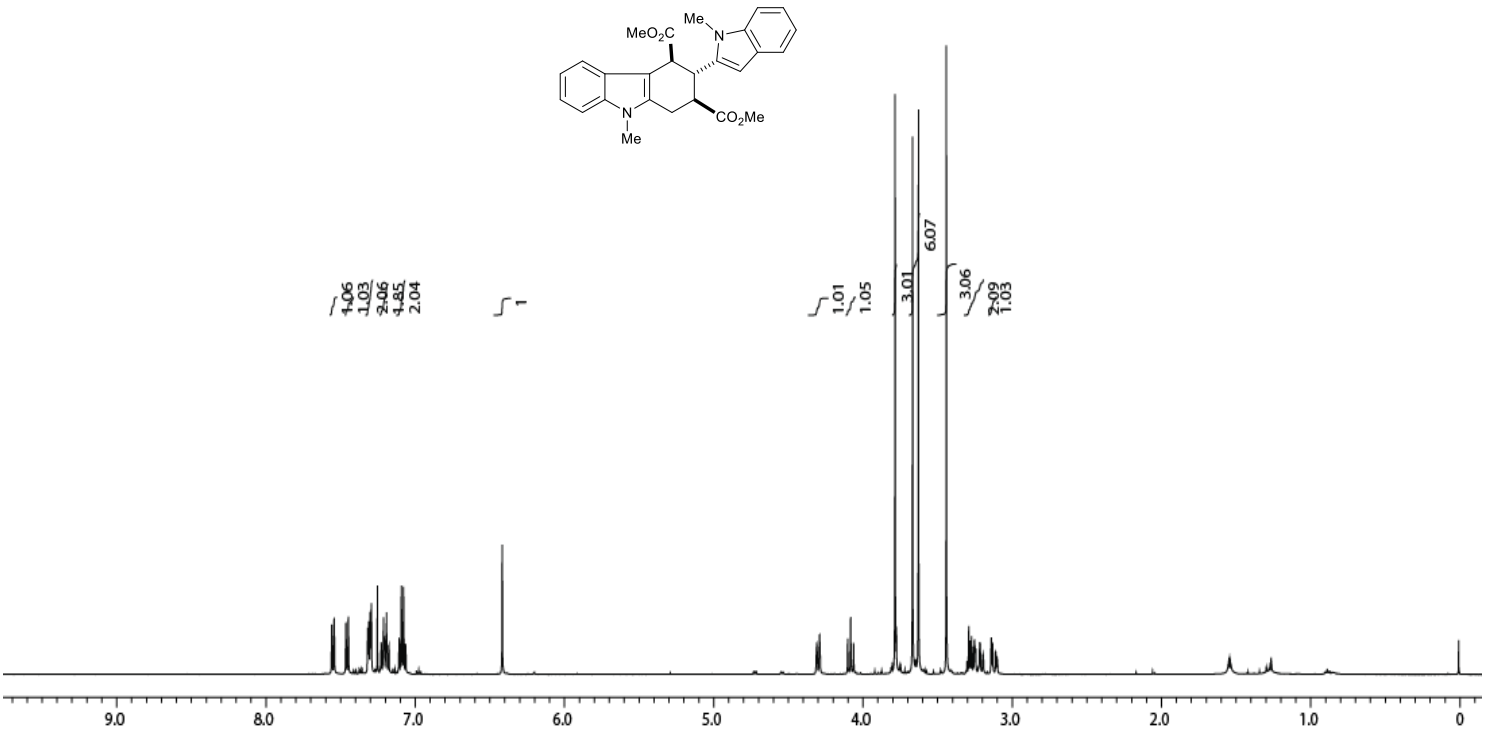

Figure S22. ^{1}H NMR spectrum of **2a** ($CDCl_3$, 500 MHz)

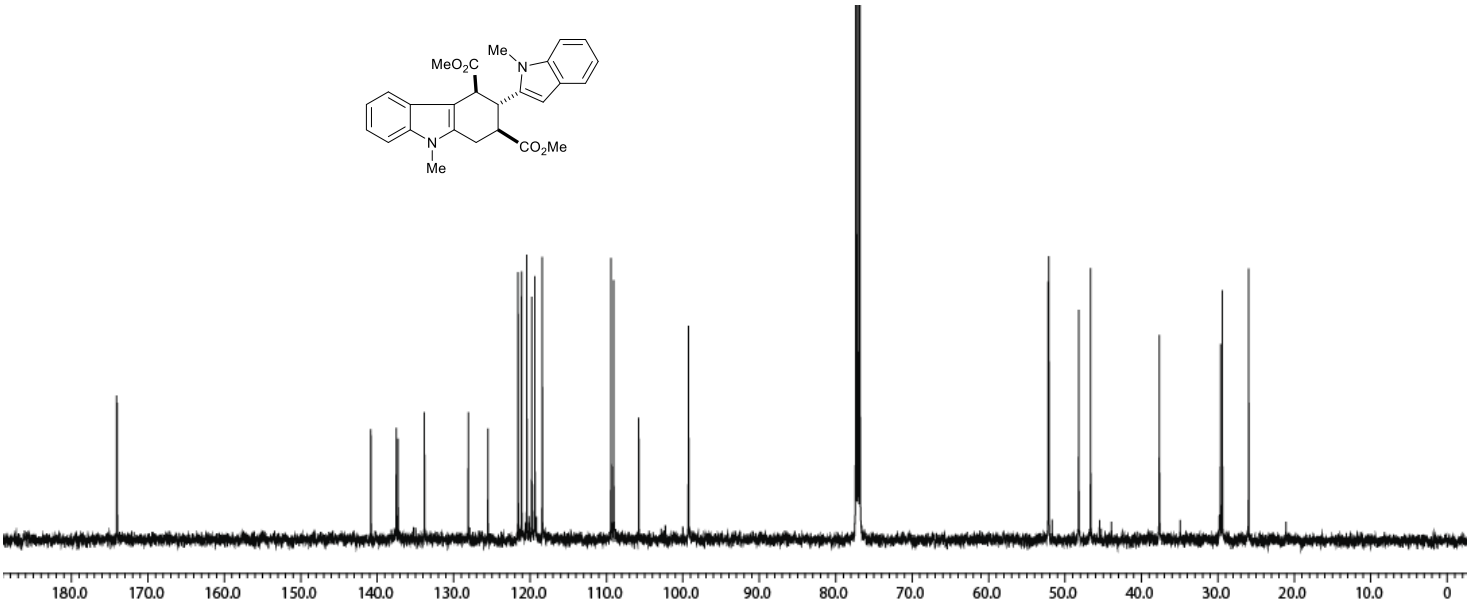

Figure S23. $^{13}C\{^{1}H\}$ NMR spectrum of **2a** ($CDCl_3$, 125 MHz)

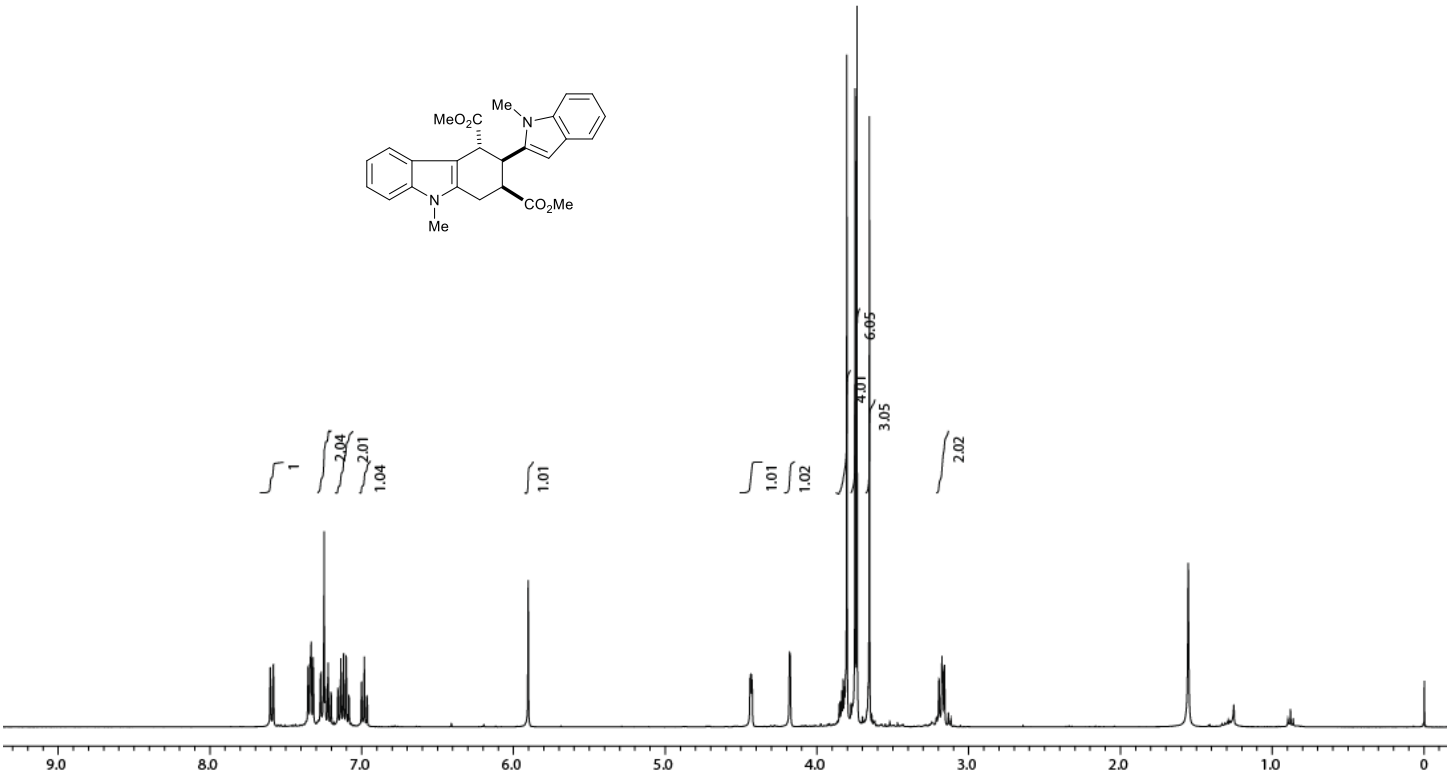

Figure S24. ^{1}H NMR spectrum of **2a** (minor diastereomer, $CDCl_3$, 500 MHz)

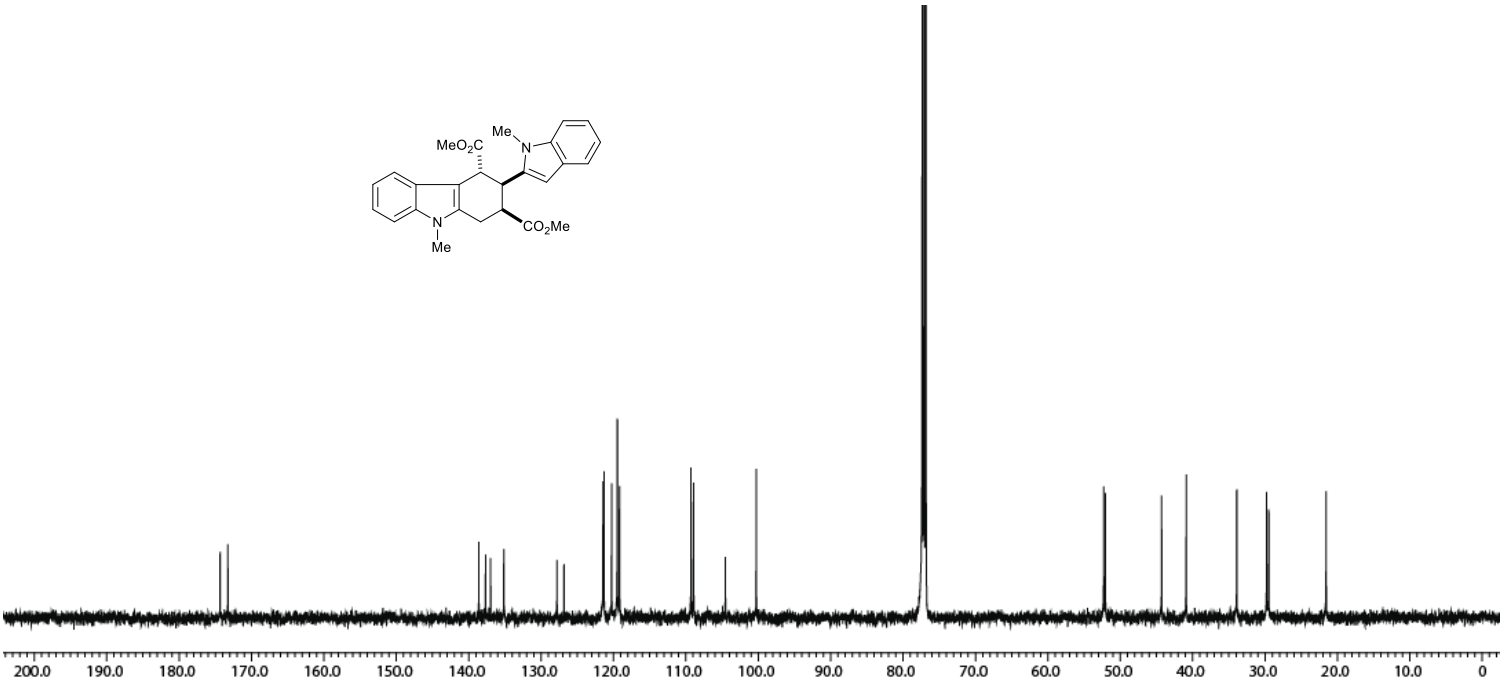

Figure S25. $^{13}C\{^{1}H\}$ NMR spectrum of **2a (**minor diastereomer, $CDCl_3$, 125 MHz)

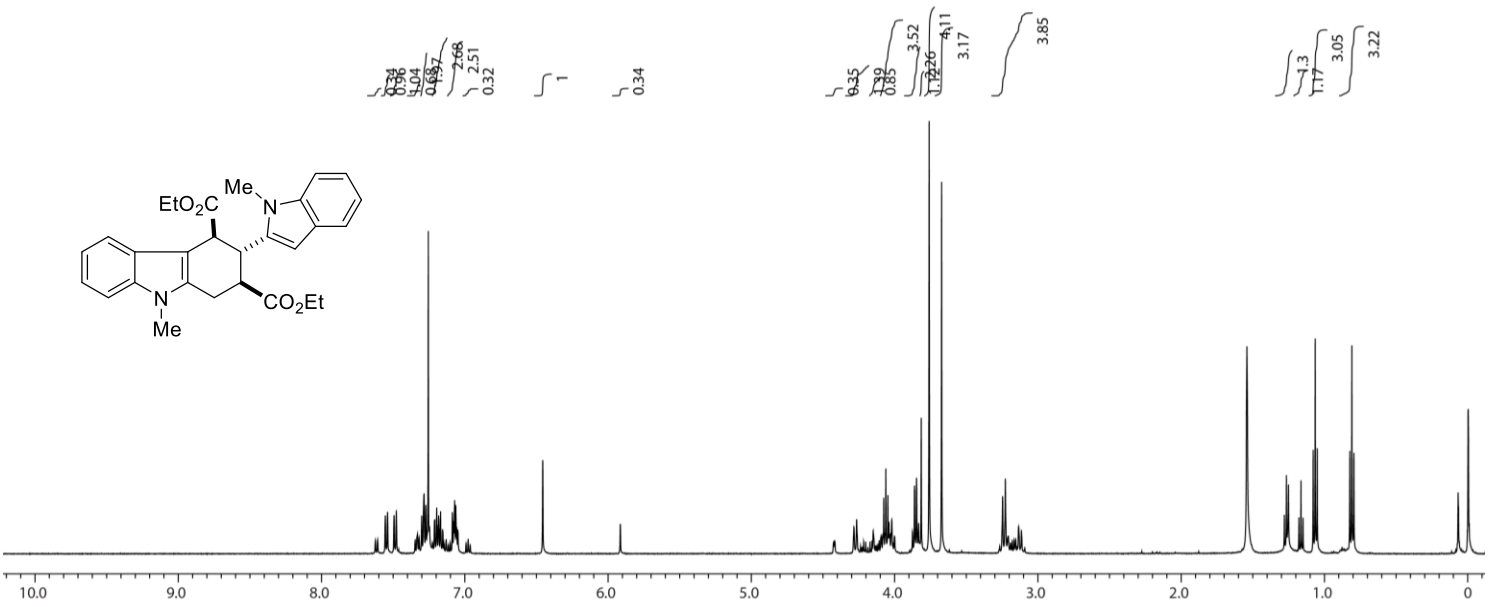

Figure S26. ^{1}H NMR spectrum of **2b** ($CDCl_3$, 500 MHz)

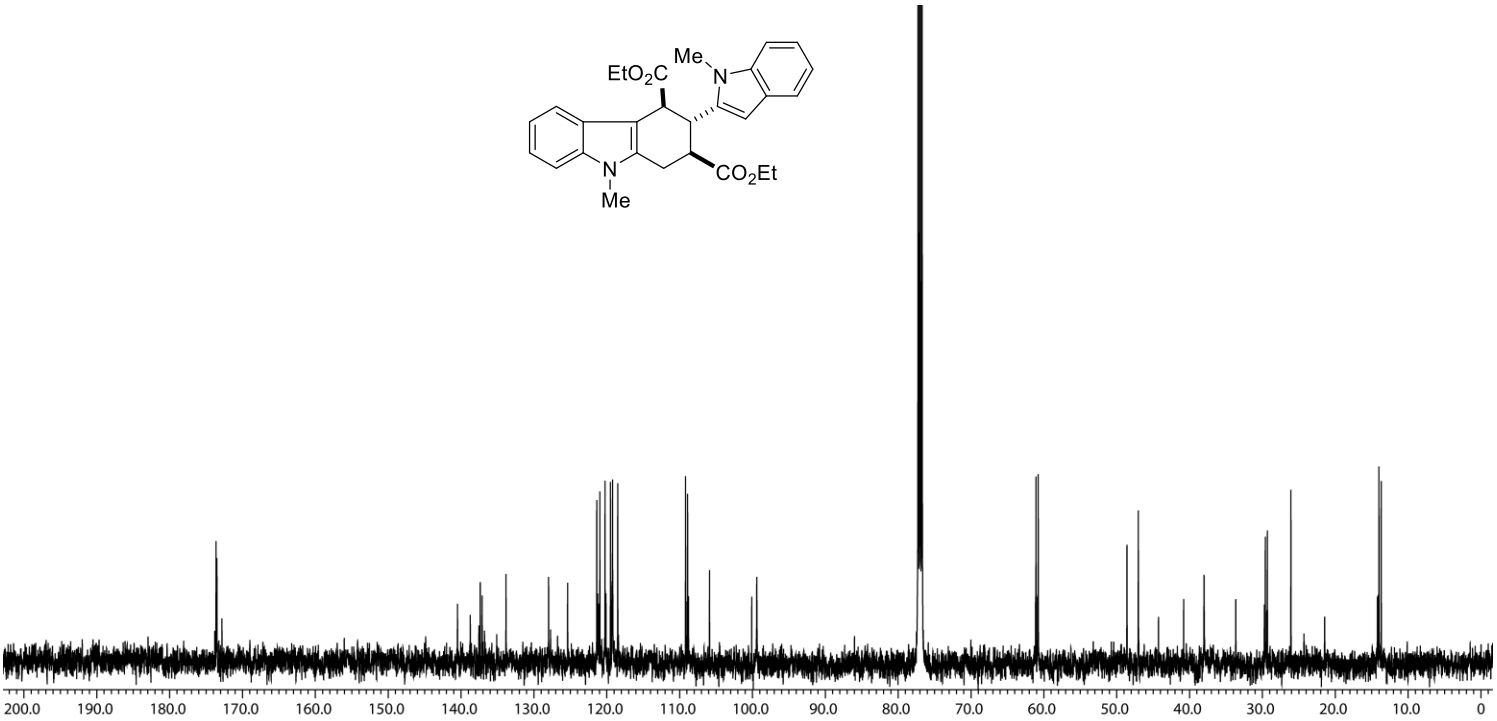

Figure S27. $^{13}C\{^{1}H\}$ NMR spectrum of **2b** ($CDCl_3$, 125 MHz)

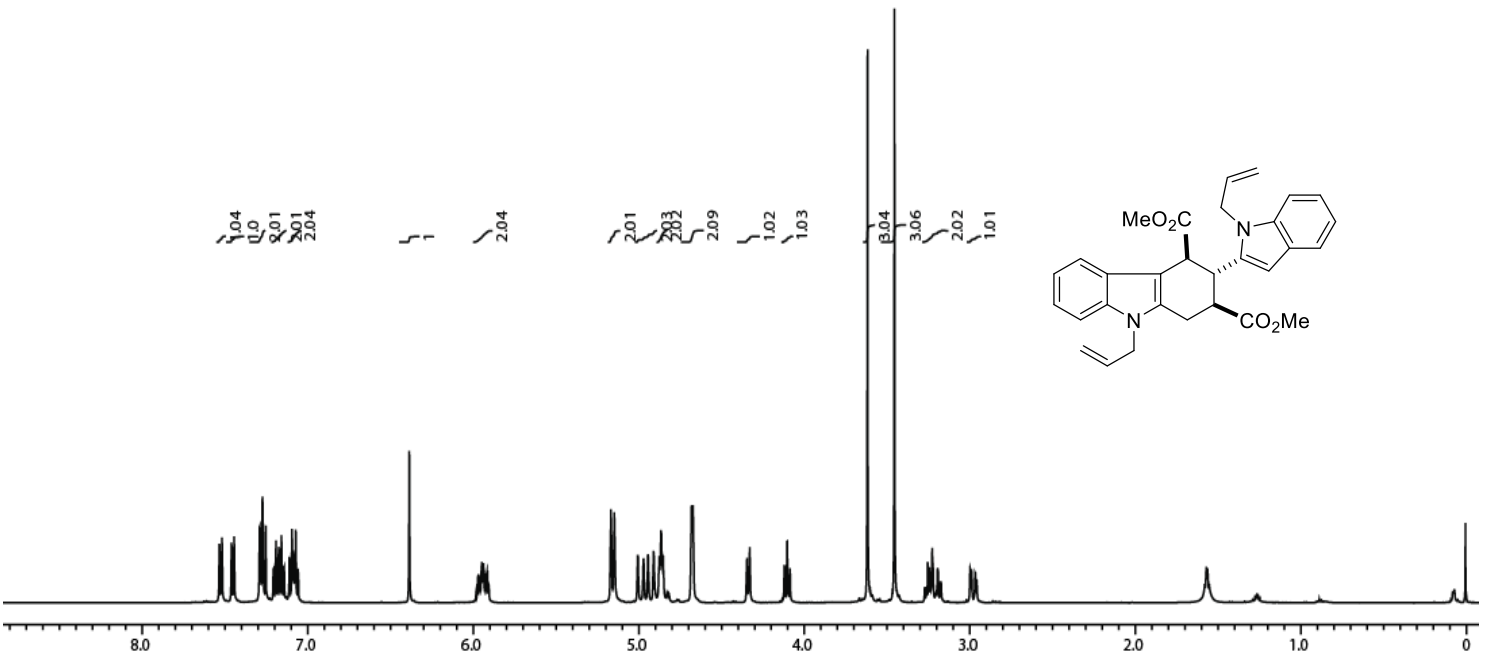

Figure S28. ^{1}H NMR spectrum of **2c** ($CDCl_3$, 500 MHz)

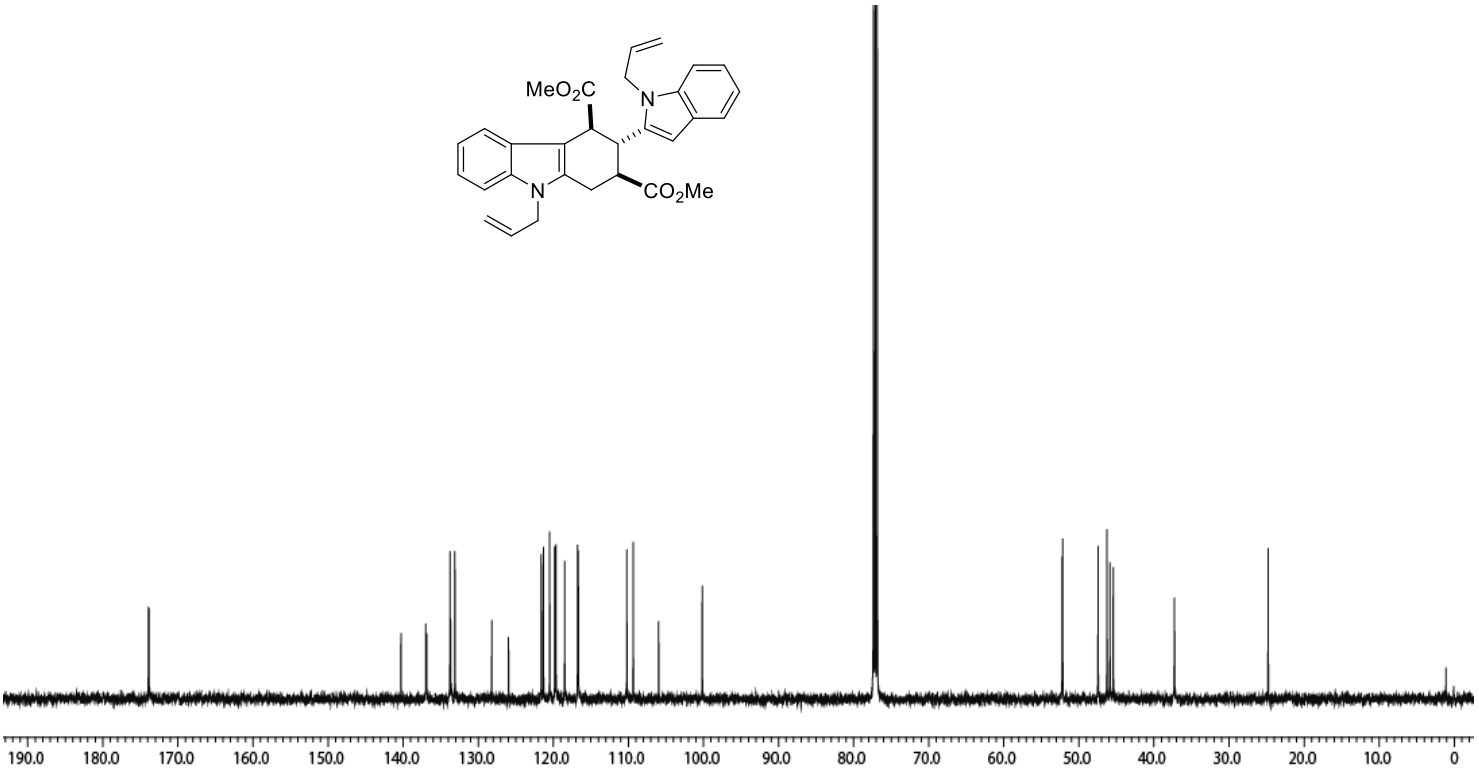

Figure S29. $^{13}C\{^{1}H\}$ NMR spectrum of **2c** ($CDCl_3$, 125 MHz)

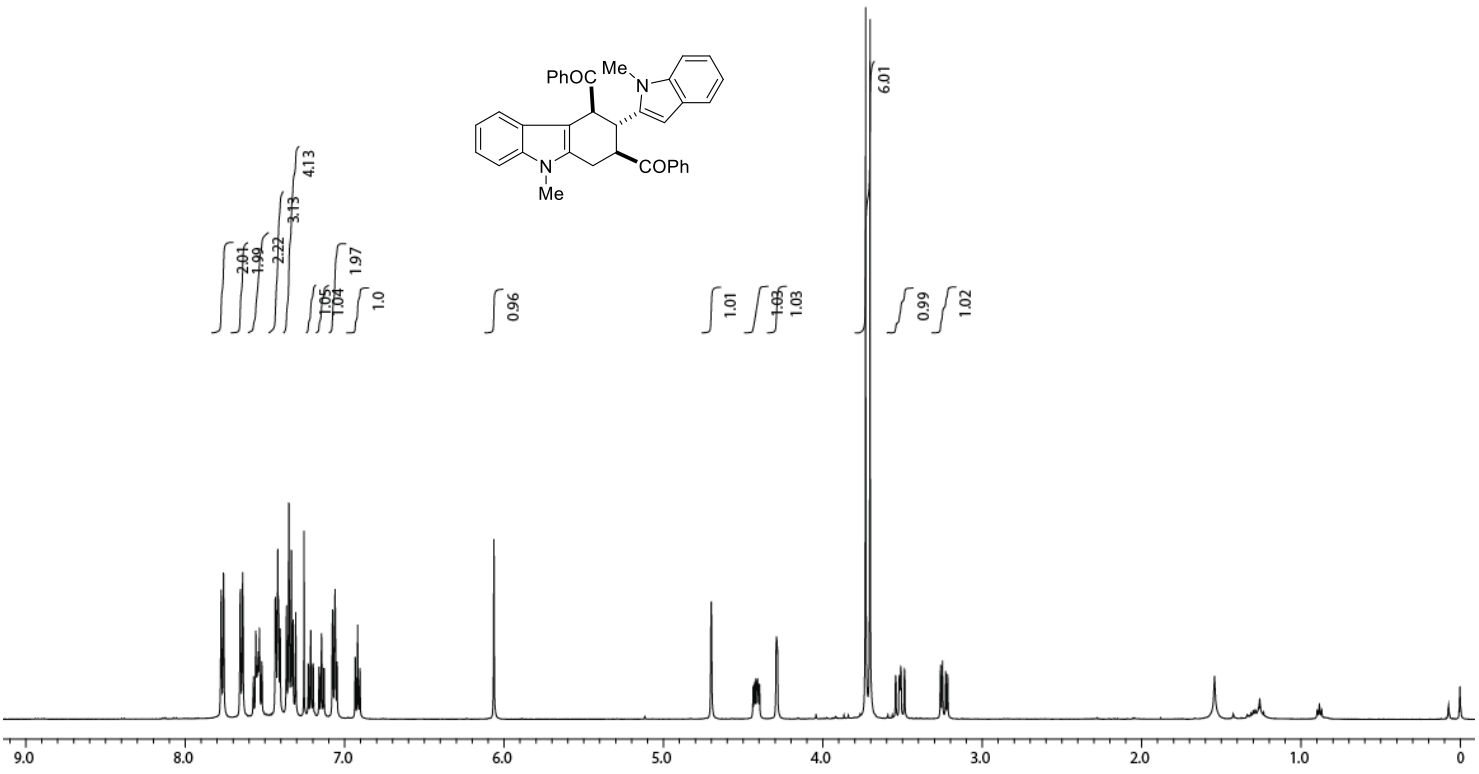

Figure S30. ^{1}H NMR spectrum of **2d** ($CDCl_3$, 500 MHz)

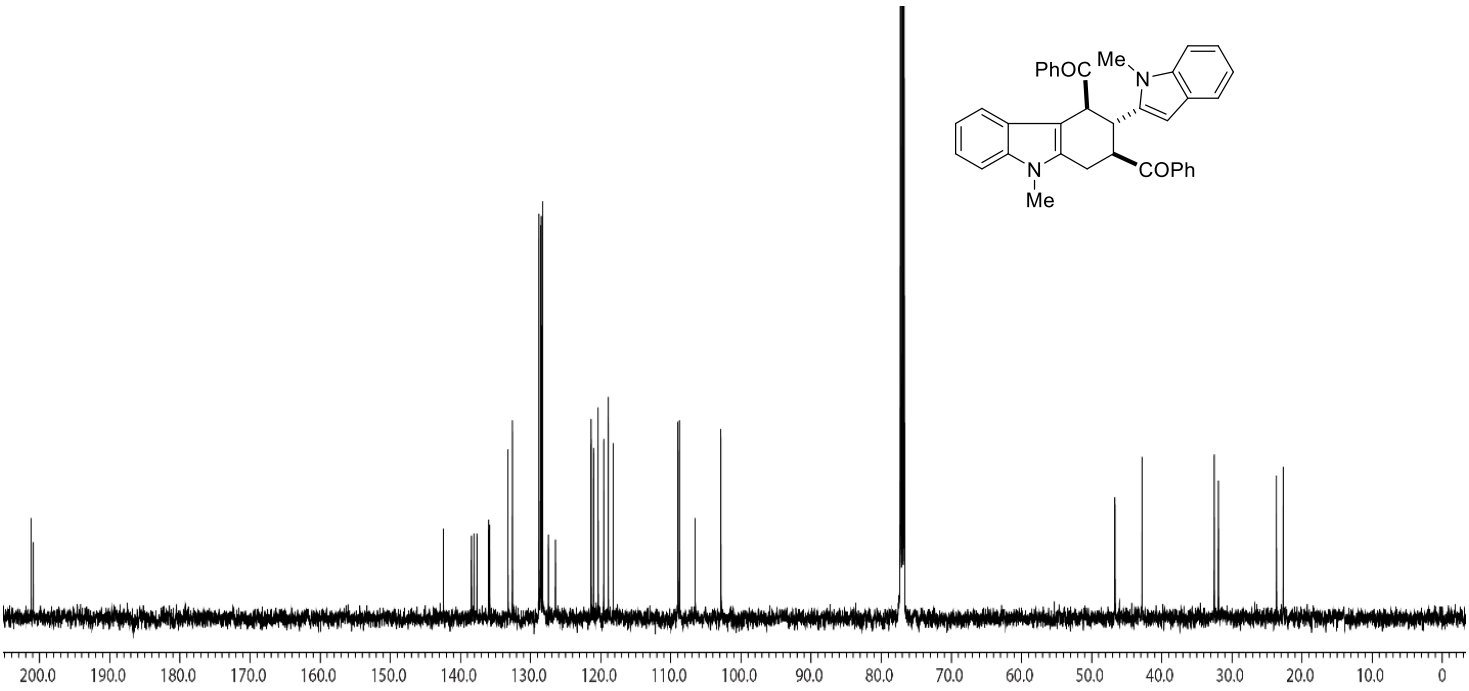

Figure S31. $^{13}C\{^{1}H\}$ NMR spectrum of **2d** ($CDCl_3$, 125 MHz)

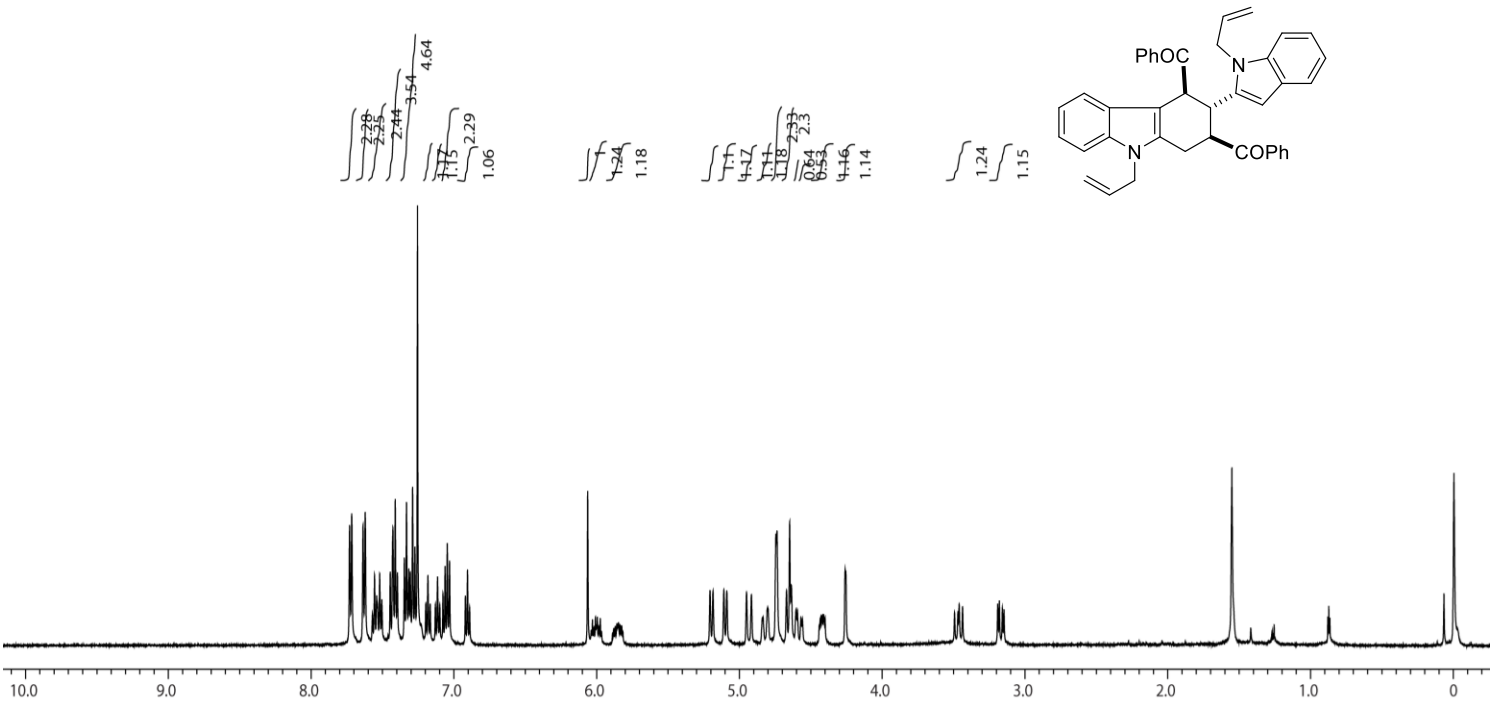

Figure S32. ^{1}H NMR spectrum of **2e** ($CDCl_3$, 500 MHz)

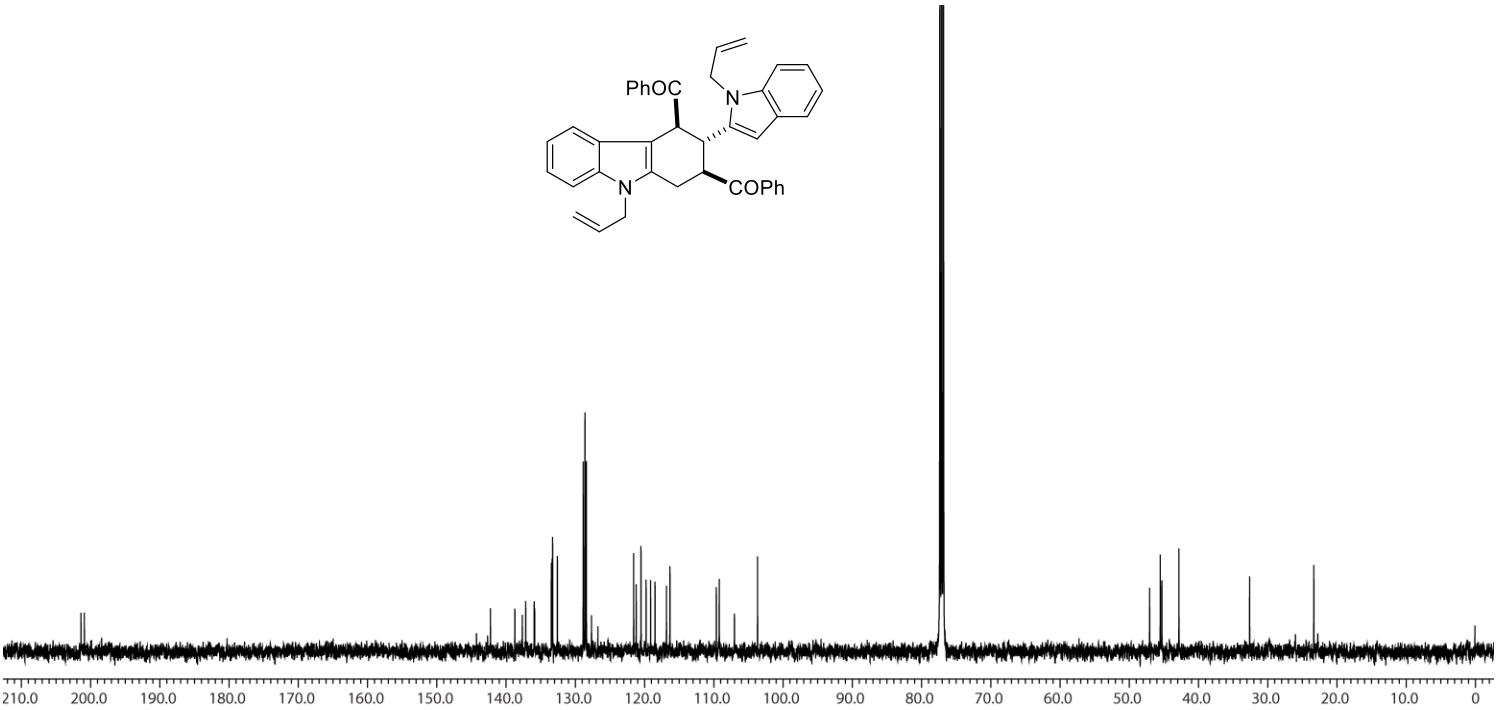

Figure S33. $^{13}C\{^{1}H\}$ NMR spectrum of **2e** ($CDCl_3$, 125 MHz)

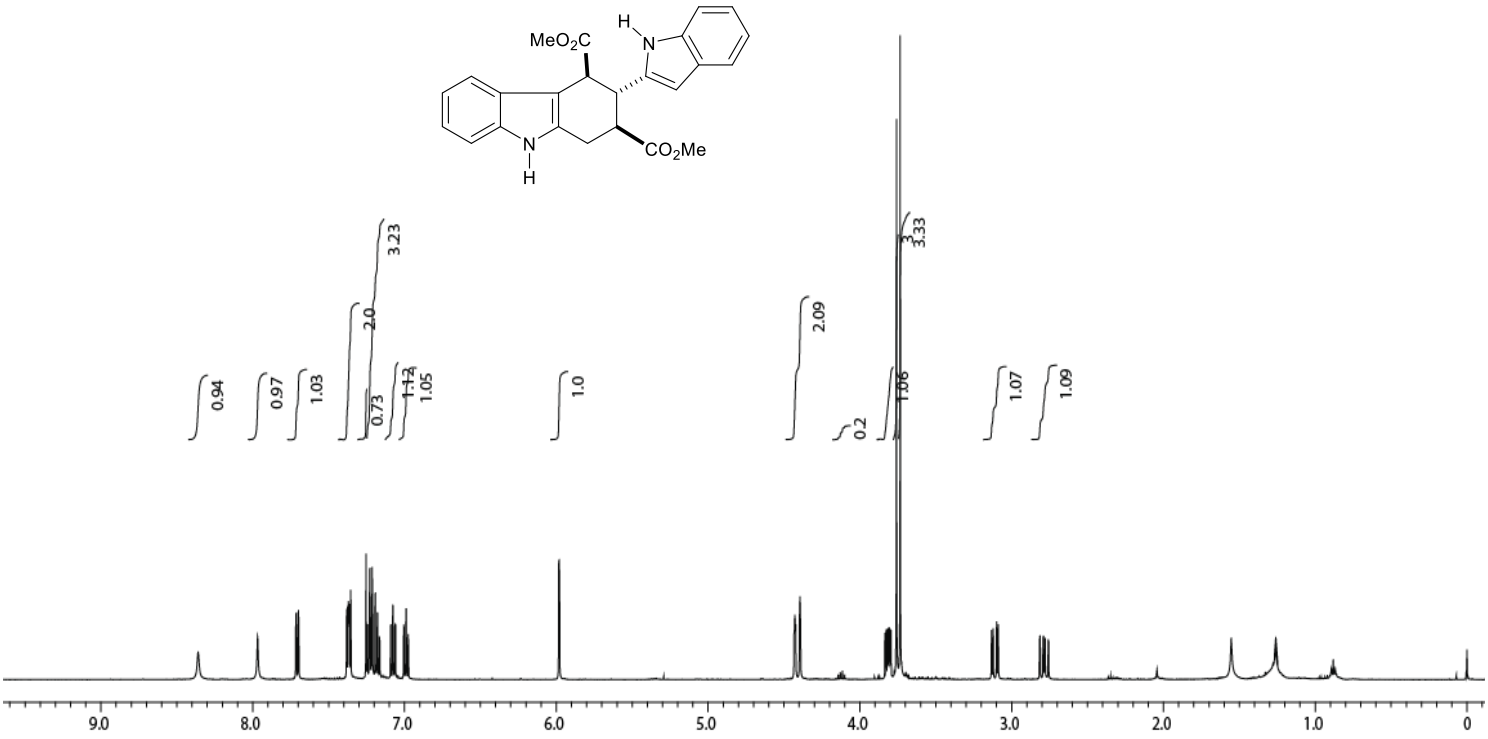

Figure S34. ^{1}H NMR spectrum of **2f** ($CDCl_3$, 500 MHz)

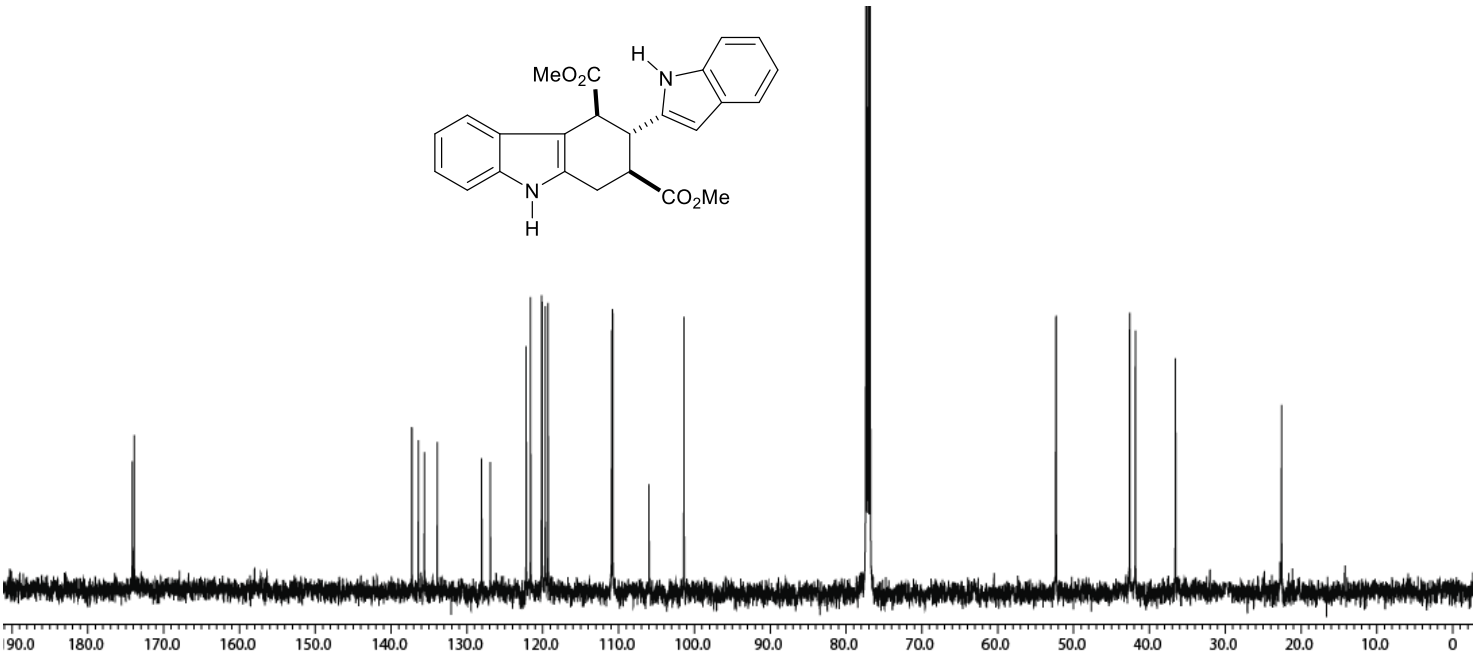

Figure S35. $^{13}C\{^{1}H\}$ NMR spectrum of **2f** ($CDCl_3$, 125 MHz)

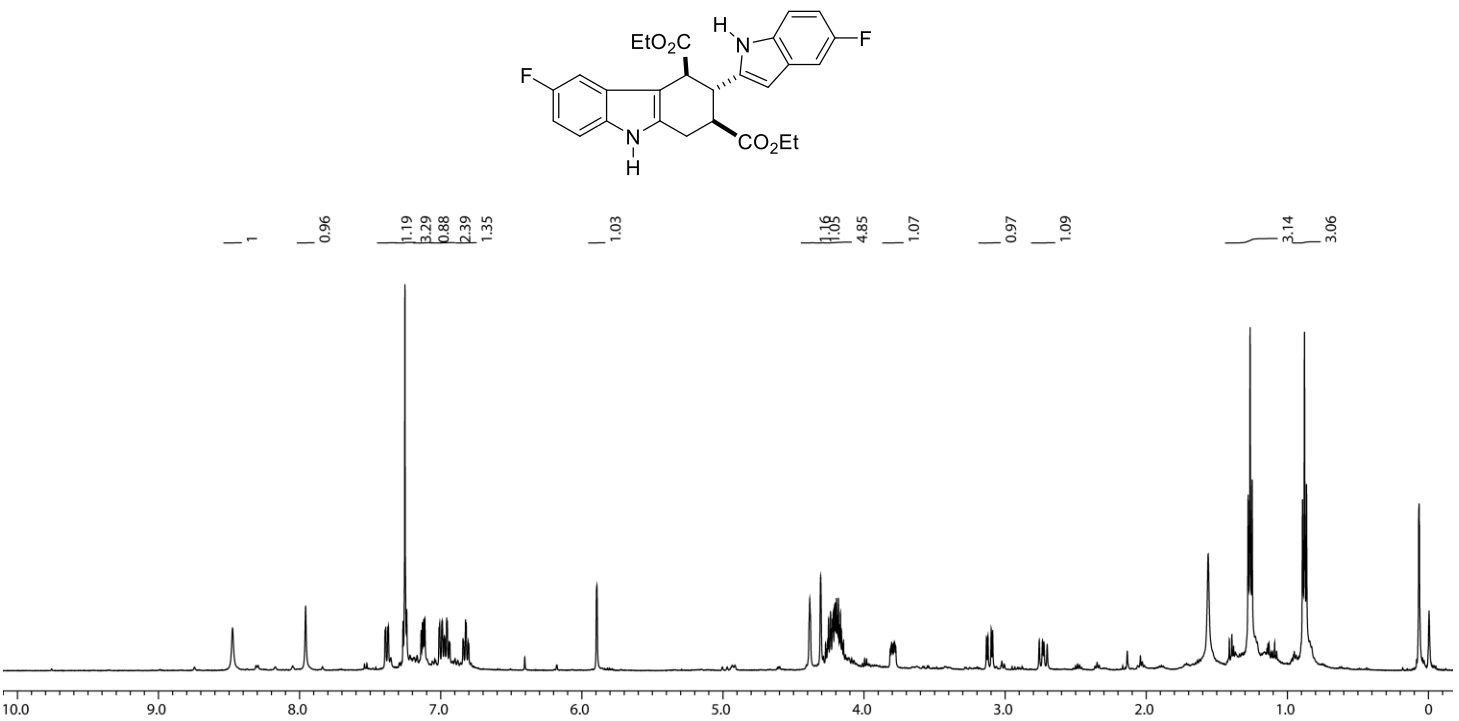

Figure S36. ^{1}H NMR spectrum of **2g** ($CDCl_3$, 500 MHz)

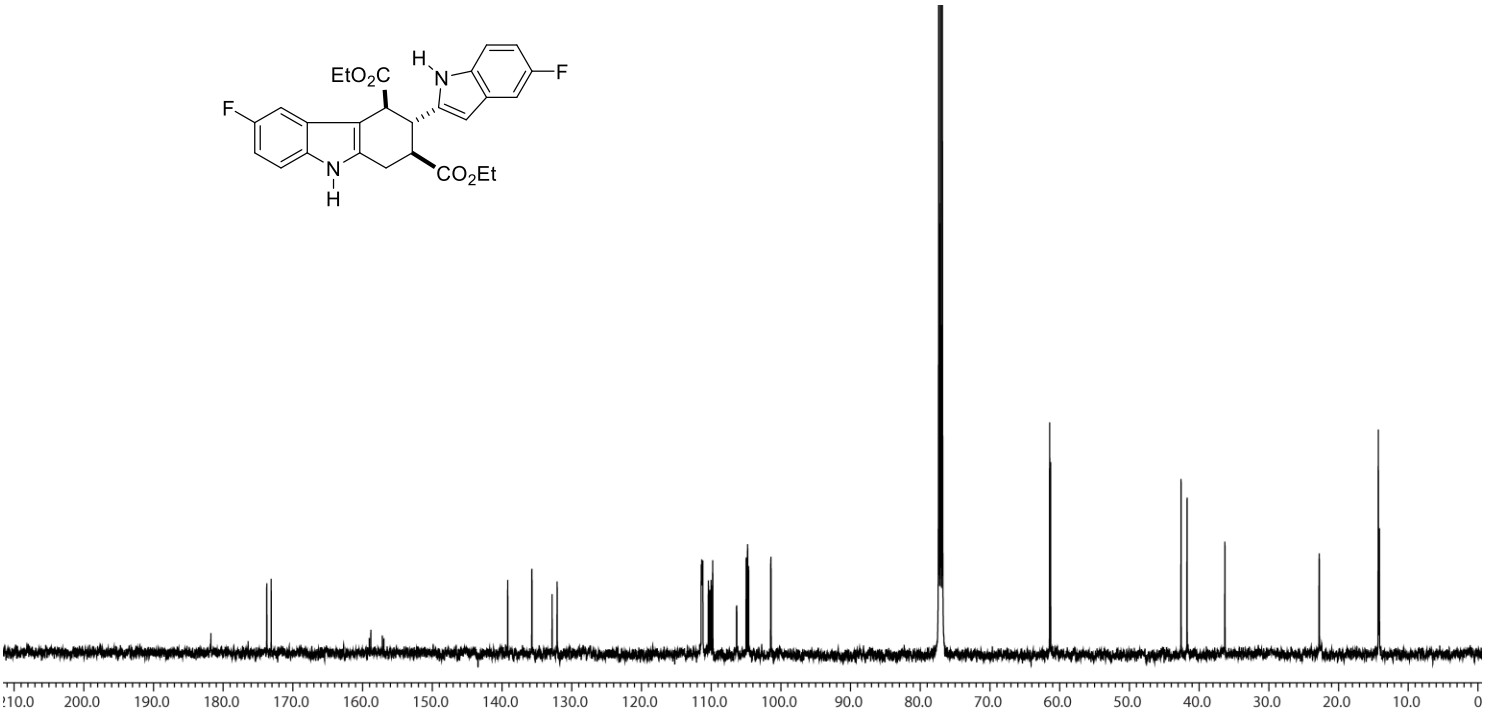

Figure S37. $^{13}C\{^{1}H\}$ NMR spectrum of **2g** ($CDCl_3$, 125 MHz)

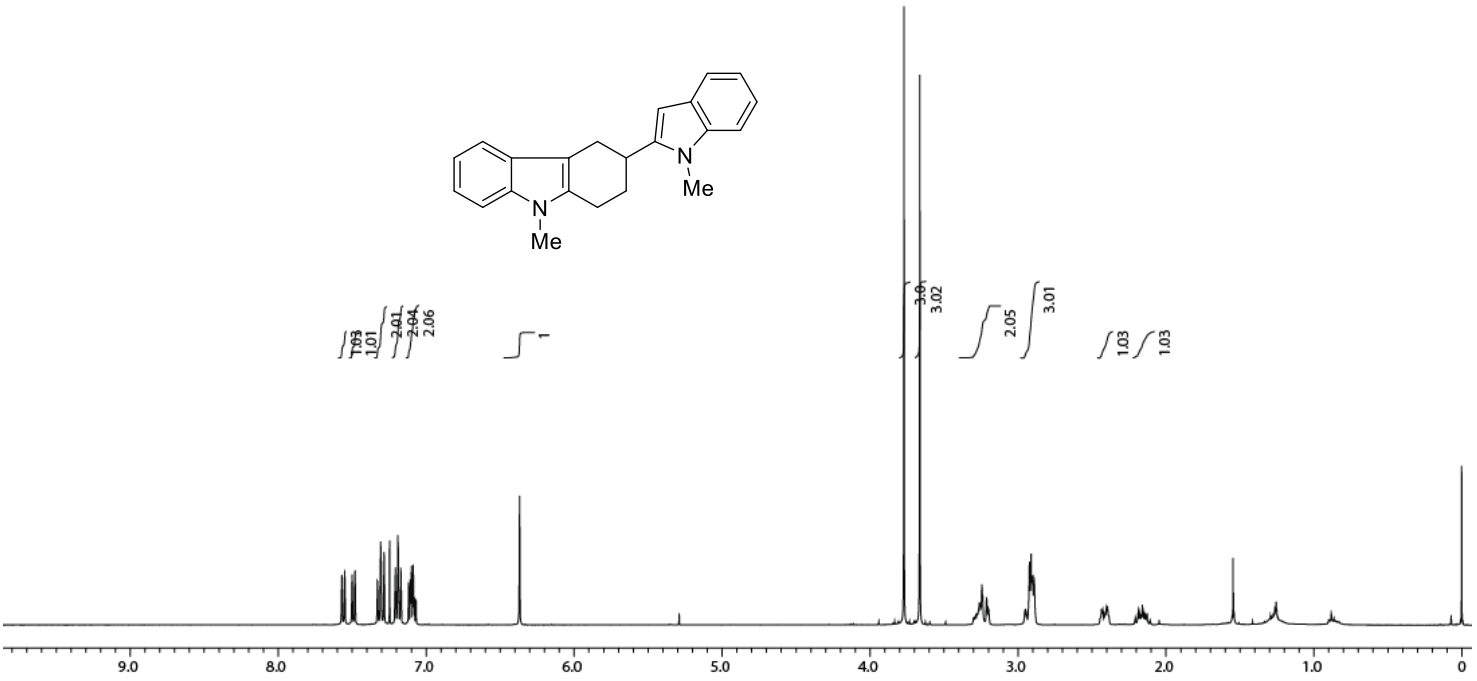

Figure S38. ^{1}H NMR spectrum of **2i** ($CDCl_3$, 500 MHz)

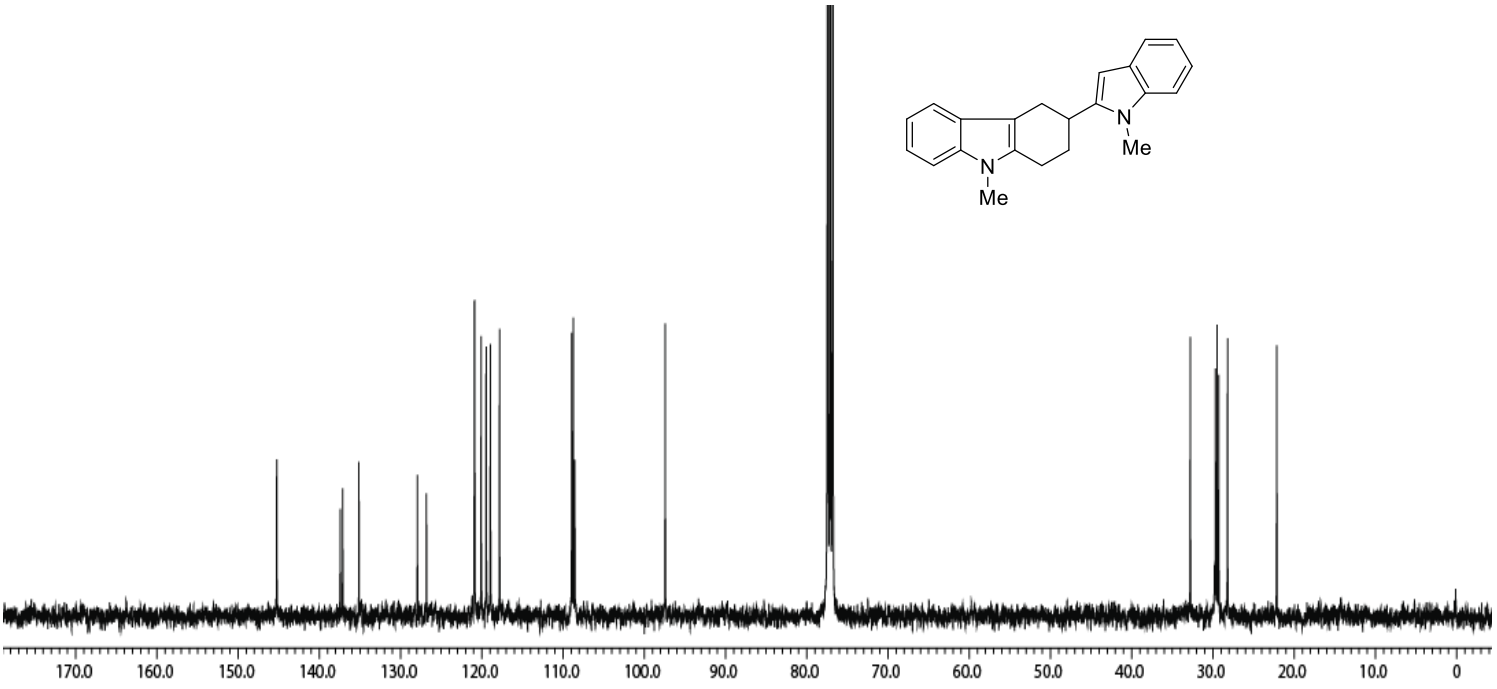

Figure S39. $^{13}C\{^{1}H\}$ NMR spectrum of **2i** ($CDCl_3$, 125 MHz)

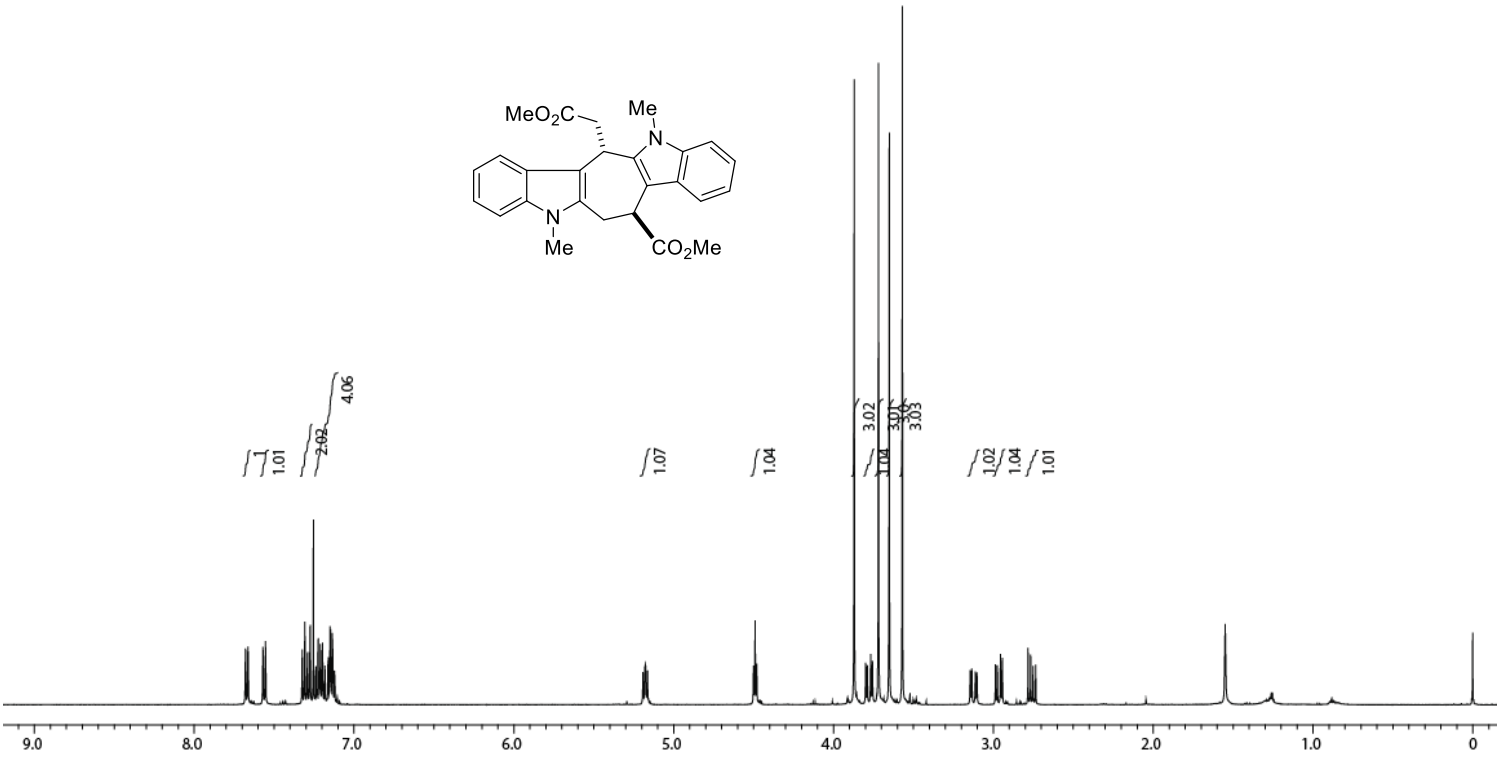

Figure S40. ^{1}H NMR spectrum of **3a** ($CDCl_3$, 500 MHz)

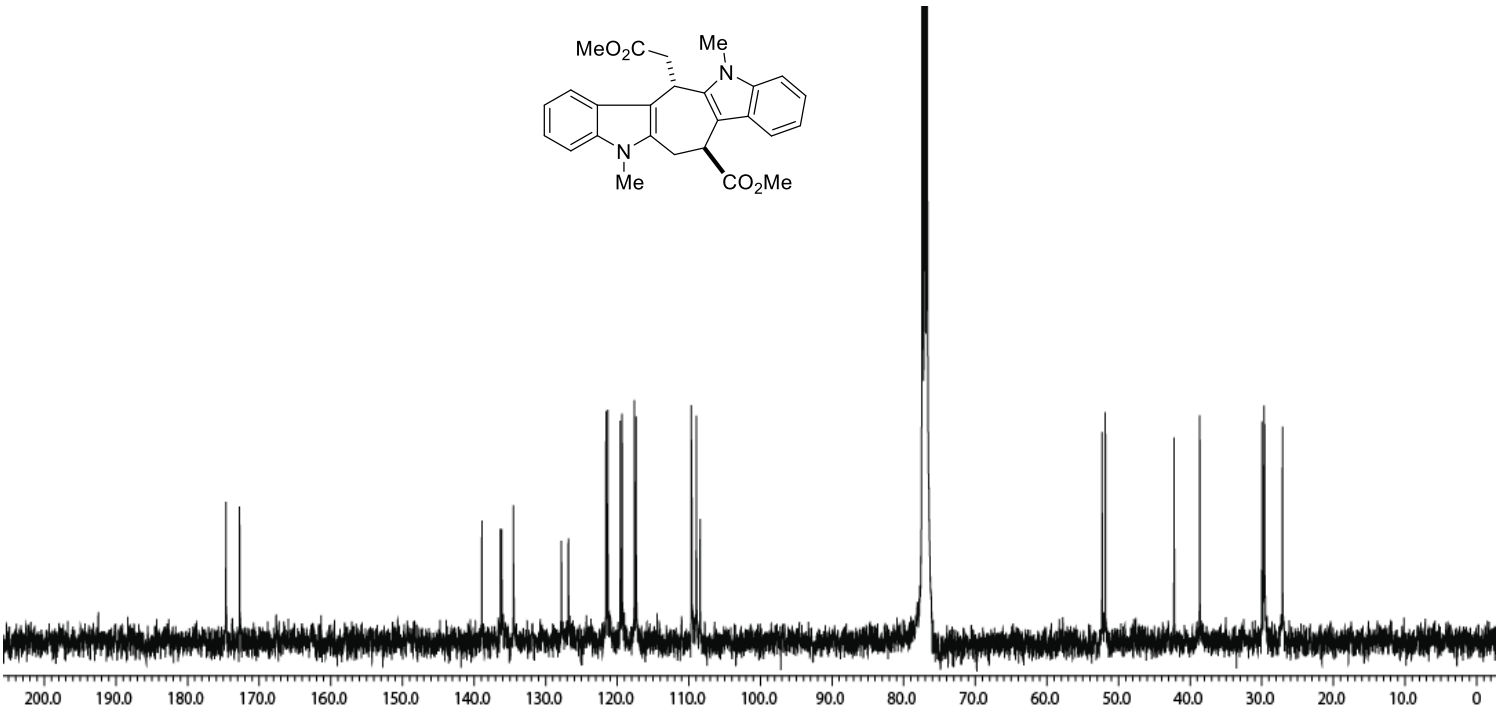

Figure S41. $^{13}C\{^{1}H\}$ NMR spectrum of **3a** ($CDCl_3$, 125 MHz)

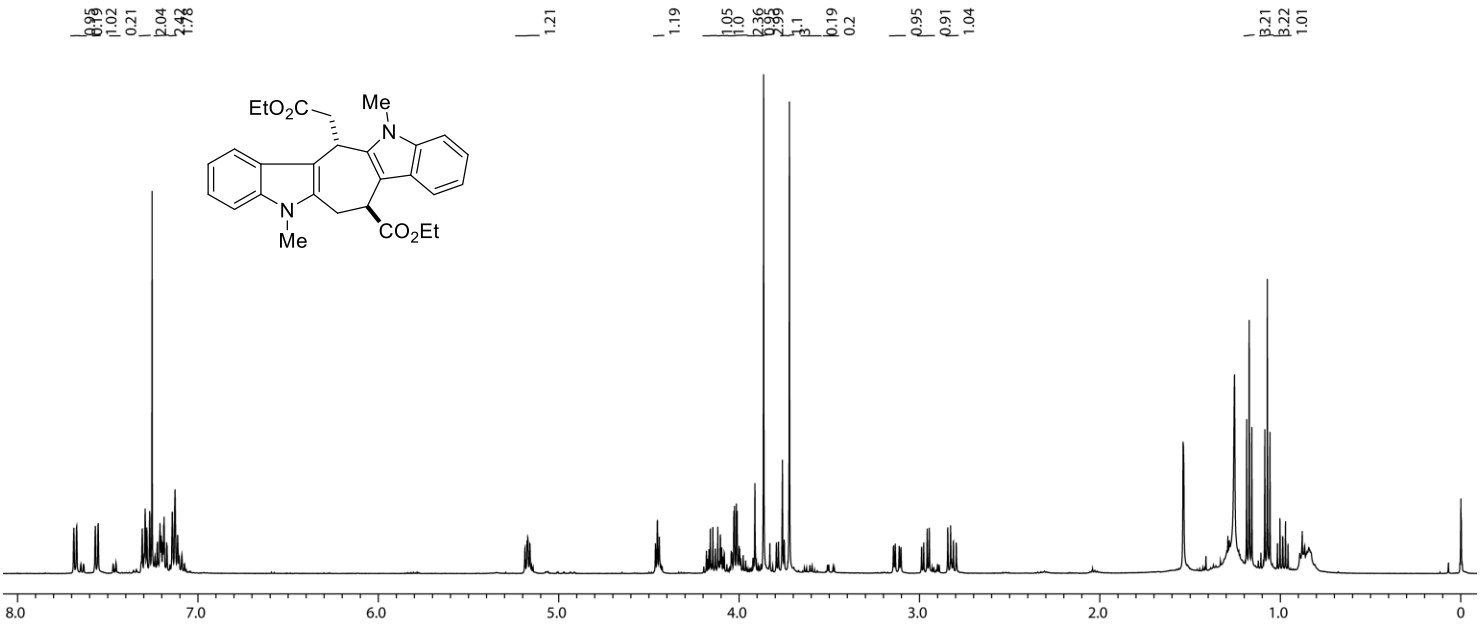

Figure S42. ^{1}H NMR spectrum of **3b** ($CDCl_3$, 500 MHz)

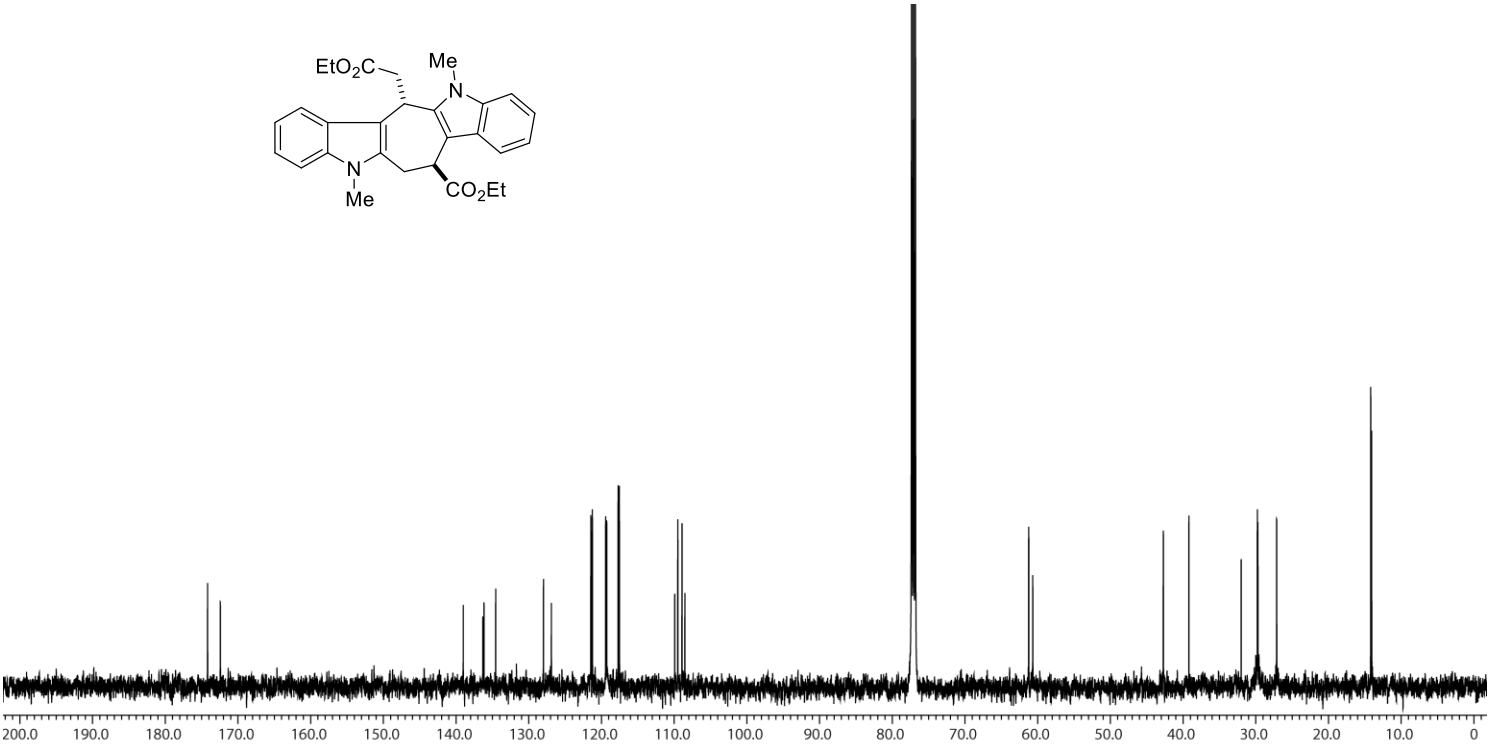

Figure S43. $^{13}C\{^{1}H\}$ NMR spectrum of **3b** ($CDCl_3$, 125 MHz)

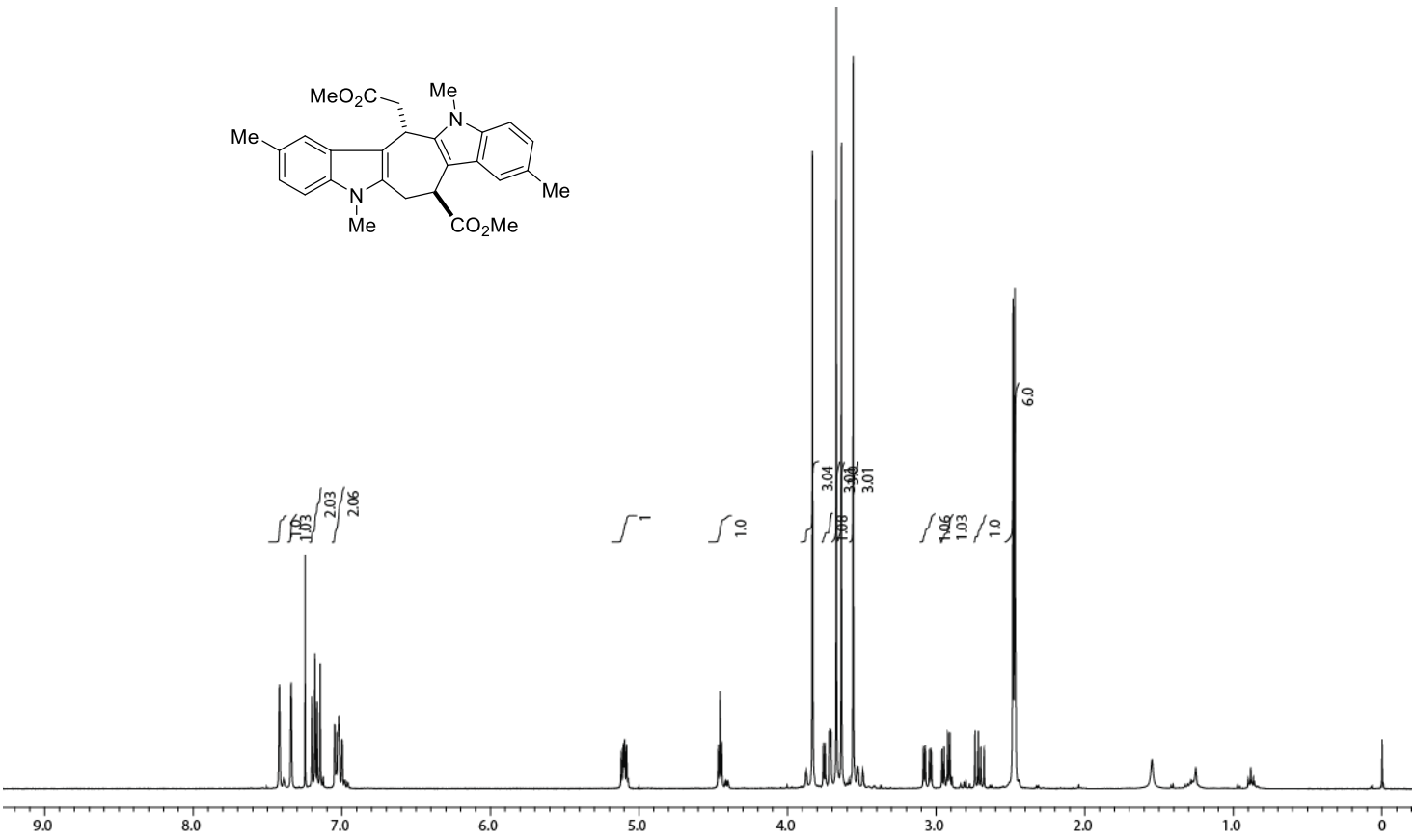

Figure S44. ^{1}H NMR spectrum of **3c** ($CDCl_3$, 500 MHz)

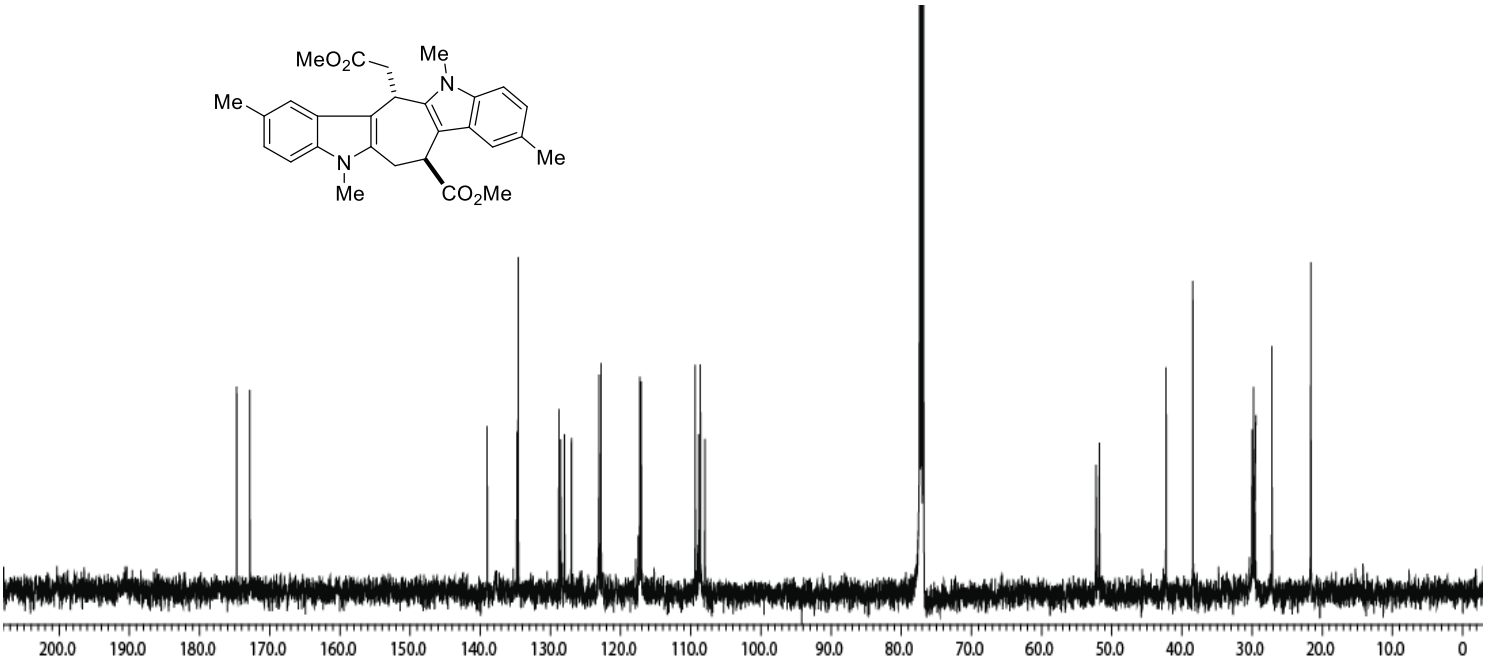

Figure S45. $^{13}C\{^{1}H\}$ NMR spectrum of **3c** ($CDCl_3$, 125 MHz)

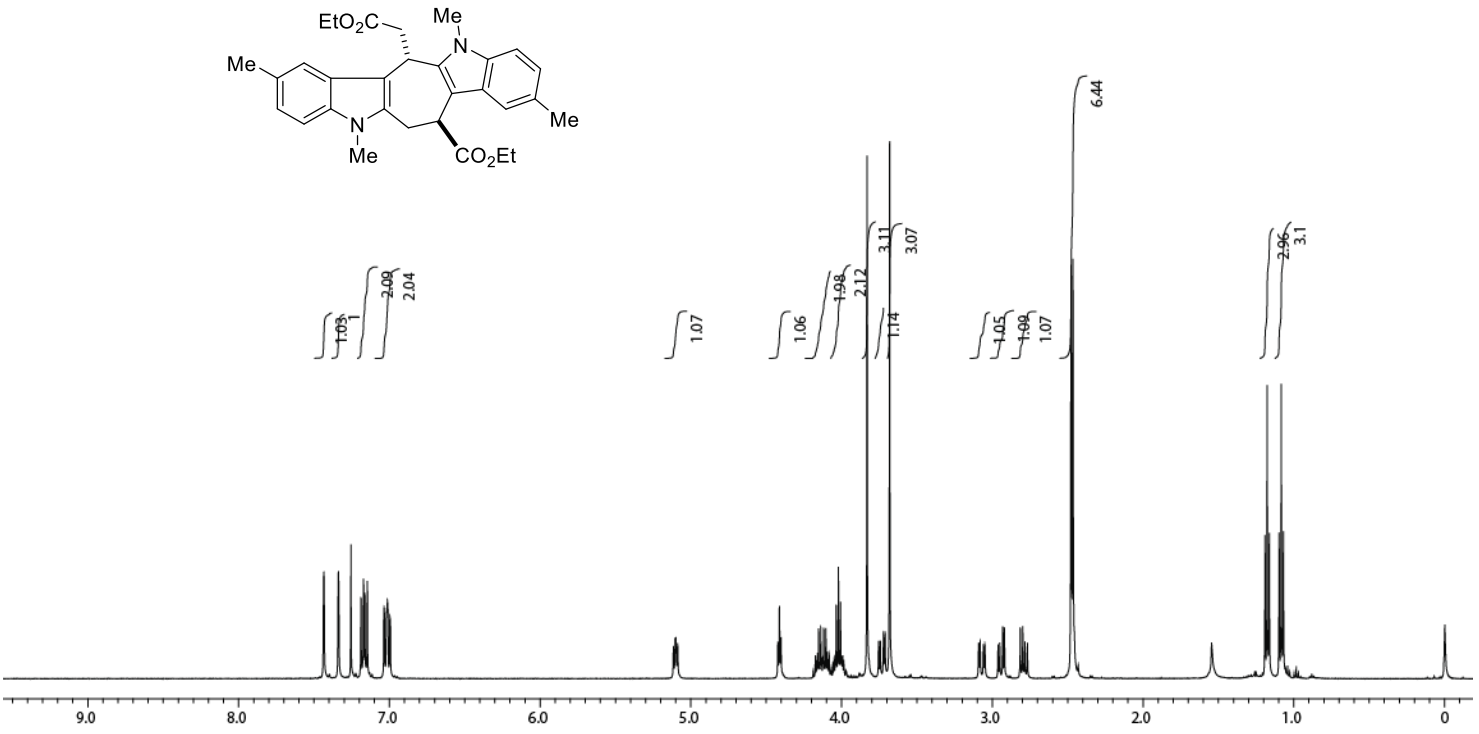

Figure S46. ^{1}H NMR spectrum of **3d** ($CDCl_3$, 500 MHz)

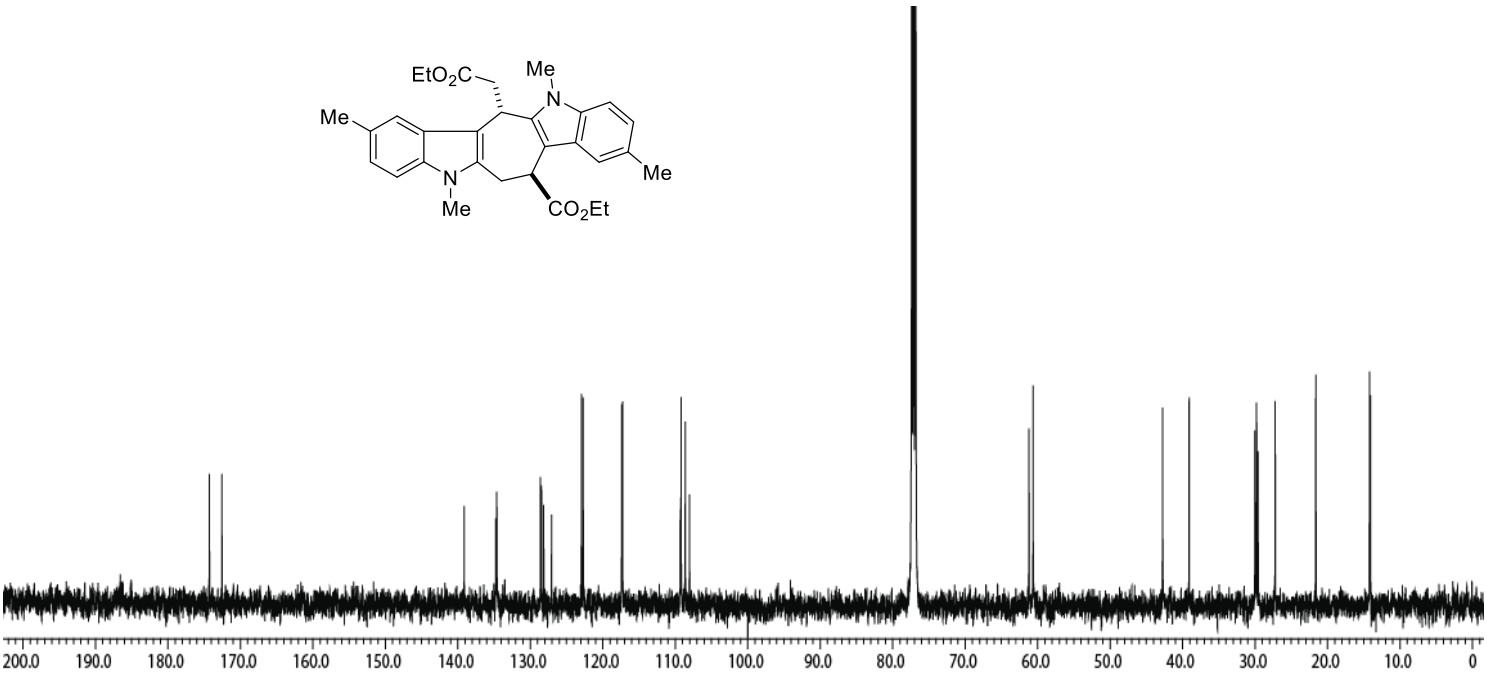

Figure S47. $^{13}C\{^{1}H\}$ NMR spectrum of **3d** ($CDCl_3$, 125 MHz)

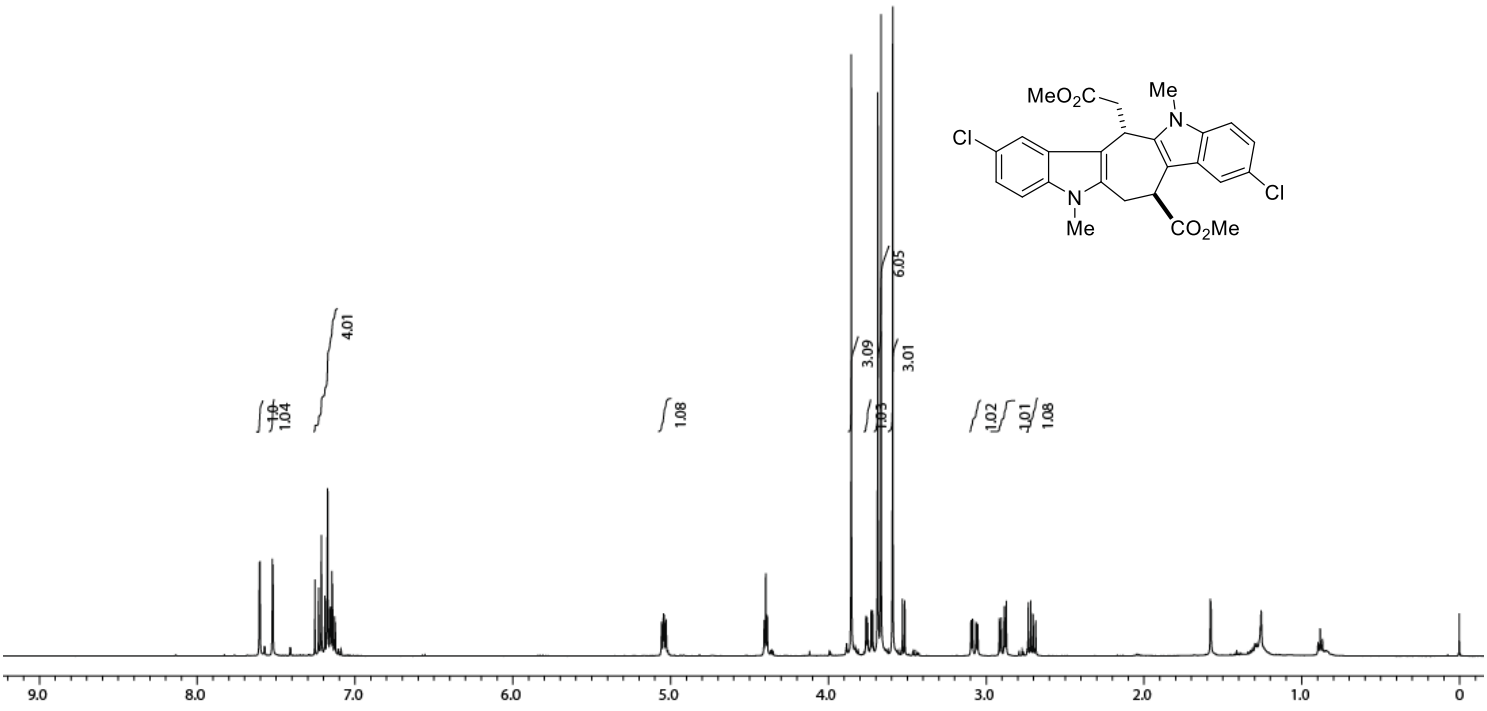

Figure S48. ^{1}H NMR spectrum of **3e** ($CDCl_3$, 500 MHz)

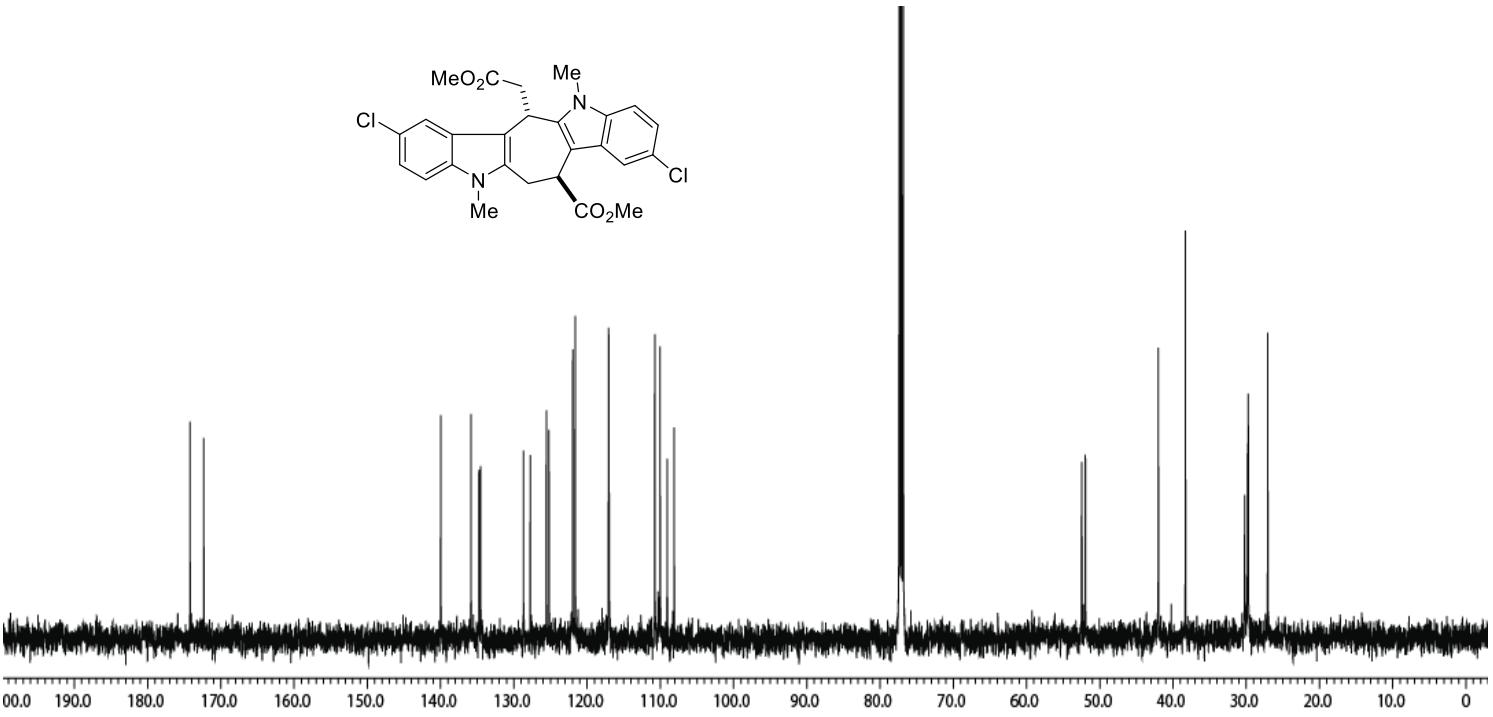

Figure S49. $^{13}C\{^{1}H\}$ NMR spectrum of **3e** ($CDCl_3$, 125 MHz)

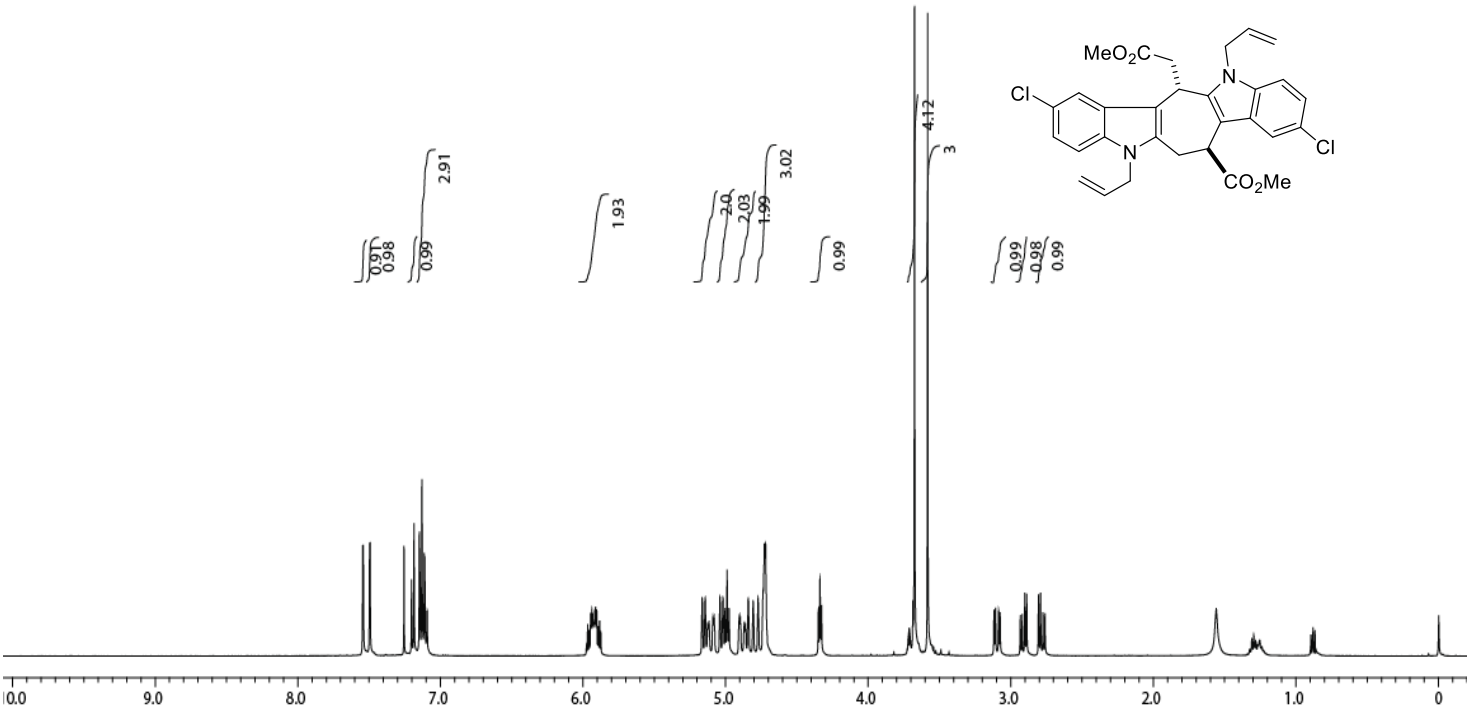

Figure S50. ^{1}H NMR spectrum of **3f** ($CDCl_3$, 500 MHz)

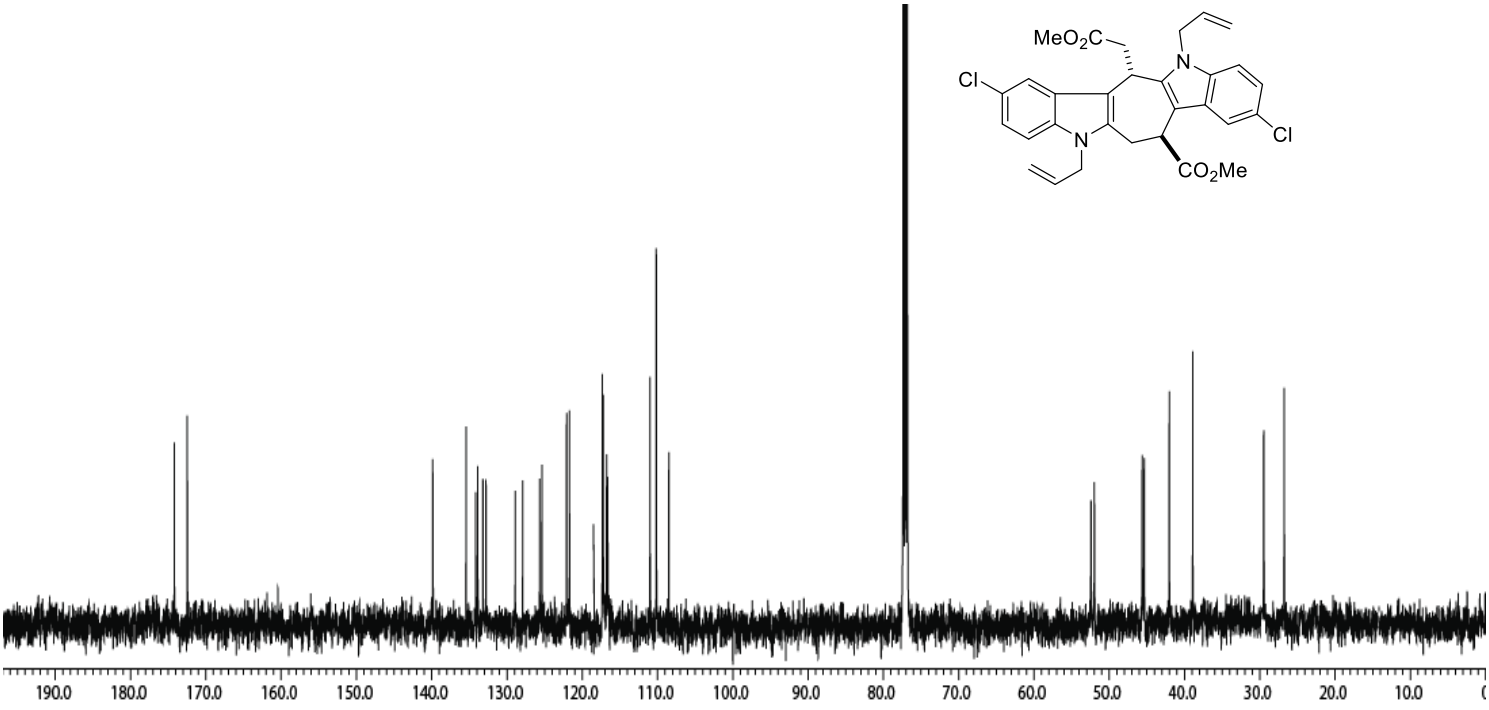

Figure S51. $^{13}C\{^{1}H\}$ NMR spectrum of **3f** ($CDCl_3$, 125 MHz)

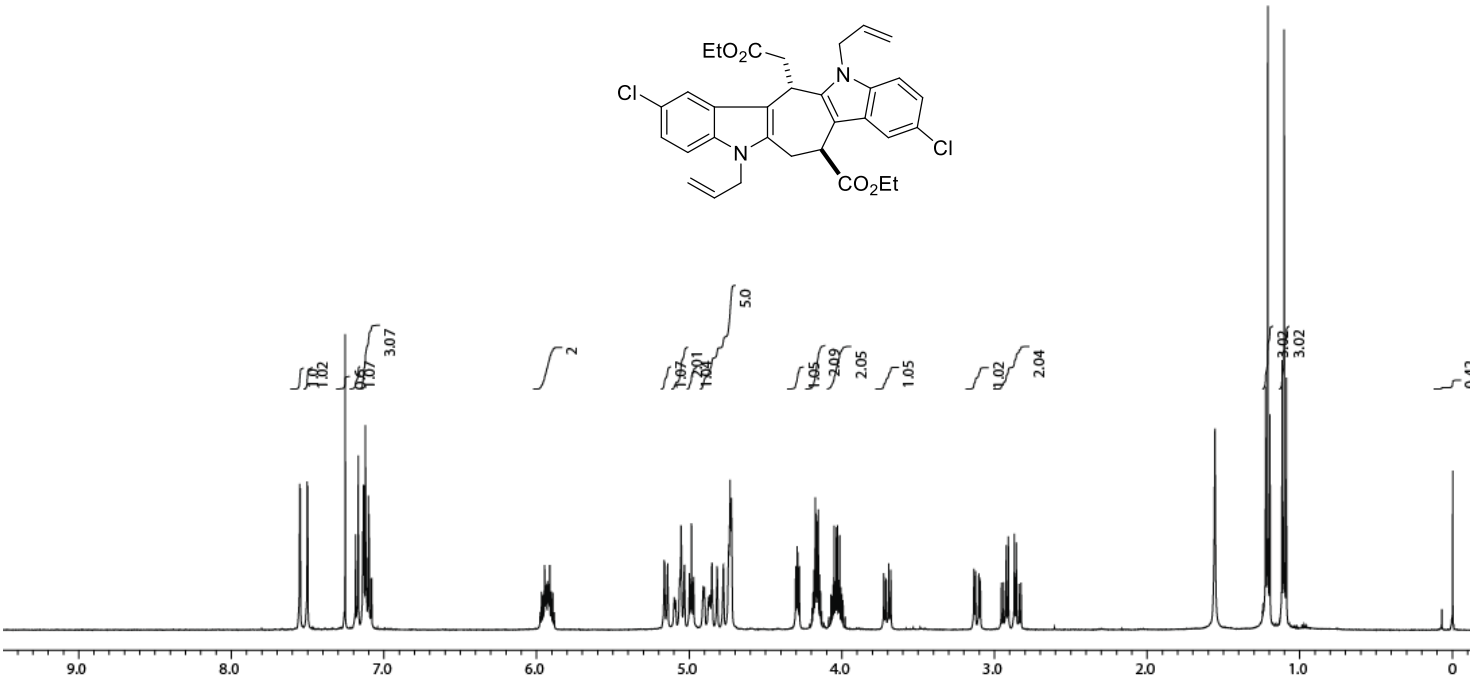

Figure S52. ^{1}H NMR spectrum of **3g** ($CDCl_3$, 500 MHz)

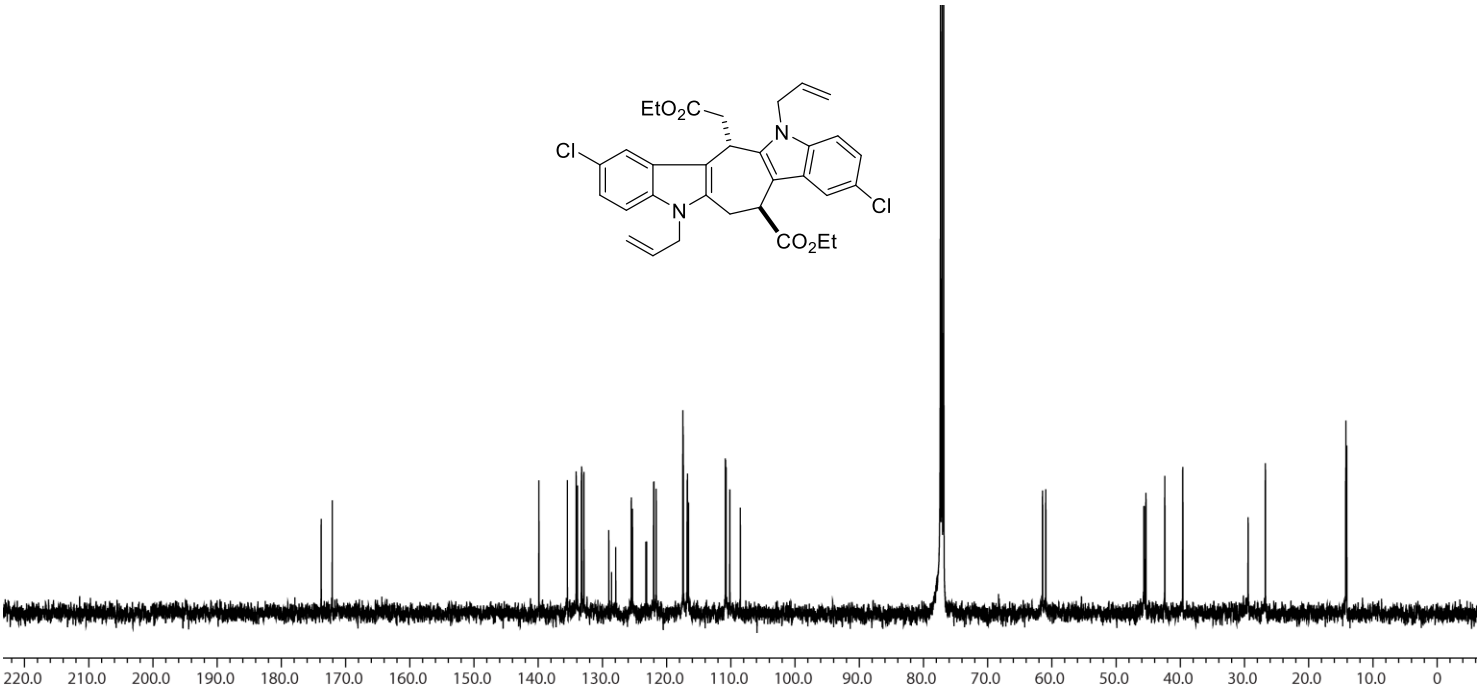

Figure S53. $^{13}C\{^{1}H\}$ NMR spectrum of **3g** ($CDCl_3$, 125 MHz)

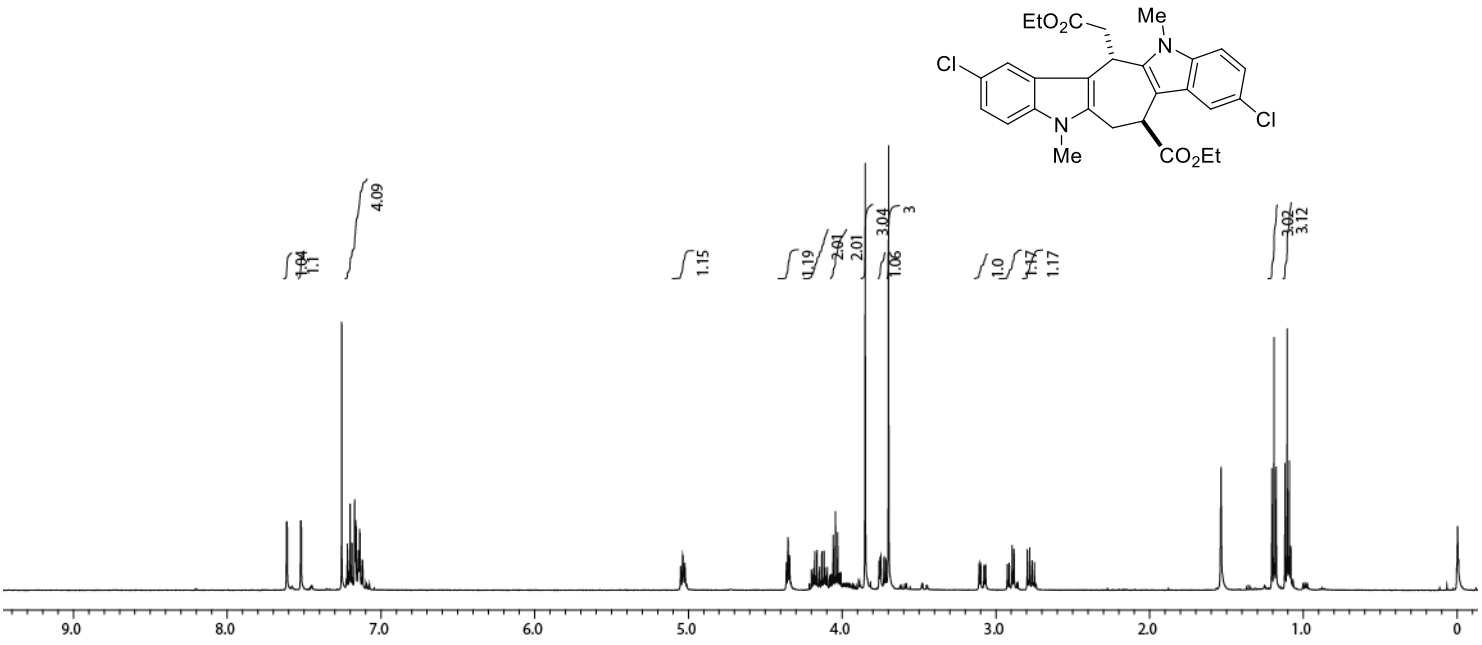

Figure S54. ^{1}H NMR spectrum of **3h** ($CDCl_3$, 500 MHz)

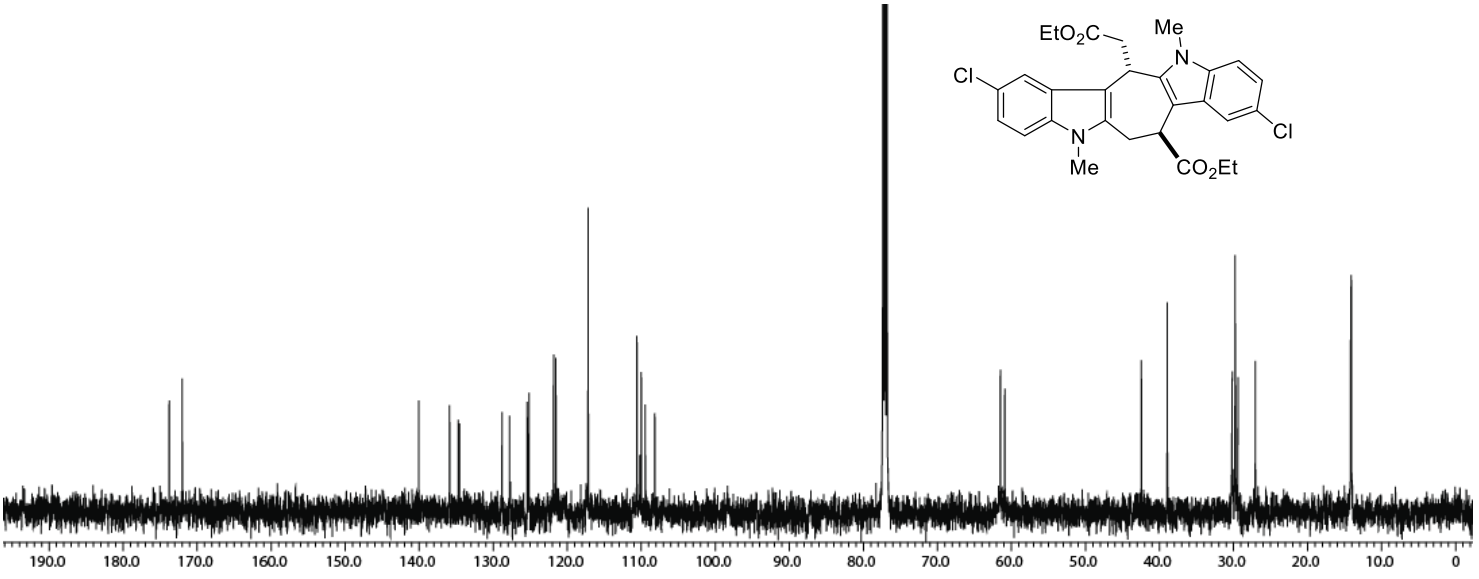

Figure S55. $^{13}C\{^{1}H\}$ NMR spectrum of **3h** ($CDCl_3$, 125 MHz)

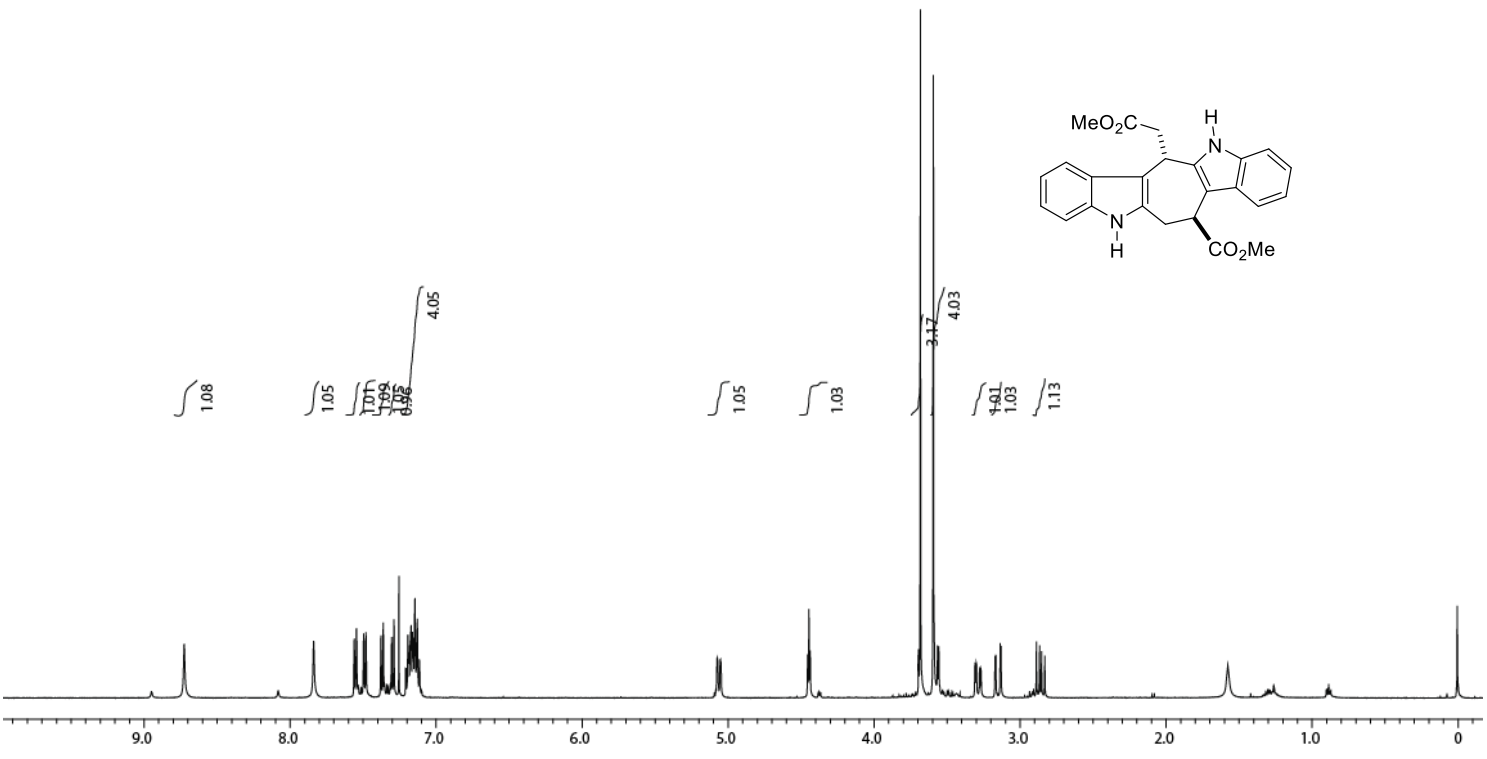

Figure S56. ^{1}H NMR spectrum of **3i** ($CDCl_3$, 500 MHz)

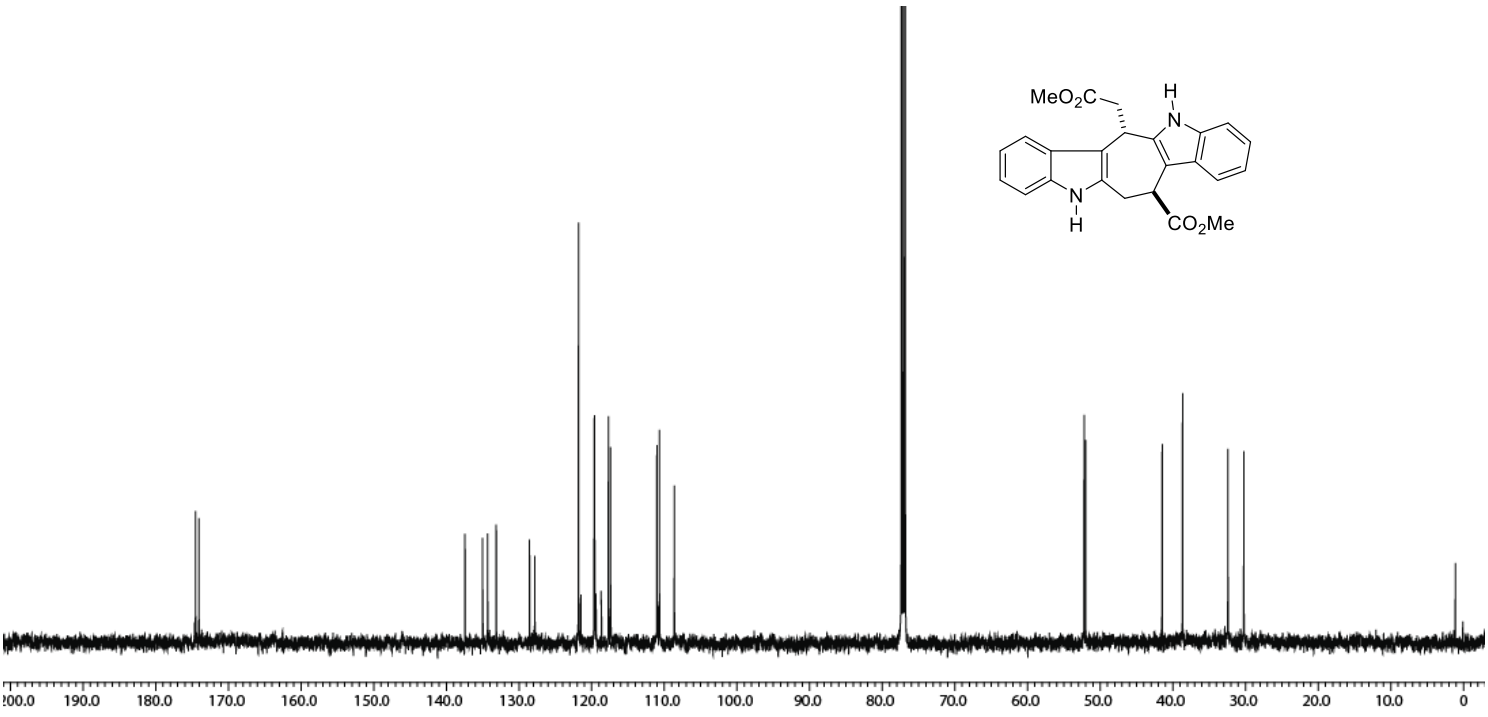

Figure S57. ^{13}C{^{1}H} NMR spectrum of **3i** ($CDCl_3$, 125 MHz)

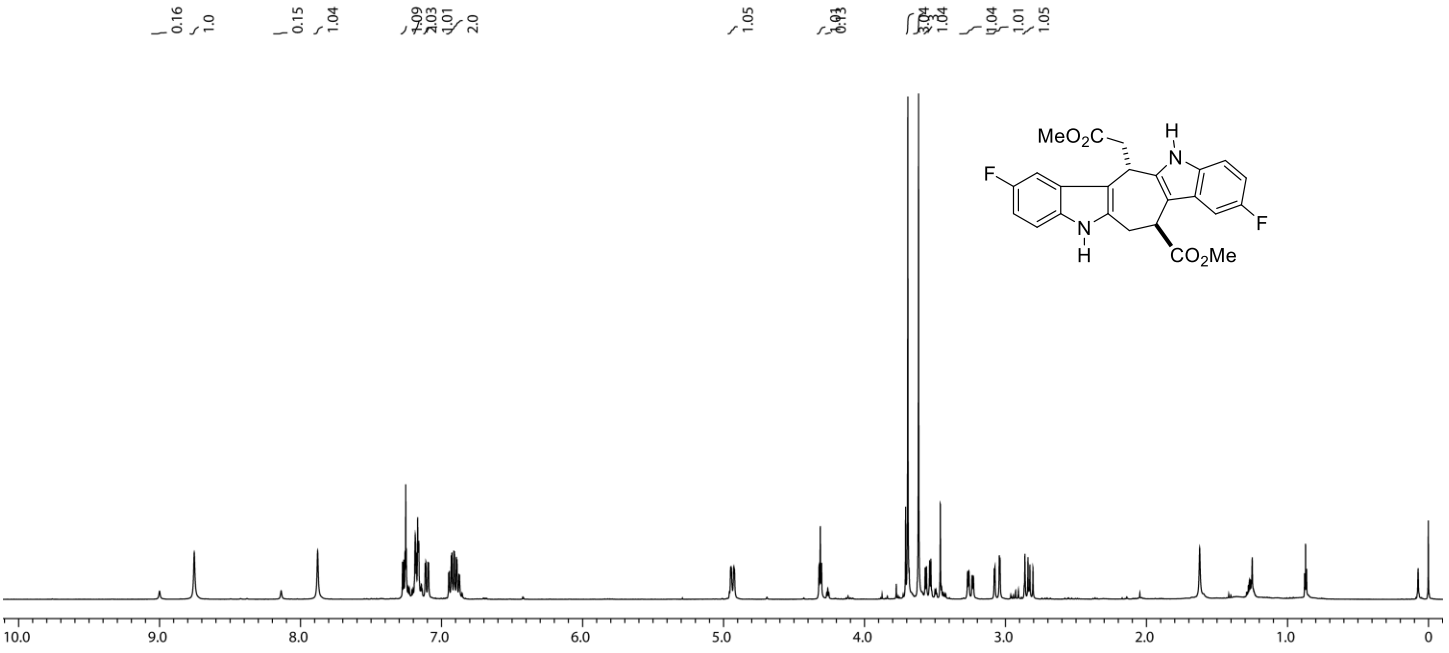

Figure S58. ^{1}H NMR spectrum of **3j** ($CDCl_3$, 500 MHz)

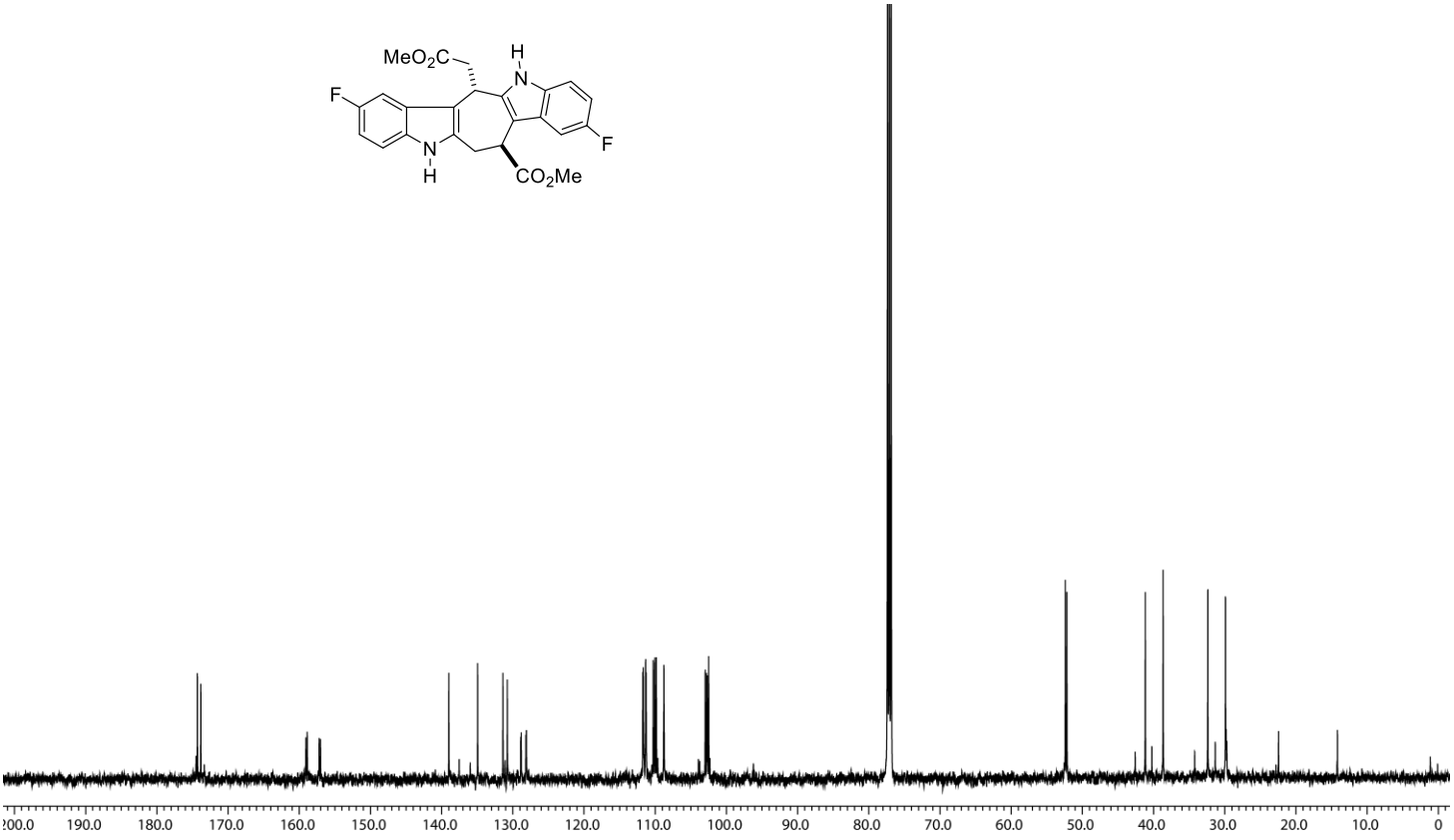

Figure S59. $^{13}C\{^{1}H\}$ NMR spectrum of **3j** ($CDCl_3$, 125 MHz)

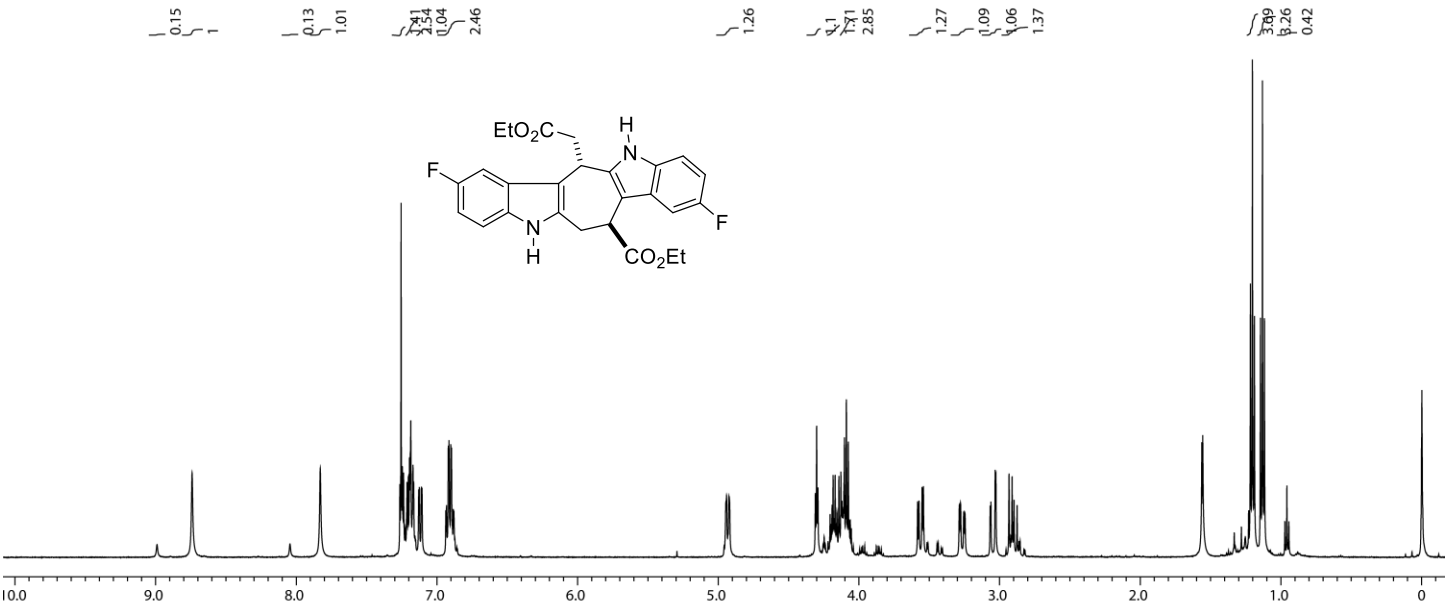

Figure S60. ^{1}H NMR spectrum of **3k** ($CDCl_3$, 500 MHz)

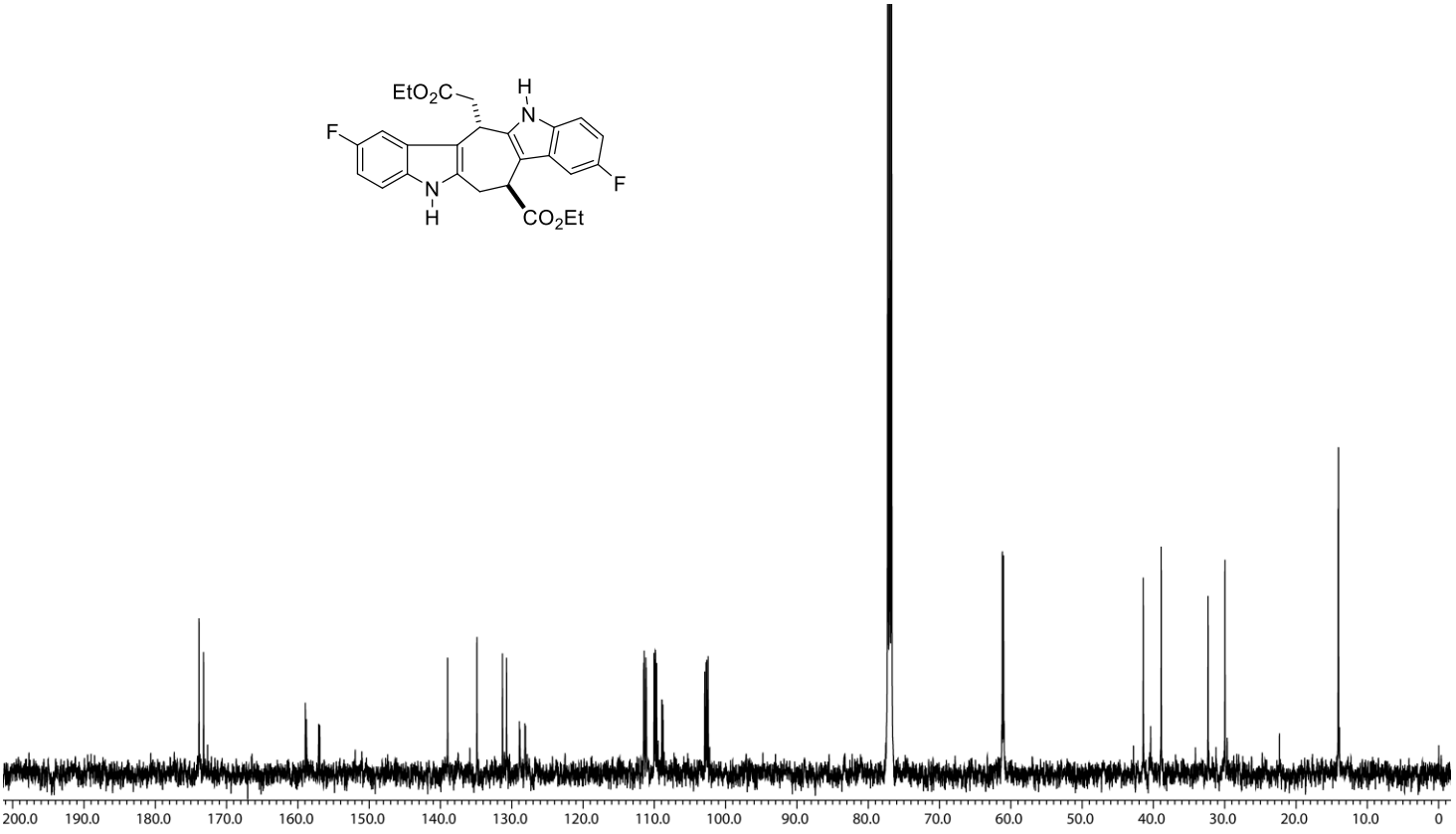

Figure S61. $^{13}C\{^{1}H\}$ NMR spectrum of **3k** ($CDCl_3$, 125 MHz)

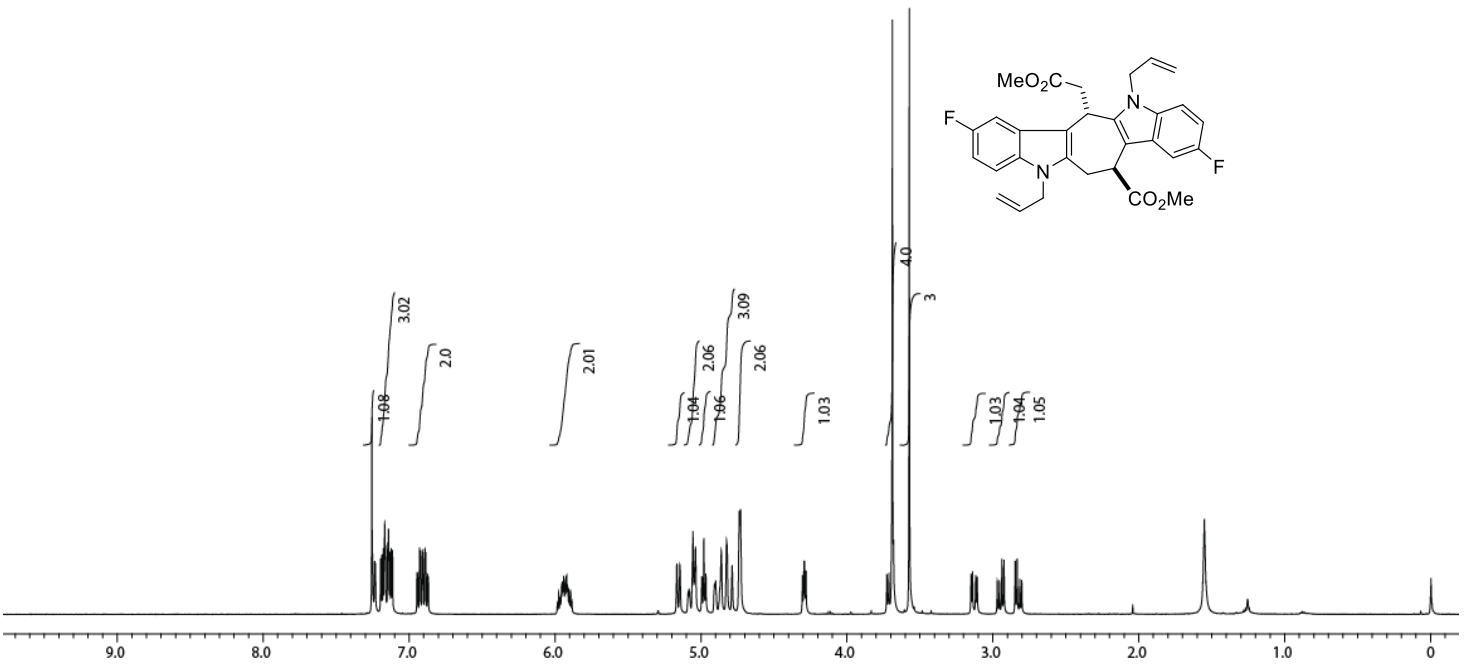

Figure S62. ^{1}H NMR spectrum of **3l** ($CDCl_3$, 500 MHz)

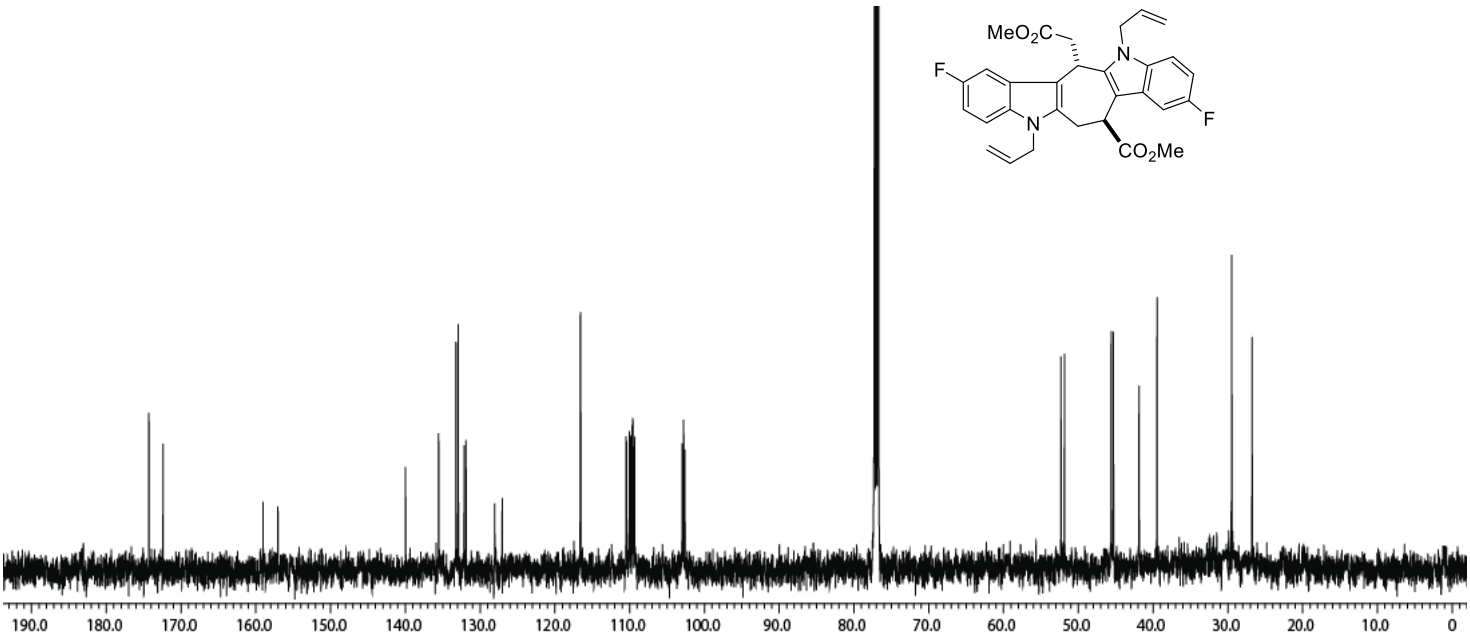

Figure S63. $^{13}C\{^{1}H\}$ NMR spectrum of **3l** ($CDCl_3$, 125 MHz)

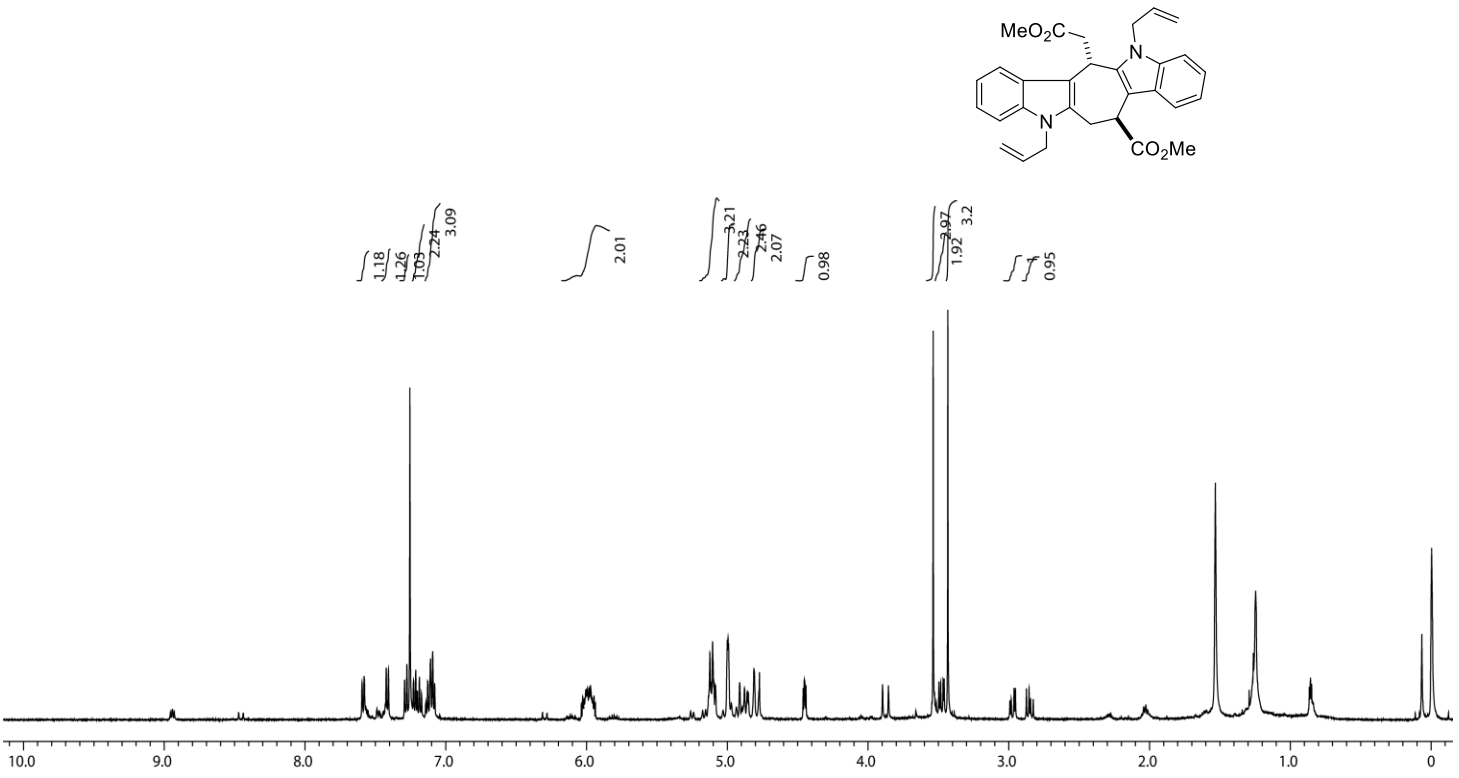

Figure S64. ^{1}H NMR spectrum of **3m** ($CDCl_3$, 500 MHz)

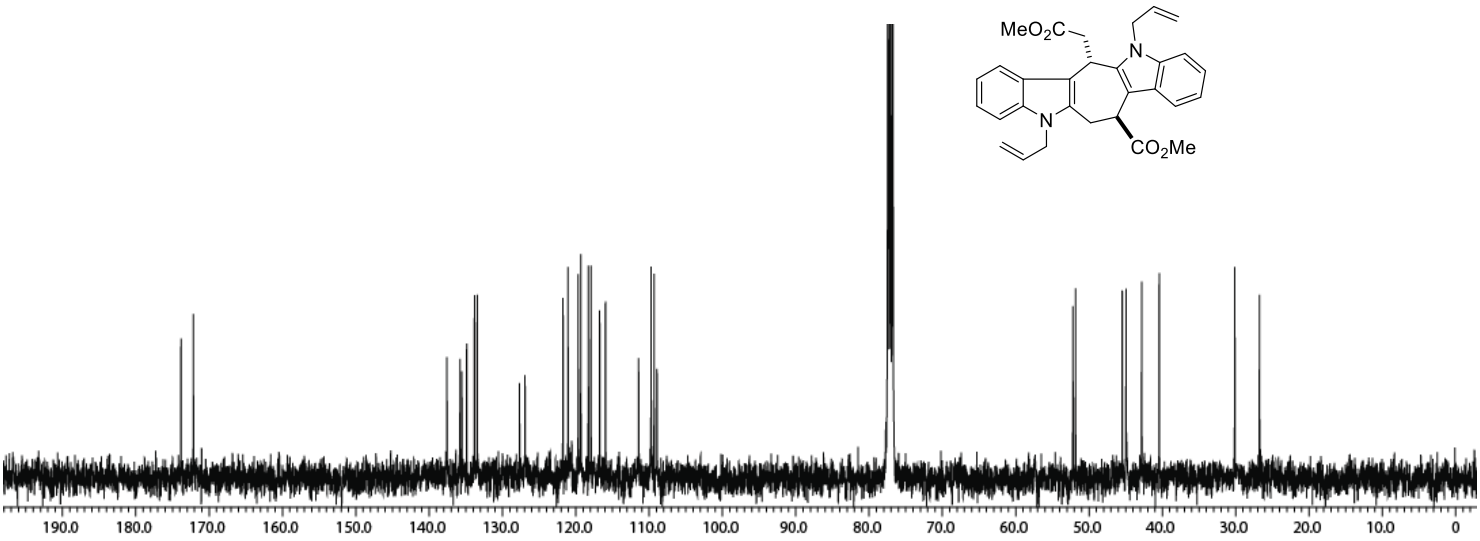

Figure S65. $^{13}C\{^{1}H\}$ NMR spectrum of **3m** ($CDCl_3$, 125 MHz)

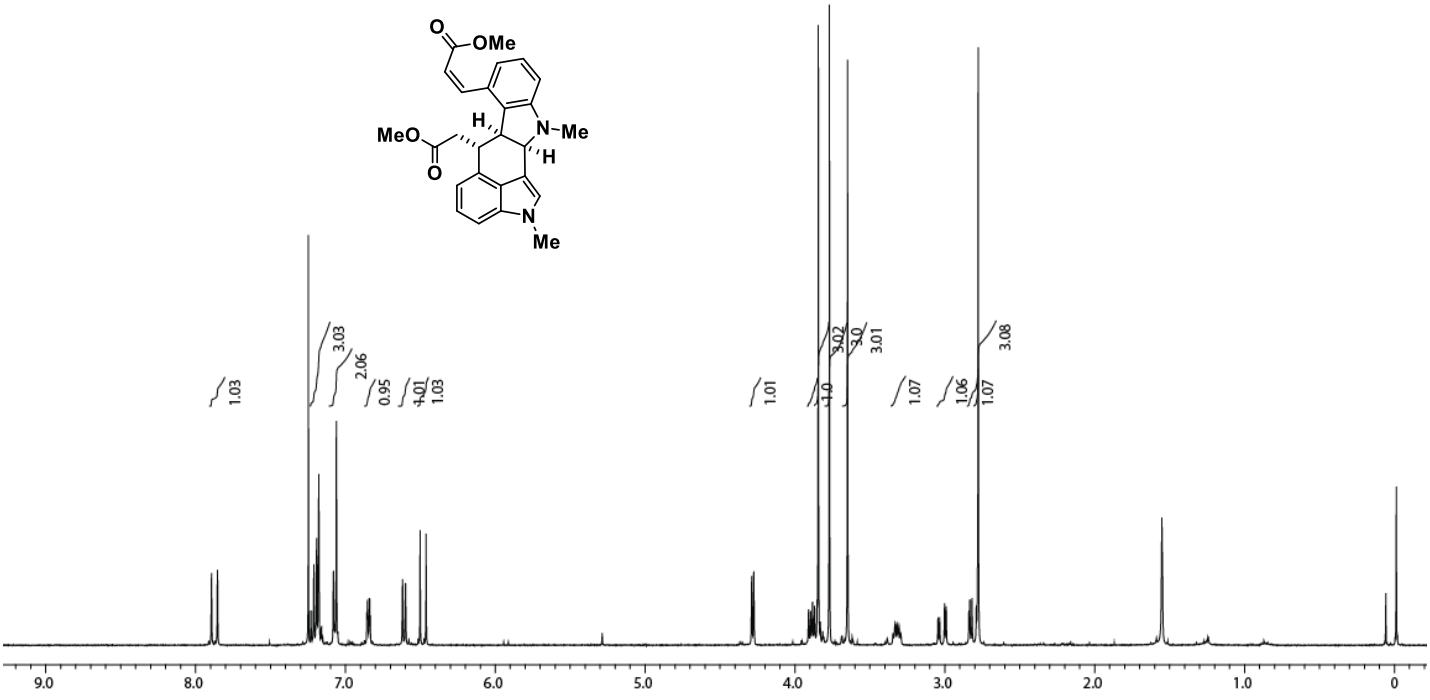

Figure S66. ^{1}H NMR spectrum of **5** ($CDCl_3$, 500 MHz)

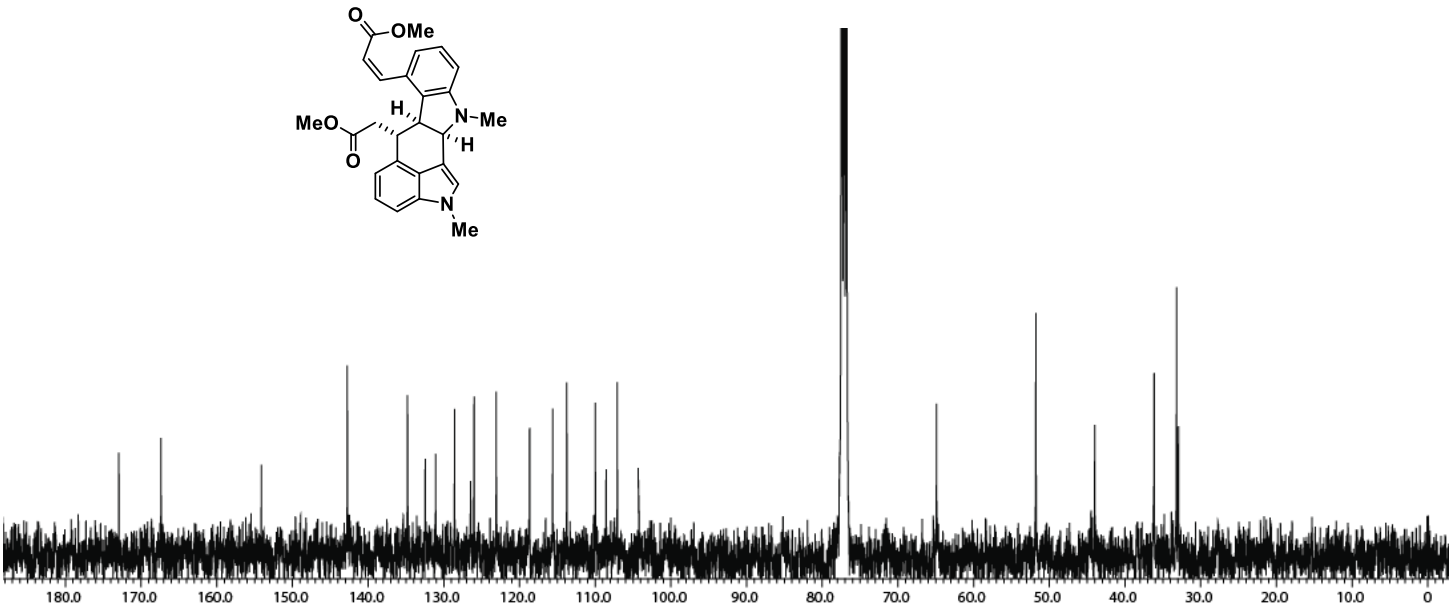

Figure S67. $^{13}C\{^{1}H\}$ NMR spectrum of **5** ($CDCl_3$, 125 MHz)